ON THE EXPERIMENTAL INVESTIGATION OF VORTEX EXCITED PRESSURE FLUCTUATIONS

by

WALTER HEINE

B.A.Sc. University of British Columbia, 1963

A THESIS SUBMITTED IN PARTIAL FULFILMENT OF

THE REQUIREMENTS FOR THE DEGREE OF

MASTER OF APPLIED SCIENCE

in the Department

of

Mechanical Engineering

We accept this thesis as conforming to the

required standard

THE UNIVERSITY OF BRITISH COLUMBIA

August, 1964

In presenting this thesis in partial fulfilment of the requirements for an advanced degree at the University of British Columbia, I agree that the Library shall make it freely available for reference and study. I further agree that permission for extensive copying of this thesis for scholarly purposes may be granted by the Head of my Department or by his representatives. It is understood that copying or publication of this thesis for financial gain shall not be allowed without my written permission.

Department of Mechanical Engineering

The University of British Columbia,
Vancouver 8, Canada.

Date September 4, 1964

ABSTRACT

Construction and calibration of a piezoelectric transducer capable of measuring acoustic level pressure fluctuations occurring on the surface of a body due to shed vortices is described. The application of the transducer as a wake survey equipment is also explained. The fluctuating pressure and wake geometry study carried out using two dimensional models of several bluff and streamlined bodies indicate that

(1) Fluctuating lift coefficient decreases with reduction in bluffness of the body.

(2) For square and rectangular cylinders, as well as for the elliptic cylinder at large angles of attack, the amplitude of fluctuating pressure is minimum at the points where static pressure is maximum.

(3) Fluctuating lift coefficient for the bodies with sharp leading edge (e.g. square and rectangular cylinders) is considerably larger than the corresponding static value, while for the circular cylinder, elliptic cylinder and the wing, the fluctuating coefficients were found to be smaller than their static counterpart.

(4) The self excited motion of the body, particularly a bluff body, does not affect either the frequency of shedding vortices or the fluctuating pressure, for frequencies above vortex resonance.

ACKNOWLEDGEMENT

I would like to express my sincere thanks and appreciation to Dr. V. J. Modi for the guidance and assistance he has given me in the presentation of this thesis. Thanks are also due to Mr. P. Hurren for his continued assistance in the experimental work, especially in the design, and construction of the pressure transducer.

Also, I would like to thank the Department of Mechanical Engineering for the use of their facilities, and the National Research Council of Canada for financial assistance given through grants in aid of research.

TABLE OF CONTENTS

LIST OF FIGURES

LIST OF SYMBOLS

a	Lateral spacing of vortices
$\bar{a}$	Semimajor axis of ellipse
AR	Aspect ratio
b	Length of face of rectangular cylinder parallel to flow
c	Characteristic chord
C'	Coefficient per unit span
ds	Elementary length
e	Eccentricity of elliptic cylinder
h	Length of face of rectangular cylinder perpendicular to flow
$\bar{h}$	Longitudinal spacing of vortices
I	Current in electromagnetic dampers
L'	Lift per unit span
P	Pressure at a point
Re	$\frac{Vc}{\nu}$, Reynolds Number
r	Damping coefficient
Kt	$\frac{\omega c}{V}$, Strouhal Number
V	Free stream velocity
$\bar{x}$	Coordinate, abscissa
$\bar{y}$	Coordinate, ordinate
α	Angle of attack
γ	Angle between pressure and lift for elliptic cylinder
ϑ	Angular spacing of taps of circular cylinder
ν	Kinematic viscosity
ρ	Density
ω	Strouhal frequency, i.e., frequency of shedding vortices

Subscripts.

fl	Fluctuating measurement
ℓ	Lower surface
L	Pertaining to lift
max	Maximum value
P	Pertaining to pressure
rms	Root mean square value
st	Static measurement
u	Upper surface
∞	Value at infinity

I. INTRODUCTION

The nature of the excitation in the study of aeroelastic instability is an important factor governing the response of a system. Hence precise determination of fluctuating pressure on elastic bodies is essential in the study of their instability characteristics.

A survey of existing literature reveals that problems involving vortex-excited fluctuating pressure characteristics have received comparatively little attention. The situations involving separation (over part of the body or during part of the cycle) have been investigated to some extent by Duncan (1),* Van de Vooren (2), Mendelson (3), Sisto (4), Stüder (5) and others. The characteristics of the wake, which forms one of the important parameters in the aeroelastic instability study, were investigated theoretically by von Karman in his classical papers (6), (7). Studies of the flow pattern in the wake of bluff cylinders using hot wire anemometers and similar flow measuring apparatus were carried out by Cometta (8) and Roshko (9), while Chuan and Magnus (10) investigated the vortex shedding as related to self excited torsional oscillations of an airfoil.

The measurement of oscillating pressure on a stationary circular cylinder was carried out by McGregor (11) and Prendergast (12). The experimental arrangement required external rotation of the model to obtain a complete distribution of fluctuating pressure.

---

* Numbers in brackets refer to bibliography

A technique involving a miniature strain gauge type transducer for oscillating pressure measurement was developed by Molyneux (13) and later modified by Molyneux and Ruddleston (14). The device was used for the experimental determination of aerodynamic derivatives by measurement of oscillating pressure and its integration over the surface of the airfoil. Their work, however, remained solely for airfoils as this was their main field of interest. The models were exposed to externally applied forced vibrations rather than oscillations resulting from the flutter phenomenon.

With all this information an important task of correlation between characteristics of the wake, oscillating pressure distribution on a body and the aeroelastic instability of that body remains.

II. STATEMENT OF THE PROBLEM

The measurement of unsteady aerodynamic pressure on a body and a survey of the associated wake and the aeroelastic instability of the body forms the subject of this experimental investigation. The project may be classified into four stages:

(i) Measurement of oscillating pressure on bluff as well as streamlined bodies, stationary and vibrating, when located in steady flow.

(ii) Experimental study of wake to associate fluctuating pressure with the wake configuration.

(iii) Measurement of critical flutter speed for the bluff and aerodynamic bodies in two degrees of freedom, plunging and torsion.

(iv) Correlation of information obtained in (i), (ii), and (iii).

III. INSTRUMENTATION, CALIBRATION AND EXPERIMENTAL SETUP

The instrumentation used in the experimental investigation corresponds as follows to the first three stages of the project mentioned in Chapter II:

(i) a pressure measuring device, a transducer, and the arrangement for calibrating it

(ii) instrumentation for wake survey

(iii) mounting of model in the wind tunnel to provide freedom of motion in plunging, and torsion, system for providing desirable stiffness and damping, arrangement for measurement of critical velocity, frequency, and amplitude during aeroelastic instability of the model.

Each of these systems is described in some detail below.

3.1.1 Wind Tunnel

The wind tunnel used for the test program was of the standard low speed, low turbulence return type with velocity control over the range of 4 to 150 feet per second and a turbulence level of less than 0.5% as indicated by sphere drag test. The tunnel was powered by a 15 horsepower direct current motor driving a commercial axiflow fan with a Ward-Leonard system of speed control. The tunnel velocity is calibrated against the pressure differential across the contraction section of 7:1 ratio. This pressure was measured on a Betz micromanometer which can be read to 0.02 millimeter of water. The test section

was 36 inches by 27 inches with corner fillets varying from 6 inches by 6 inches to 4 3/4 inches by 4 3/4 inches to compensate for boundary layer growth. The spatial variation of velocity was found to be less than 0.25%. The aerodynamic outline of the tunnel is given in Figure 1.

3.1.2 Calibration of Betz Manometer

A standard pitot tube placed in the test section was used in conjunction with a Lambrecht Manometer to measure the dynamic pressure head. The readings obtained from these measurements were then compared with the readings of the pressure differential across the contraction section as measured by the Betz manometer. The accuracy of Betz manometer was found to be adequate for the purpose (Figure 2).

3.2 Models

The models used were all of a light weight balsa construction. Five different models were made:

(i) a 2 inch sqare cylinder

(ii) a 1 1/2 by 3 inch rectangular cyliner

(iii) a 2 inch diameter circular cylinder

(iv) an elliptic cylinder with semimajor axis of 3 inches and semiminor axis of 3/8 inch

(v) a 6 inch chord NACA 4412 airfoil section wing

All models were constructed to span the entire wind tunnel test section thus simulating two-dimensional flow. The models were made out of solid balsa with the exception of the wing which was made up of stiffening ribs with stringers and covered with a 1/16 inch balsa sheet. The models are

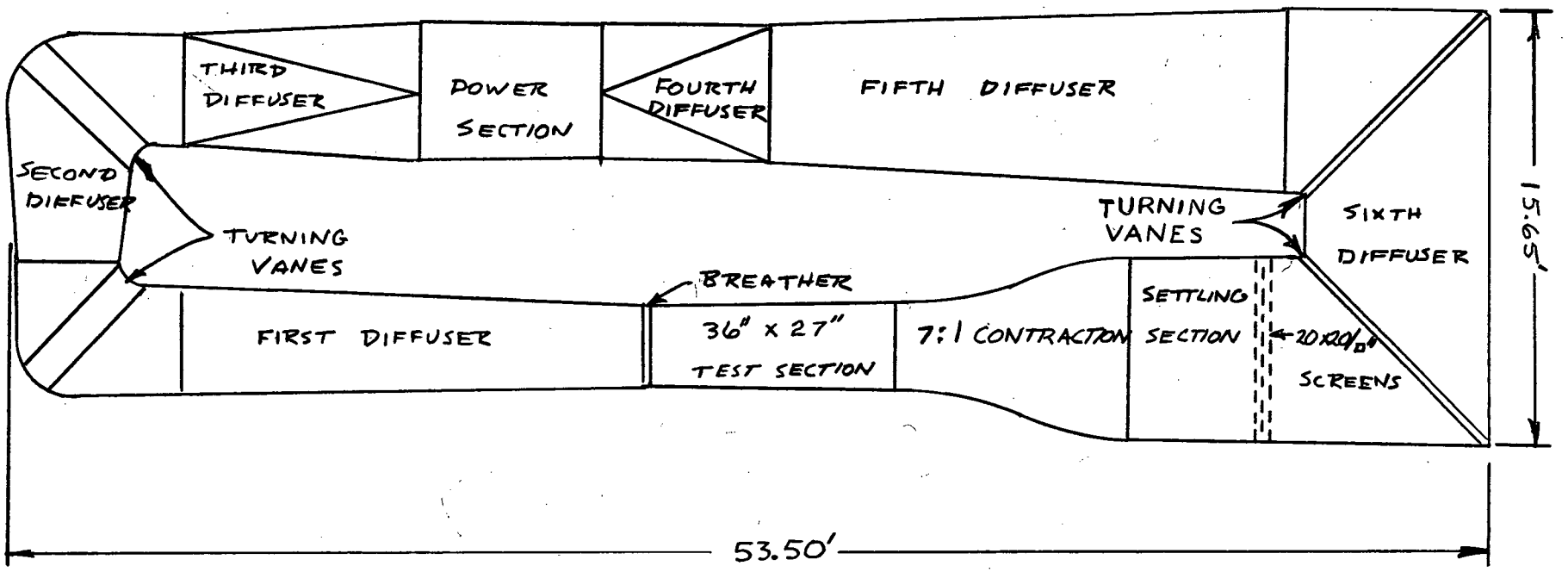

Figure 1. Aerodynamic Outline of Wind Tunnel

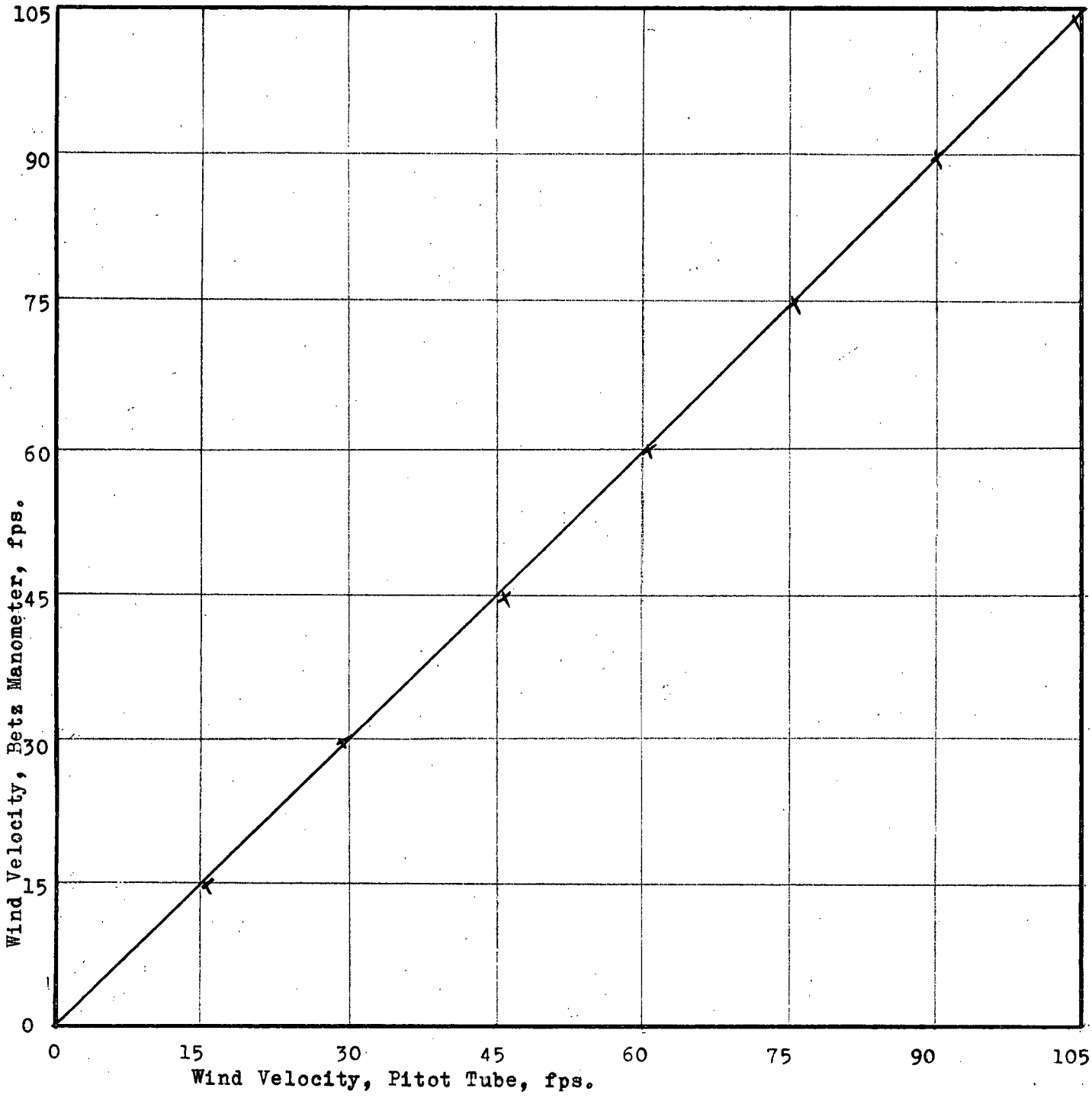

Figure 2. Calibration Curve: Wind Tunnel

shown in Figure 3.

A copper strip 3/4 inch wide, was placed at midspan to accommodate the pressure taps in the elliptic cylinder and airfoil. For the circular cylinder, a copper ring of 2 inch diameter and 3/4 inch width was used, while the square and rectangular cylinders used 3/4 inch wide aluminum blocks for positioning the static pressure holes. Models with the location of the pressure taps are shown in Figure 4.

Each model was supported by a 1/2 inch diameter shaft which extended beyond the tunnel walls, the shaft in turn being supported by a system of air bearings (Figure 5a).

3.3 Model Mounting System

The mounting system essentially consisted of a channel section, a steel frame supporting the air bearings at the top and bottom of of the tunnel section which provided the plunging degree of freedom to the model. Positive alignment between upper and lower air bearings was achieved by the use of 2 1/2 by 2 1/2 inch angle irons bolted at the ends, while the several adjusting bolts provided along the frame side helped in vertical positioning of the model. The upper and lower channels were machined to provide accurate alignment between the air bearings supporting the lateral shafts. The above arrangement was identical to that used by Smith (15).

For the study of flutter phenomena it was essential to incorporate the torsional degree of freedom. This was achieved by providing a set of torsional air bearings which were similar to the lateral air bearings but on a smaller scale. The torsional air bearings were designed to be mounted in the upper and lower lateral support shafts (Figure 5b).

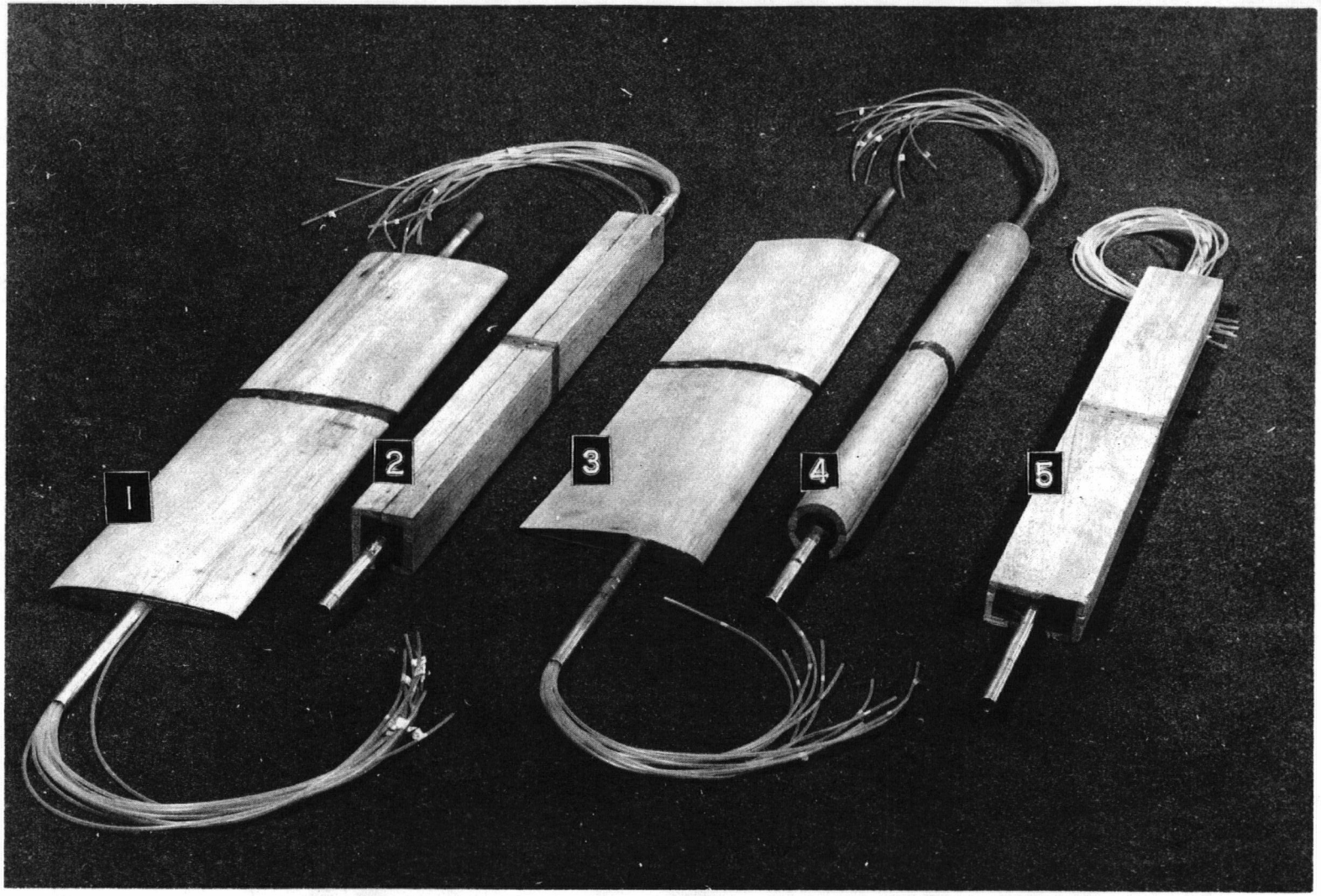

Figure 3. Experimental Models. 1. Elliptic Cylinder 2. Square Cylinder 3. NACA 4412 Section Wing 4. Circular Cylinder 5. Rectangular Cylinder AR = 1/2,2

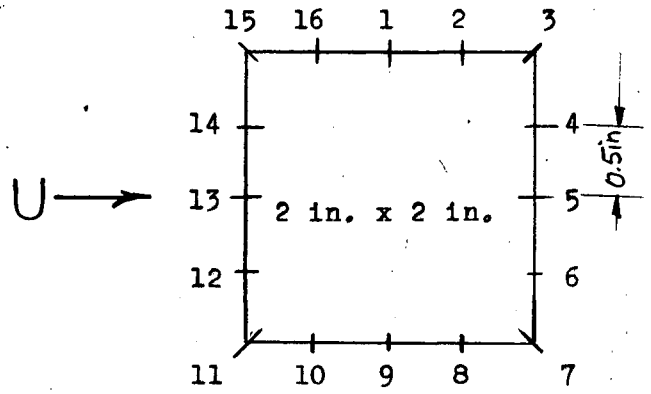

(a) Square Cylinder

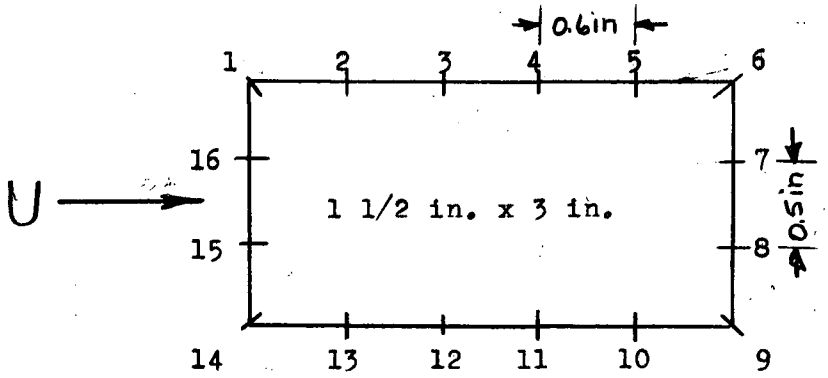

(b) Rectangular Cylinder

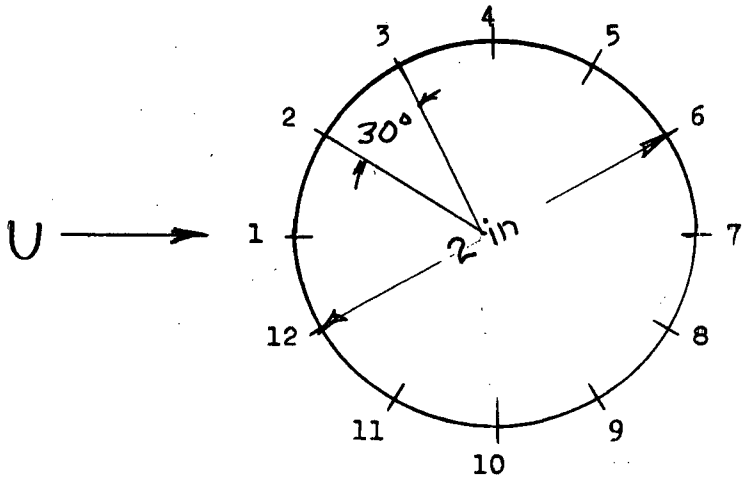

(c) Circular Cylinder

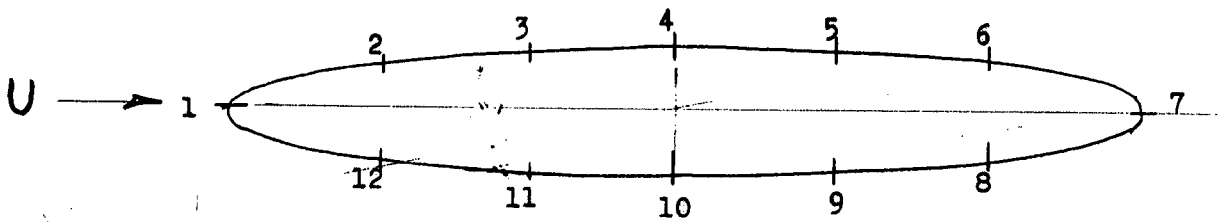

(d) Elliptic Cylinder

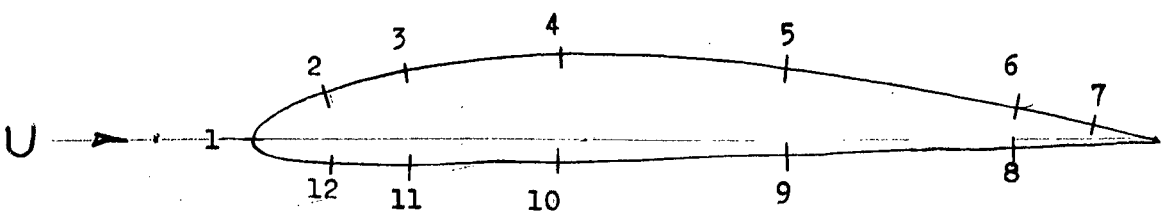

(e) NACA 4412 Airfoil

Figure 4. Location of Pressure Taps on Models

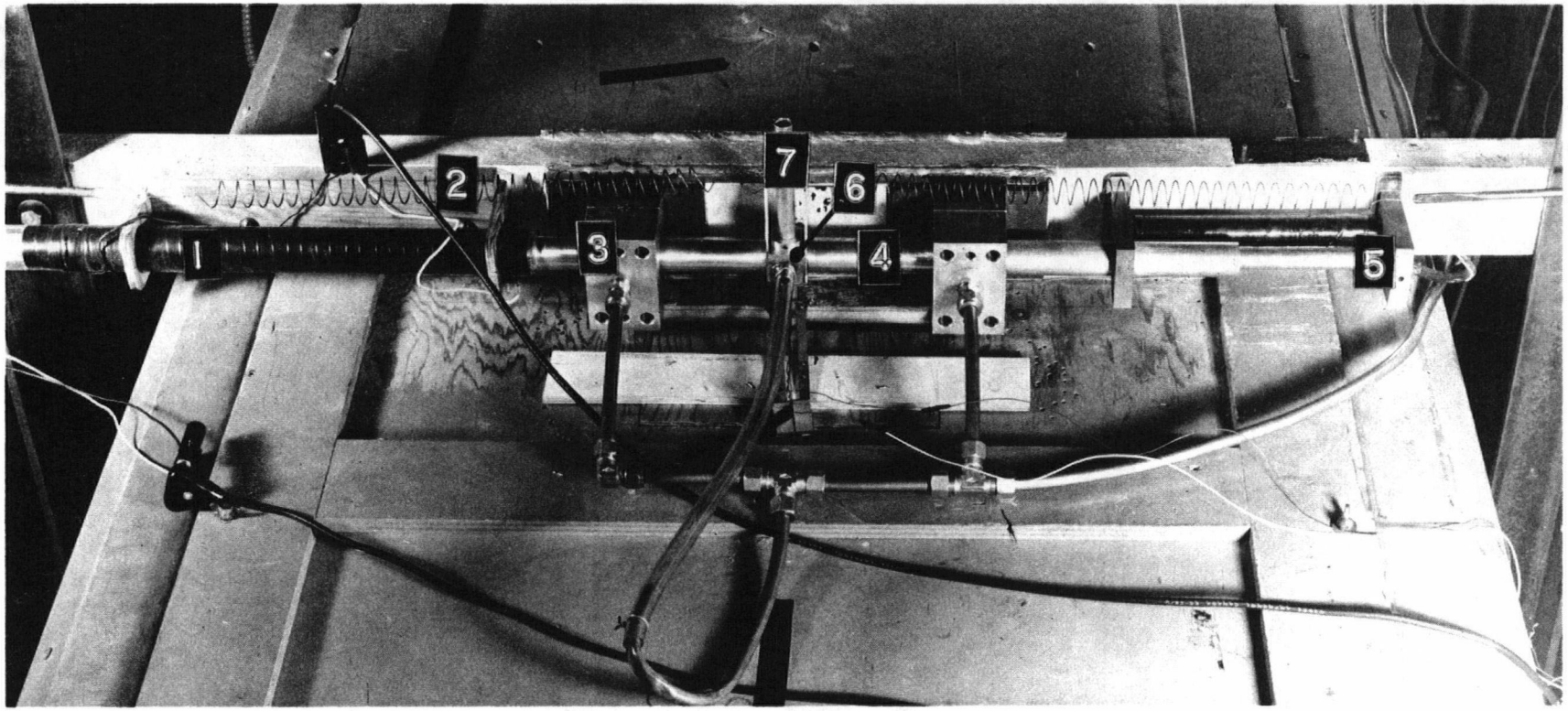

Figure 5a. 1. Lateral Displacement Transducer 2. Lateral Stiffness Spring 3. Lateral Air Bearing 4. Lateral Support Shaft 5. Lateral Damper 6. Torsional Air Bearing 7. Model Shaft

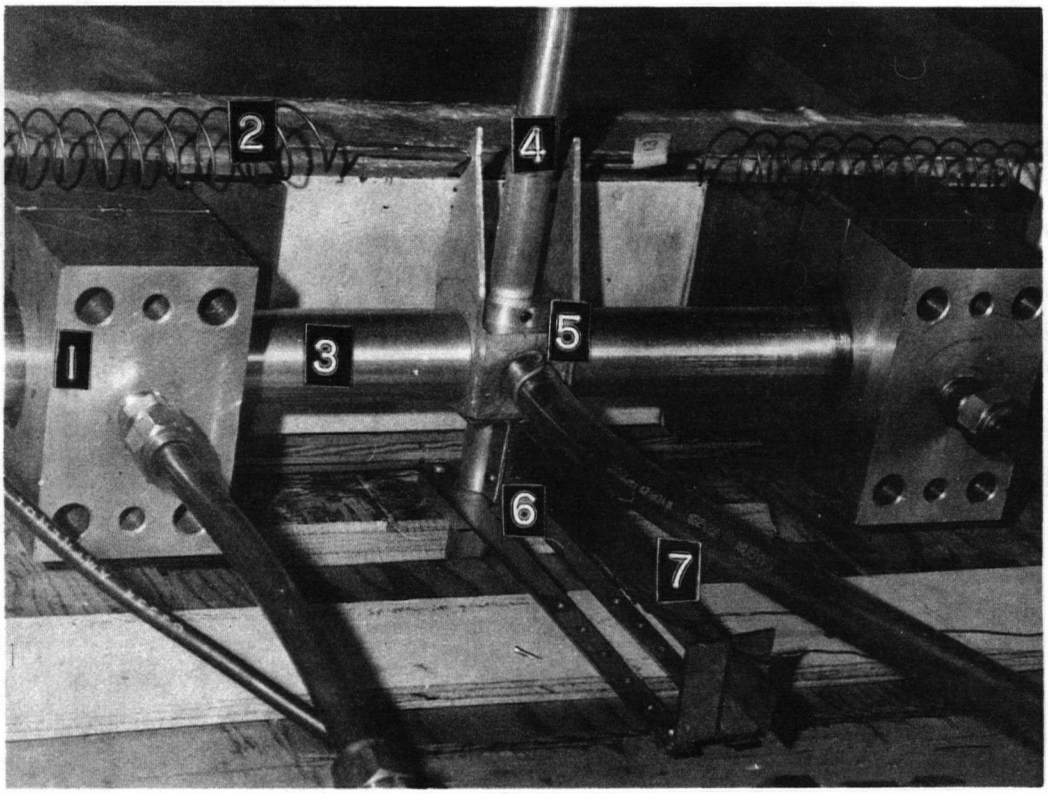

Figure 5b. 1. Lateral Air Bearing 2. Lateral Stiffness Spring 3. Lateral Support Shaft 4. Model Shaft 5. Torsional Air Bearing 6. Torsional Displacement Transducer 7. Torsional Stiffness Spring

Figure 5. Details of Model Mounting System

The air bearing carries a load on a shaft passing through the bearing in a similar manner to an oil journal bearing. Air is supplied through an orifice (Figure 6) at a pressure P_o. Due to viscous forces acting along the sides of the shaft and bearing walls the pressure drops to some value P_1. Application of a load causes the shaft to position itself eccentrically with respect to the bearing. The distance between shaft and bearing now becomes less on the side opposite to the load. The reduction in distance between shaft and journal on the side opposite to the load increases the viscous forces on the air flowing through the bearing thus decreasing the flow out of the bearing. Since the volumetric flow is now decreased, the pressure drop $(P_o - P_1)$ is decreased and since P_o is constant P_1 must increase. The opposite effect occurs on the load side where the distance increases. A pressure differential is therefore set up which supports the load. A quantitative analysis of air bearings is given by Laub (16).

Air for the bearings was supplied by an Ingersoll-Rand 2-stage compressor, pumping into a 250 cubic foot storage tank. Air was carried from the tank by a flexible hose to a throttling valve which distributed air at 60 pounds per square inch to all air bearings from the main supply at 118 pounds per square inch.

Lateral stiffness was supplied by springs attached between the mounting frame and the torsional air bearing. For torsional stiffness, cantilever springs were used. This was done by taking a strip of beryllium-copper and attaching it at one end to the torsional air bearing serving as the root and at the other end in such a way as to restrain torsional

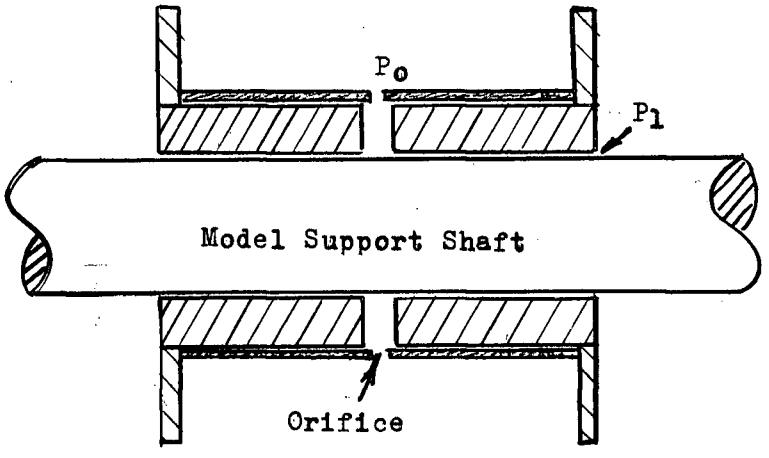

Figure 6. Cross-section of Air Bearing

motion. The details of the two mode stiffnesses are shown in Figure 5.

3.4 Pressure Transducer

The main problem encountered in the investigation was the design and calibration of a dynamic pressure transducer suitable for the measurement of fluctuating pressure on the surface of the models, which may be stationary or oscillating and may be located in unseparated or separated flow. Acoustic level pressure variations in the frequency range of 2 to 200 cycles per second made most of the commercially available transducers unsuitable for the purpose. The ideal transducer would be one with high sensitivity, linear response, and neutral to variations in atmospheric conditions. With this ideal in mind a variety of transducers involving the principle of strain gage, capacity change, resistance change and piezoelectricity were designed.

The resistor and capacitor type transducers failed to provide enough sensitivity for the size of the transducer intended. A strain gage type of transducer designed according to the arrangement suggested by Perry (16) was found to be quite sensitive to static pressures but relatively insensitive to pressure fluctuations of acoustic level. The tests conducted with a diaphragm of 2 inches diameter and 0.002 inch thickness revealed rather extreme sensitivity of the transducer output to the minor imperfections in the diaphragm. Increase in diaphragm thickness only reduced the sensitivity without improving the situation substantially. It is believed that with a relatively stiff diaphragm the strain gage transducer suggested by Perry may be used for measurement of static or

large amplitude dynamic pressure but further investigation is necessary to make it suitable for minute pressure fluctuations.

Transducers using Rochelle salt, quartz, and ceramic piezoelectric crystals in the form of a phonograph cartridge as used in the arrangement shown in Figure 7 were found to be highly sensitive and capable of measuring intended low level pressure changes on a body. The insensitivity of the device to static pressure did not present any problem as the intention was to measure fluctuating pressure rather than static pressure. Crystals of Rochelle salt and quartz were discarded in preference to the ceramic type because of their sensitivity to temperature changes. Thus the piezoelectric transducer using a ceramic crystal met the necessary requirements adequately and hence was used for the pressure measurement throughout the experiment.

In a piezoelectric device it can be shown that the voltage output is directly proportional to the force applied across one of the sensitive dimensions of the crystal (17). This phenomenon is due to the characteristics of the crystal structure and advantage was taken of this property to provide a linear pressure transducer.

The oscillating pressures at the surface of the body were sensed by pressure taps and transmitted by polyethylene tubing to the transducer. It was important to determine the effect of length and diameter of the tubing on sensitivity and phase lag. Experiments carried out with tubing of different diameter and lengths revealed considerable dependence of sensitivity on the diameter of the tube.

With very fine tubing (0.010 inches diameter) response of the

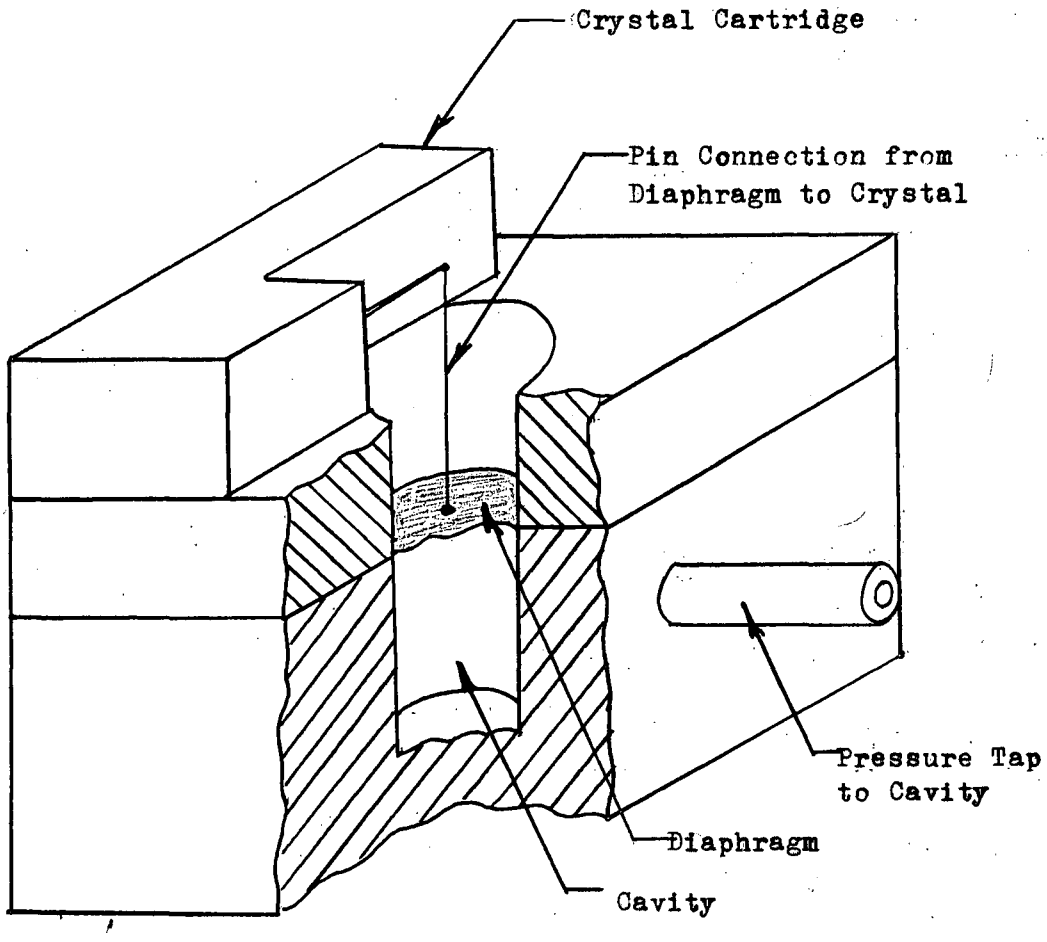

Figure 7a. Schematic

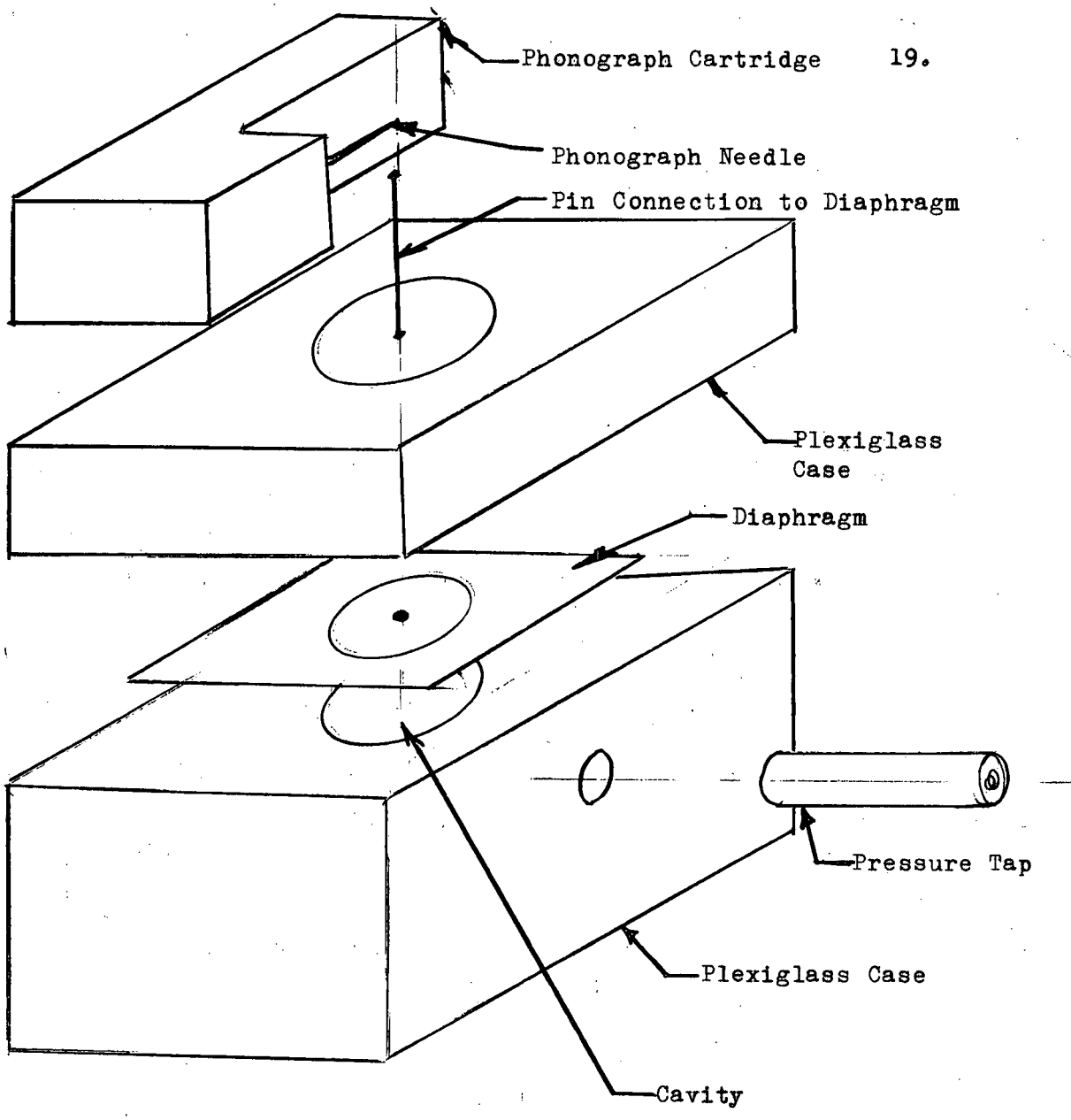

Figure 7b. Exploded View

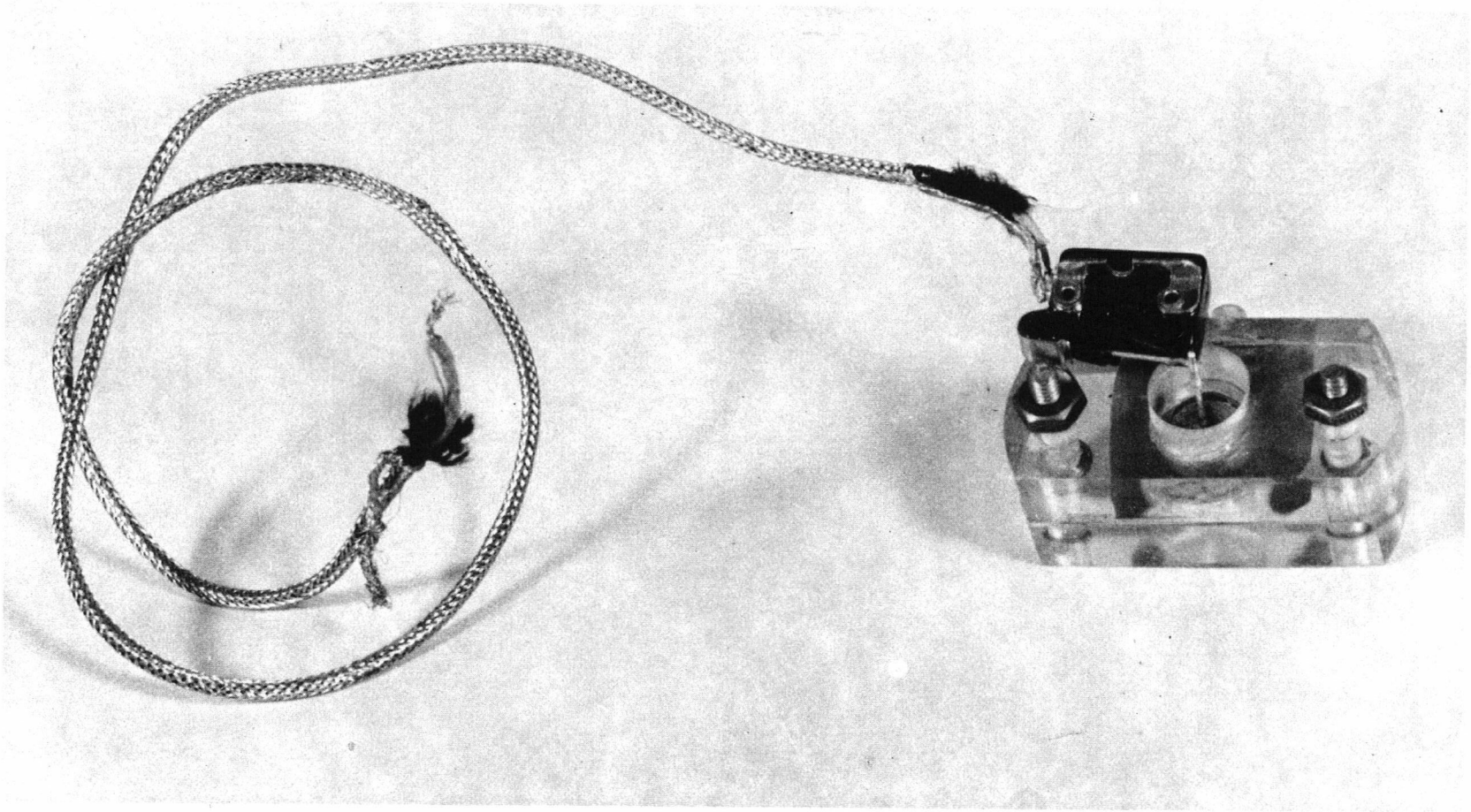

Figure 7E. Assembly

Figure 7. Pressure Transducer

transducer was almost negligible while with a large diameter tubing (1/8 inch inside diameter) the transducer response was observed to be turbulent. The tube size of 0.07 inch inside diameter showed no loss in the sensitivity and hence was used in the experiment. To study the effect of length of the tubing on phase shift, the fluctuating pressure at a point on a model was transmitted to two identical pressure transducers, one located within the model and the other located at the end of 30 inches of 0.07 inch diameter tube. No measureable phase lag was observed in the frequency range of 10 cycles per second to 70 cycles per second (Figure 8). This made it possible to locate the pressure transducers outside the tunnel thus eliminating inertia effects which would be present if the transducer were located inside the model.

To establish the technique of construction giving transducers of identical performance three units were constructed and calibrated although only one of them was used. The arrangement was made to connect the pressure taps separately. This was accomplished by allowing the pressure tubes to hang freely from the bottom of the model and to be individually connected to an acoustically dead chamber designed to eliminate the interference from external noise.

The acoustically dead chamber was constructed from 3/4 inch plywood lined with 1 inch thick foam rubber. The chamber was then placed on a 1 inch foam rubber pad to eliminate mechanical vibrations transmitted through the floor. The acoustically dead chamber with transducer in place is shown in Figure 9.

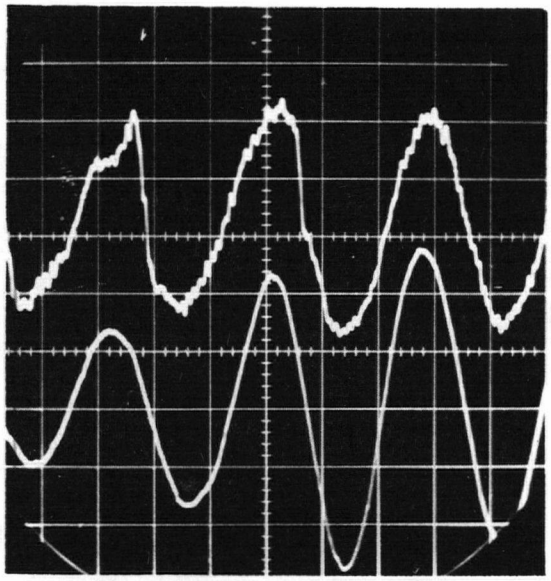

Figure 8. Effect of Tube Length on Phase,
67 cycles per second

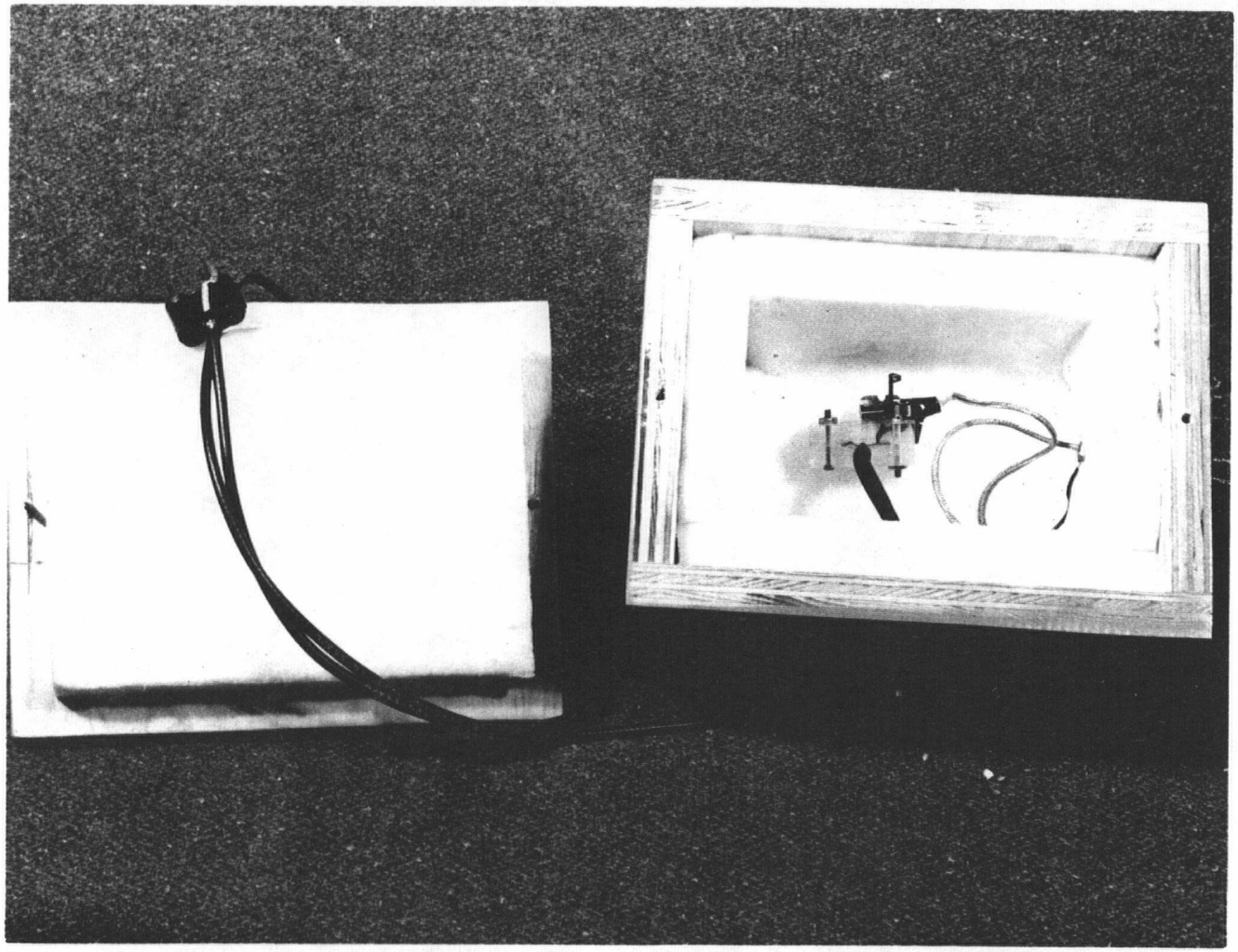

Figure 9. Pressure Transducer as Located in Acoustically Dead Chamber

3.4.1 Calibration of Pressure Transducer

Calibration of the pressure transducer was carried out in two different ways. In the first arrangement the calibration was attempted using a fluctuating pressure source consisting of a fixed cylinder with a reciprocating piston. The piston was driven through an eccentric whose speed and eccentricity could be varied so as to provide pressure fluctuations of varied amplitude and frequency. Two pressure taps were taken from the top dead centre of the cylinder with one connected to a sound level meter and the other to the pressure transducer. The arrangement was found to have some inherent limitations.

(i) The apparatus was rather crude and would require considerable improvement before it could be used for refined calibration.

(ii) Mechanical nature of the device introduced considerable noise thus distorting the signal.

(iii) With the available driving unit it was not possible to attain frequencies beyond 30 cycles per second, while it was necessary to obtain a calibration curve up to 100 cycles per second.

Although the magnitudes of the pressures obtained from the mechanical oscillating pressure source were found to be inaccurate as compared to that predicted by the theory or measured by the Sound Level Meter, it was observed that the output of the crystal transducer was linear in the frequency range of 0 to 25 cycles per second. This information

proved to be helpful in later calibration.

The second arrangement made use of a University ID-60 horn driver in conjunction with a General Radio 1551 sound level meter as shown in Figure 10. The horn driver produced the oscillating pressure inside the calibration box, constructed of mild steel, which was sensed by the microphone of the sound level meter and by the crystal transducer. The frequency of pressure oscillations was controlled by a Hewlett - Packard 202 A low frequency generator and amplified by a Bogen 60 watt Amplifier.

The calibrations were conducted by holding a constant pressure level at varying frequency. This was made possible by keeping the Db sound level, as detected by the sound level meter, at a constant value and varying the frequency of the generator. From the data obtained curves representing variation of output with frequency were plotted as shown in Figure 11. From these plots it was straight forward to obtain the relation between pressure and voltage output of the transducer for a given frequency. It was possible to relate the Db readings of the sound level meter to pressures in pounds per square inch by the fact that the Dbs are defined as a function of pressure ratios with a reference pressure of 0.0002 microbars. The plots of pressure versus voltage output were found to be linear (Figure 12).

Due to the limitations imposed by the amplifier and horn driver the minimum frequency obtainable was 15 cycles per second. It thus remained to calibrate the transducer in the low range of 0 to 15 cycles per second. This was achieved by extrapolation

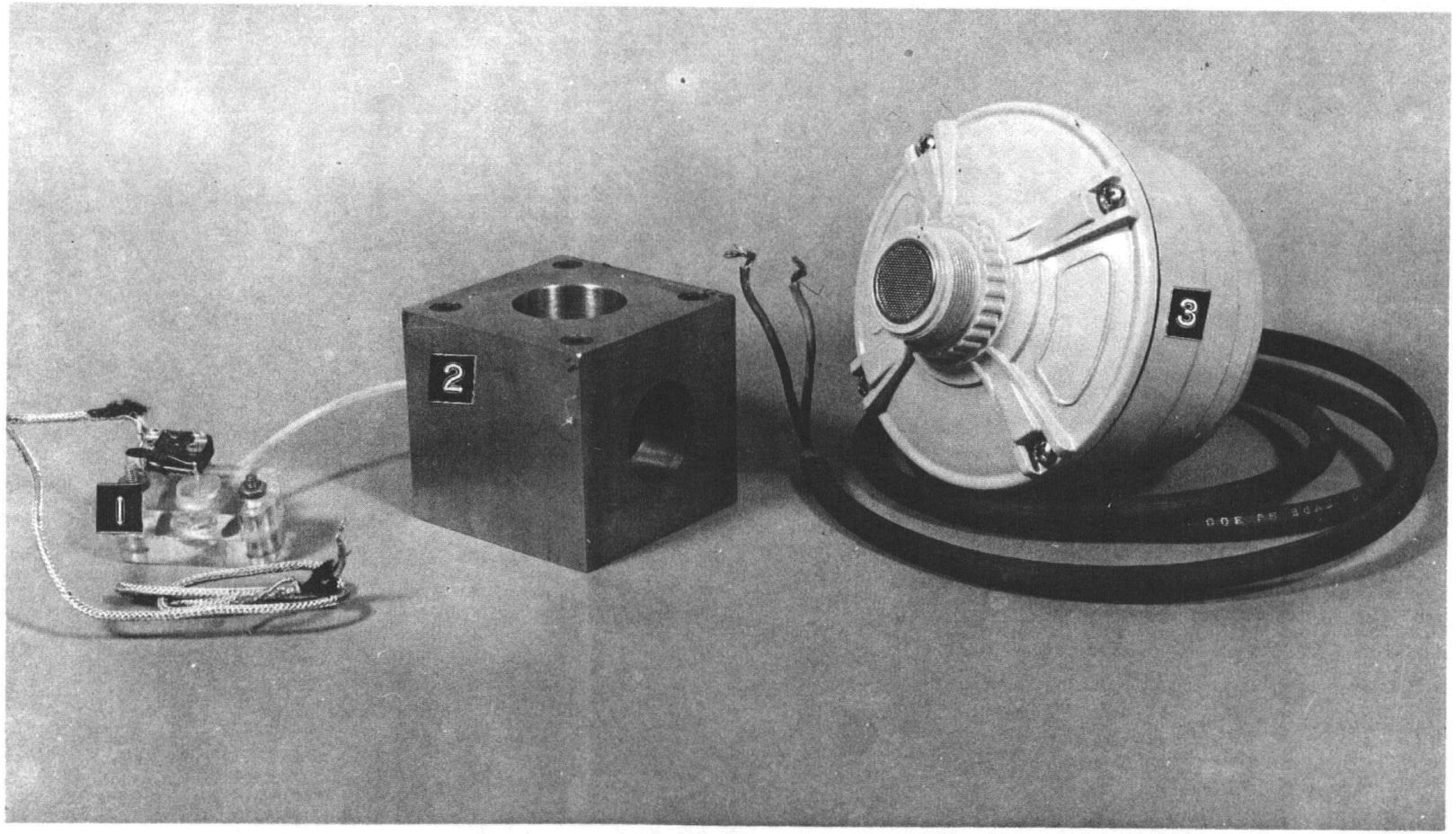

Figure 10a. Details 1. Pressure Transducer 2. Calibration Box 3. Horn Driver

Figure 10b. Assembly 1. Bogen Amplifier 2. Sound Level Meter 3. Horn Driver 4. Calibration Box 5. Acoustically Dead Chamber

Figure 10. Calibration Setup

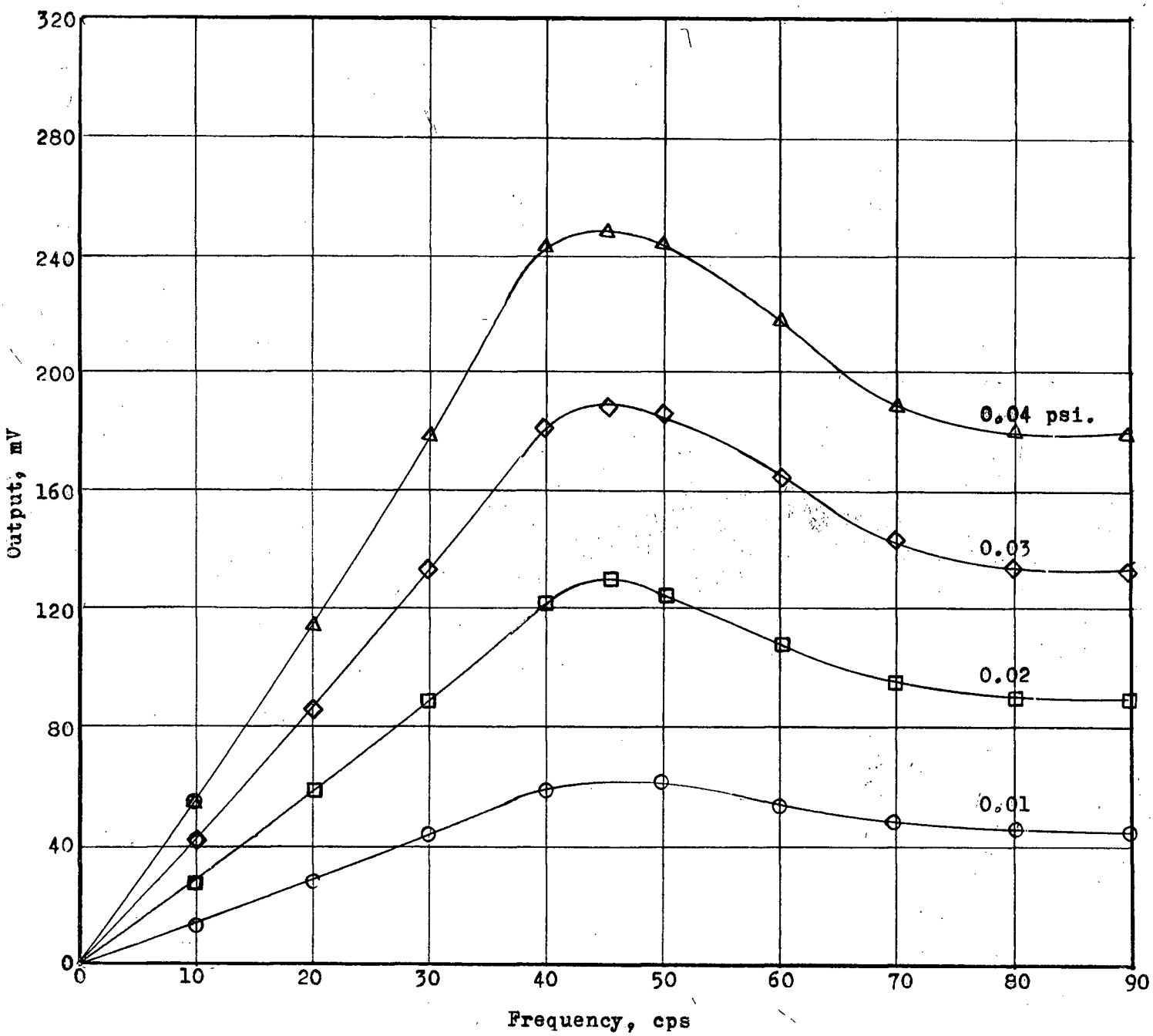

Figure 11. Calibration Curve: Variation of Output with Frequency

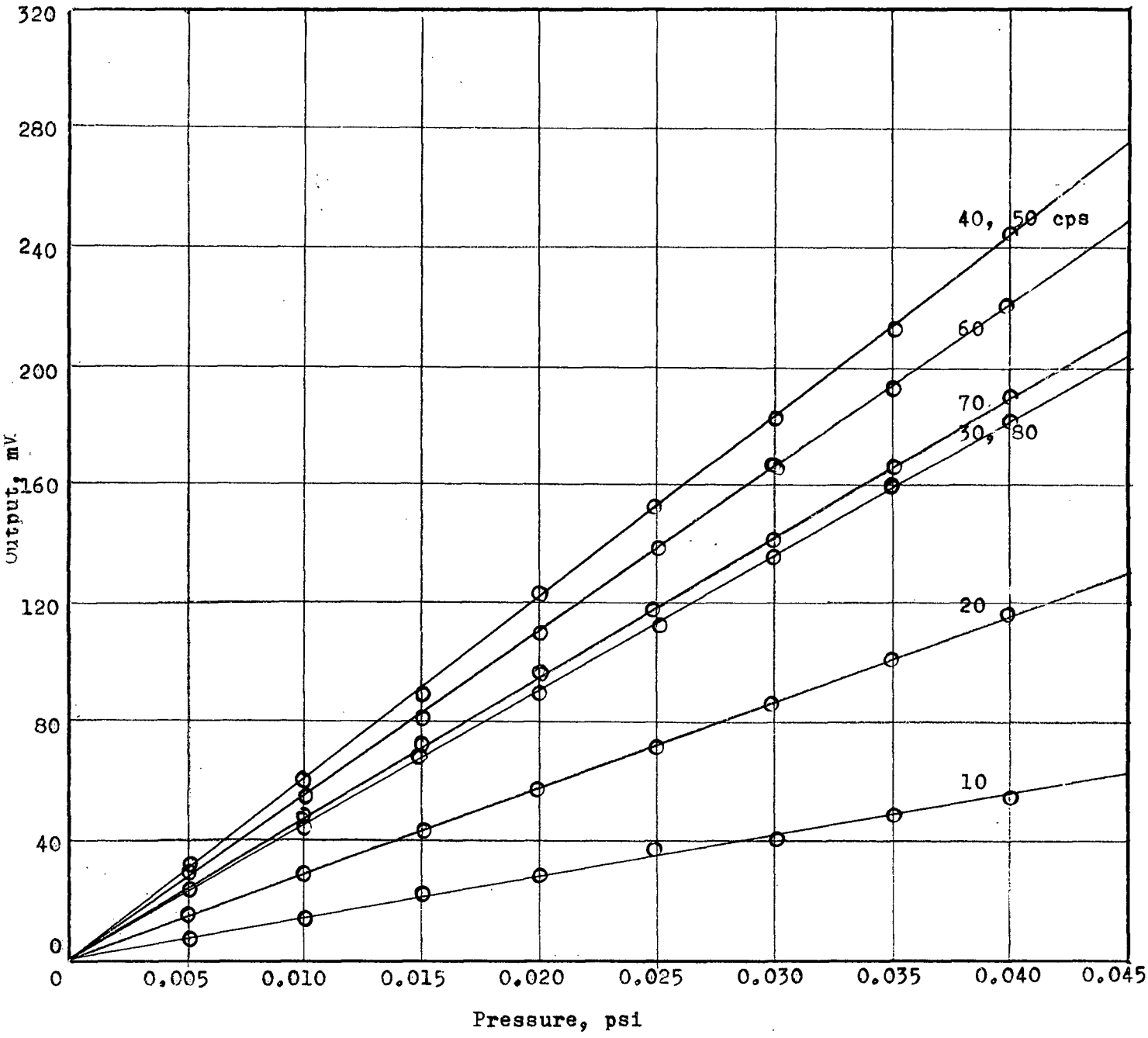

Figure 12. Calibration Curve: Variation of Output with Pressure

based on the fact that the variation of voltage output with frequency was found to be linear in the range of interest in both of the calibration procedures.

The calibration was checked by comparing the pressure fluctuations on the surface of a stationary circular cylinder registered by the pressure transducer with those obtained by McGregor (11). The comparison between the two sets of results is presented in Figure 41.

3.5 Wake Survey Equipment

Preliminary surveys of the wake behind a circular cylinder, carried out with hot wire anemometer equipment, gave the impression that it would be rather difficult to locate, precisely, the shed vortices. The fundamental signal was completely camouflaged by the random background noise which was difficult to suppress with the available equipment. An attempt to eliminate the background noise was made with the use of an integration oscilloscope, but it was found that the random voltages superimposed on the fundamental signal triggered the sweep at different points in the fundamental cycle each time so no build-up occurred. Thus the integration oscilloscope could not properly detect the fundamental signal.

The Karman vortex street causes velocity fluctuations and accompanying these are pressure fluctuations. As the transducer was designed to measure fluctuating pressure, a possibility existed that it might serve as a wake survey instrument.

A simple experiment showed that a pressure transducer placed in a stationary body located in the airstream would sense the frequency of the vortices shed from that body. It was surprising to note that the output from the crystal transducer gave a more clearly defined indication of the fundamental shedding frequency than the output from the hot wire anemometer. Proof that the frequency was that of the shed vortices was obtained by comparison of the Strouhal number as determined from the frequency recorded by the transducer to the Strouhal numbers over a given range of Reynolds number for a circular cylinder as given by Fung (18). Thus the pressure transducer designed to measure the acoustic level pressure variations can be used to determine the frequency of the shedding vortices behind test bodies.

Further experimentation revealed that a pressure tap placed at the tip of a slender probe when used in conjunction with the pressure transducer could be used effectively as a wake survey device (Figure 13). A 36 inch length of tubing was used to transmit the pressure fluctuations at the probe tip to the transducer. Using the probe and the transducer in this manner gave by movement of the probe in the wake an indication of the vortex locations. The output signal from the pressure transducer with the probe in the wake was much clearer than the corresponding signal from hot wire anemometer equipment. Experimentation with the probe in the wake of a circular cylinder yielded a value of 0.29 for the ratio of lateral to longitudinal spacing between the adjacent vortices which is little higher than the theoretically established value of 0.281.

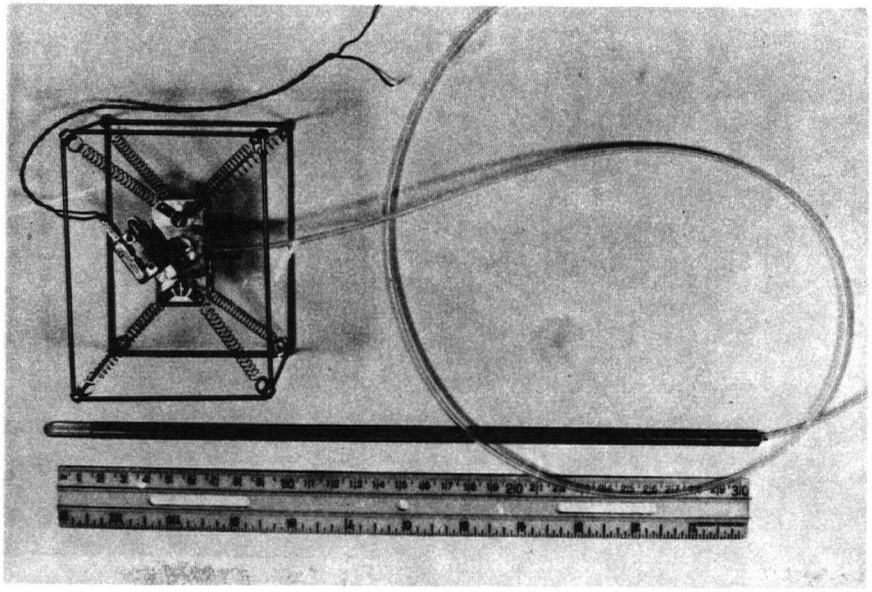

Figure 13. Wake Survey Probe

3.6 Bending and Torsional Displacement Transducers

The lateral displacement transducer was an inductive coil type developed by Smith (15). Two coils were used, one as the primary and the other as the secondary. They were concentrically mounted so as to provide an annular region through which the lateral shaft could pass. A signal of 20,000 cycles per second was fed in to the primary coil which was sensed by the secondary coil through inductance. The amplitude of the signal received by the secondary coil was dependent on the number of primary turns cut off by the lateral shaft, i.e. on the plunging displacement of the model.

The output from the secondary coil was an amplitude modulated signal. By filtering the carrier frequency; i.e. the 20,000 cps signal fed to the primary, an exact time-history of the lateral displacement was obtained.

The torsional displacement was measured by sensing strain in one of the torsional cantilever springs used to provide torsional stiffness to the model. The strain gages were mounted at the root of the cantilever spring and the signal was fed through an Ellis Bam-1 strain gage bridge amplifier. Both lateral and torsional displacement outputs were fed into a Tektronix 502A oscilloscope.

3.6.1 Calibration of Displacement Transducers

The lateral displacement transducer was calibrated by

displacing the aluminum lateral support shaft in the annular region of the transducer in equal increments and noting the output. This calibration showed the lateral transducer to be linear within 1% (Figure 14).

The torsional displacement transducer was calibrated by displacing the end of the cantilever spring in equal increments and noting the output. The tolerances of linearity were found to be comparable to those of the lateral displacement transducer (Figure 15).

3.7 Electromagnetic Damping

The damping, in addition to inherent damping with the system, was introduced by means of electromagnetic eddy current dampers. The dampers created a magnetic field to which the aluminum shaft carrying the model was exposed. Eddy currents induced in the shaft dissipated energy from the oscillating system.

The damping was found to be almost viscous. For higher currents the damping was still as close to viscous as it was for lower currents. Damping levels were controlled by the amount of D. C. current passing through the electromagnet. The calibration curve is shown in Figure 16.

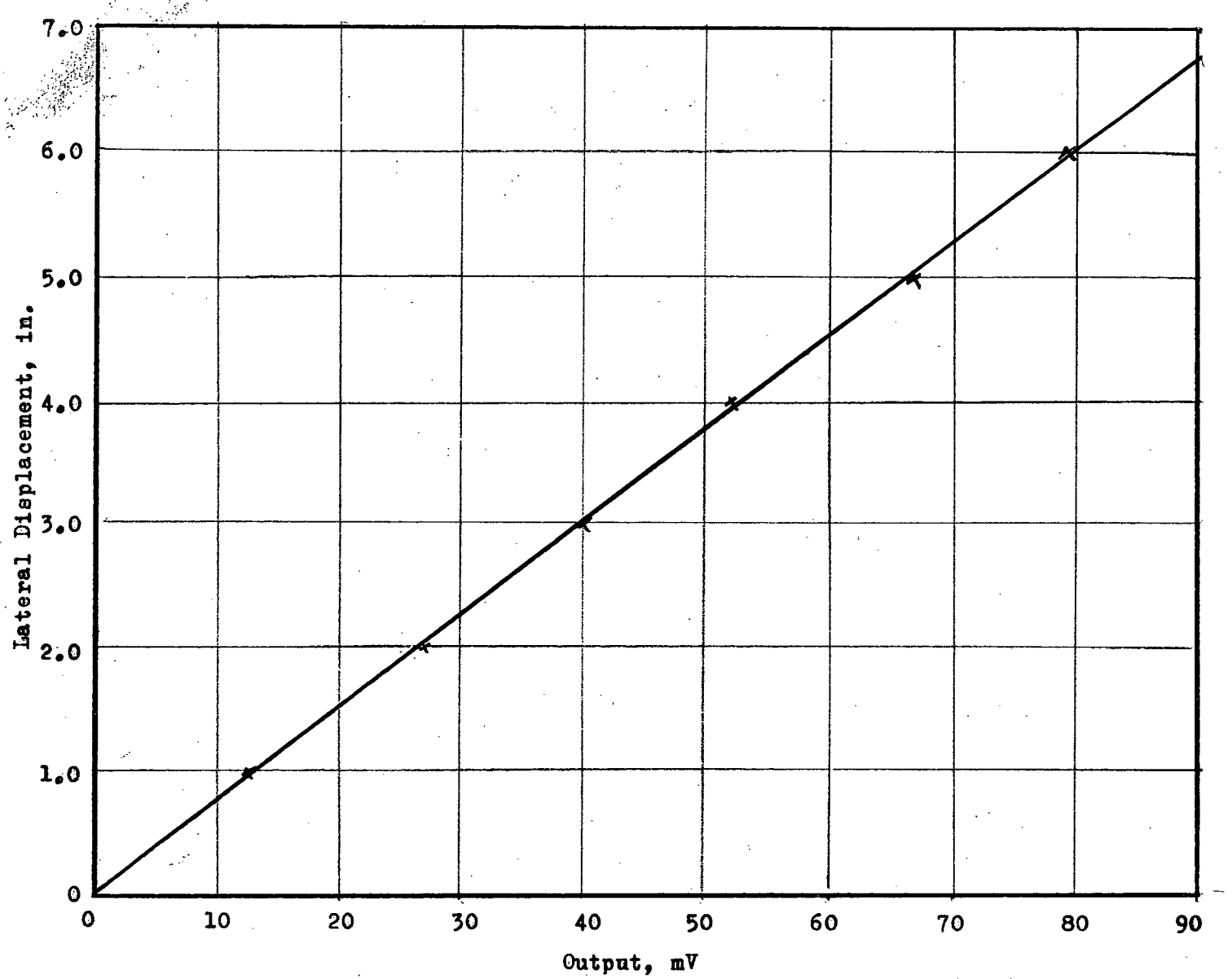

Figure 14. Calibration Curve: Lateral Displacement Transducer

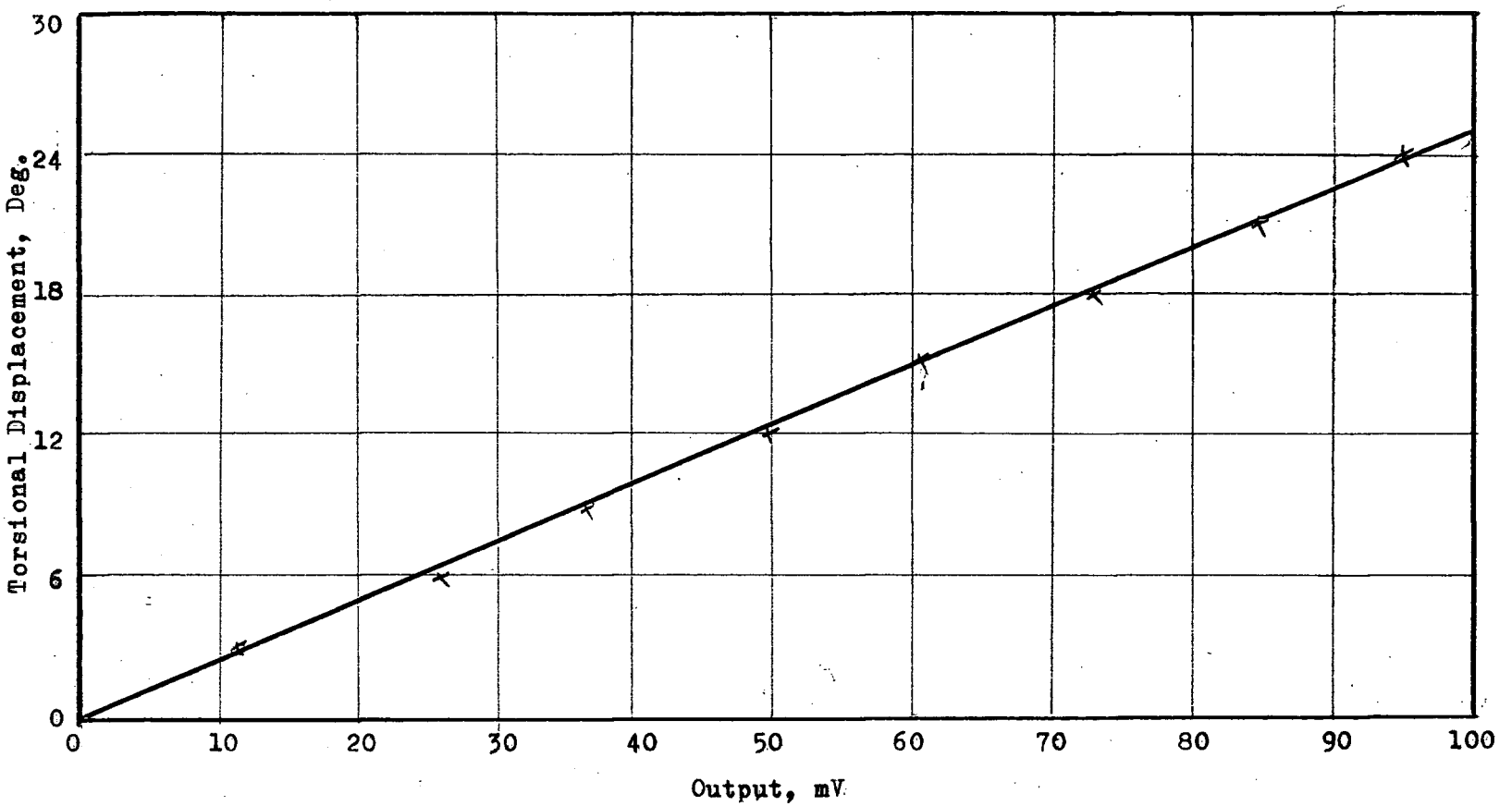

Figure 15. Calibration Curve: Torsional Displacement Transducer

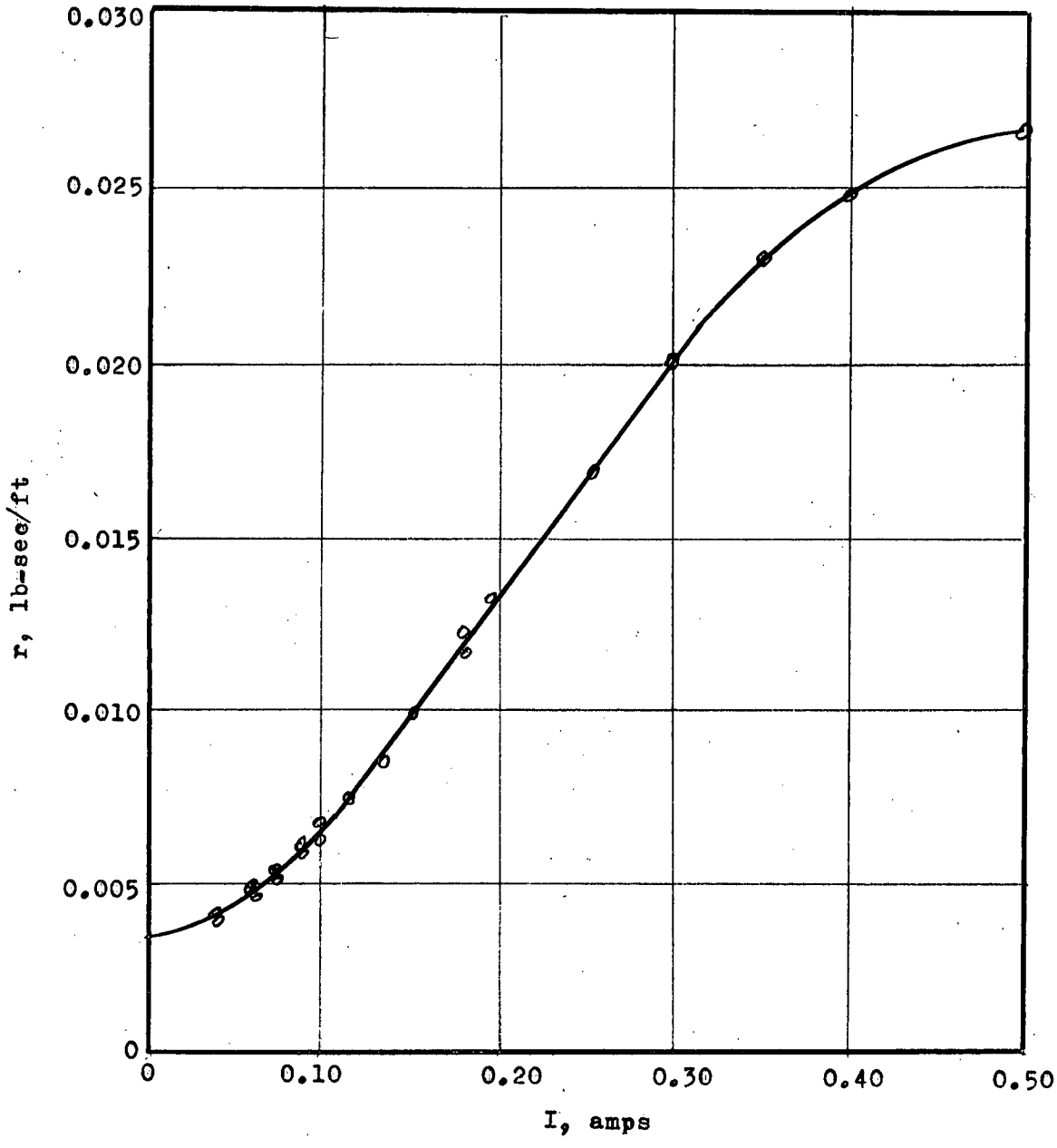

Figure 16. Calibration Curve: Electromagnetic Damper

3.8 Experimental Test Procedures

3.8.1 Static and Oscillating Pressure Measurements

Measurements of static and oscillating Pressures were made separately for each individual pressure tap. The tubings from the taps were connected individually first to a Lambrecht manometer for static pressure measurements and second to the pressure transducer for oscillating pressure measurements.

The transducer output was fed directly to the Tektronix 502A oscilloscope. The grid inscribed onthe oscilloscope screen made it possible to read with the accuracy of less than 1% full scale. All readings of pressure fluctuations were made peak to peak and in the case of amplitude modulated signals the maximum amplitude only was recorded and taken to be the maximum pressure fluctuation at that point. The readings from the oscilloscope were recorded in millivolts and conversion to pounds per square inch was made using the calibration curves. The frequency of pressure oscillations was noted during each test as output of the pressure transducer was a function of frequency. The experimental test setup is shown in Figure 17.

Pressure measurements were made with all the models initially stationary. The square, rectangular, elliptical cylinders and wing were tested at various angles of attack and the variation of static and fluctuating pressure distribution was noted. These measurements with stationary models were carried out as several values of Reynolds number.

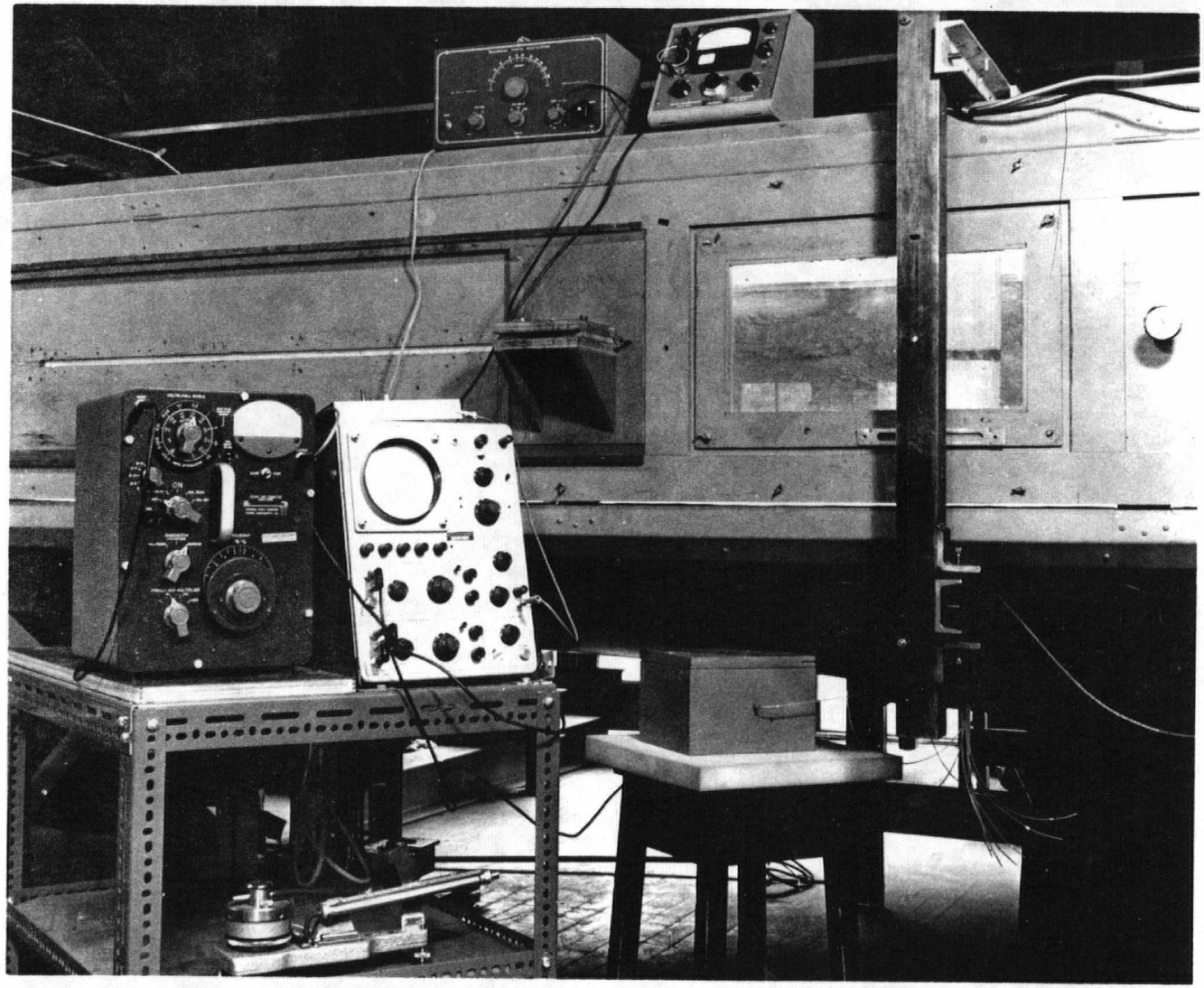

Figure 17. Equipment and Test Section

Once the models were tested when stationary, air was supplied to the bearings, and tunnel speed was varied until the model executed self excited oscillations. The effect of motion on the oscillating pressure distribution was noted.

The oscillating pressures as well as the model oscillations were recorded photographically.

3.8.2 Amplitude Measurements

The individual model was made free to oscillate by supplying air to the lateral and torsional air bearings which permitted two degrees of freedom. Once the body was in motion, the nature of oscillations was observed on the oscilloscope. Since the oscilloscope was of the dual beam type it was possible to display and photograph the two degrees of freedom of motion simultaneously. It was also possible to observe the effect of torsional and lateral displacements on the oscillating pressure distribution by the dual beam feature.

3.8.3 Wake Measurements

The probe connected to the pressure transducer was placed in the wake of each body and slightly to one side. The pressure fluctuations produced by the wake were displayed on the screen of the oscilloscope along with those produced at a point on the surface of the model. The probe, located on the same side of the model as the point, was then moved from the vicinity of the body down stream until the two signals were in phase.

The procedure was repeated with the probe on the opposite side. Twice the difference between the two readings gave the vortex spacing in the flow direction. It was found that this measurement could be made with a fair degree of accuracy. For example, Figure 35 shows two such traces in phase, the upper trace being the pressure oscillations at the surface of the body (tap 1) and the lower trace the oscillations at the probe tip.

The probe was moved across the wake of the models to obtain the spacing in the direction perpendicular to the airstream. The measurements were made by noting the distance between the maximum fluctuations to either side of the wake. This measurement could be made but not with the accuracy of the longitudinal distance since the maximum fluctuations appeared over a substantial distance rather than attaining a well defined peak.

3.8.4 Strouhal Numbers

Comparison of the frequency of the pressure oscillations of the circular cylinder with published data on Strouhal frequencies showed the two frequencies to be identical. The trace obtained by the pressure transducer sensing the oscillating pressures at the surface of the model displayed the frequency of vortex shedding in a more defined manner than was obtainable with hot wire anemometer equipment. All Strouhal frequency measurements were therefore made from the fluctuating pressure trace at the surface of the model.

Strouhal frequencies were recorded at various Reynolds numbers for the circular, square, rectangular and elliptic cylinder at high angles of attack (no pressure fluctuations were observed at low angles of attack in the case of the elliptic cylinder).

3.8.5 Static Lift Coefficient Versus Angle of Attack

Circular Cylinder and NACA 4412 Section Wing

Pressure distributions and static lift coefficients on the circular cylinder and NACA 4412 airfoil are well established and it was not necessary to measure them during this experiment.

Square and Rectangular Cylinders

Static lift coefficients were determined by graphical integration of the pressure distributions about the model.

The lift for a square or rectangular cylinder can be obtained from the relation:

$$L' = \int_0^c (P_3 - P_1)\, dS_1 \cos\alpha + \int_0^{c_2} (P_4 - P_2)\, dS_2 \sin\alpha$$

Defining lift coefficient as:

$$C_L' = \frac{L'}{\frac{1}{2}\rho V^2 c}$$

(where c is the length of a face on the square cylinder and the length of the longest face on the rectangular cylinder) gives:

$$C_L' = \frac{L'}{\frac{1}{2}\rho V^2 c} = \int_0^1 \frac{(P_3 - P_1)}{\frac{\rho}{2} V^2}\, d\left(\frac{S_1}{c}\right) \cos\alpha + \int_0^1 \frac{(P_4 - P_2)}{\frac{\rho}{2} V^2}\, d\left(\frac{S_2}{c_2}\right) \frac{c_2}{c} \sin\alpha$$

i.e.

$$C_L' = \int_0^1 (C_{p_3} - C_{p_1})\, d\left(\frac{S_1}{c}\right) \cos\alpha + \int_0^1 (C_{p_4} - C_{p_2})\, d\left(\frac{S_2}{C_2}\right) \frac{C_2}{c} \sin\alpha$$

Here the subscripts 1, 2, 3, and 4 denote the value of the parameter at the faces as shown in Figure 18.

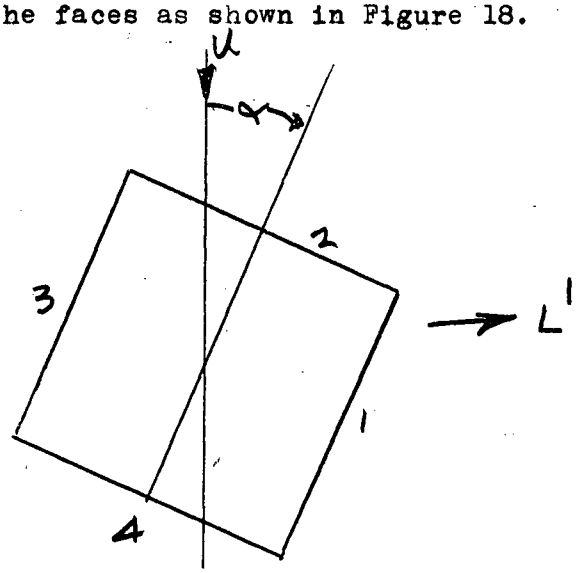

Figure 18

here

$$C_{p_n} = \frac{P_n}{\frac{\rho}{2} V^2} \qquad n = 1, 2, 3, 4$$

α - angle of attack.

<u>Elliptic Cylinder</u>

The lift for the elliptic cylinder can be obtained from the following relation:

$$dL' = P_\ell \, dS_\ell \cos\gamma_\ell - P_u \, dS_u \cos\gamma_u$$
$$= (P_\ell - P_u)\, d\pi$$

$$L' = \int_0^{c\cos\alpha} (P_l - P_u)\, dx$$

giving the lift coefficient per unit span as:

$$C_L' = \int_0^{\cos\alpha} \left[\frac{(P_l - P_\infty)}{\frac{1}{2}\rho V_\infty^2} - \frac{(P_u - P_\infty)}{\frac{1}{2}\rho V_\infty^2} \right] d\left(\frac{x}{c}\right)$$

i.e.

$$C_L' = \int_0^{\cos\alpha} (C_{p_l} - C_{p_u})\, d\left(\frac{x}{c}\right)$$

The subscripts l and u denote the lower and upper surfaces respectively of the elliptic cylinder as shown in Figure 19.

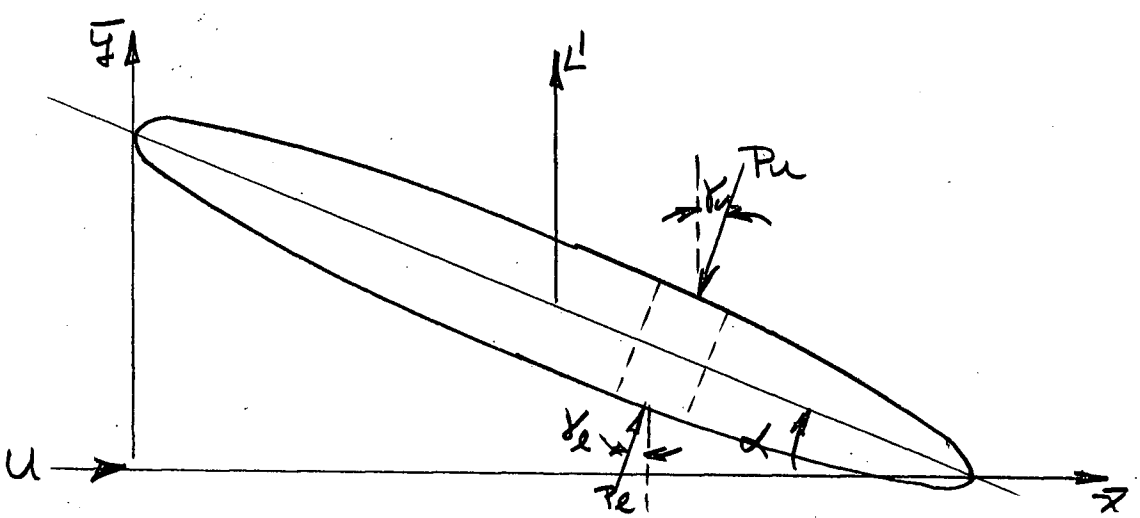

Figure 19.

3.8.6 Fluctuating Lift Coefficients

From phase difference measurements around a model under test it was observed that:

(a) all pressure fluctuations occurring on the same surface,

i.e. the lower or the upper surface, were in phase with one another

(b) pressure fluctuations on the upper surface were 180° out of phase with those on the lower surface.

The graphical integration was performed in a manner similar to the one presented before with the exception that here the oscillating pressure distribution was integrated over the top and bottom surfaces separately and the two results were added to get the total fluctuating lift coefficient.

All measurements of oscillating pressures and lift coefficients as presented here are peak to peak.

Thus:

L'_{fl} = fluctuating lift per unit span

$$= \oint P_{fl.} \cos\alpha \, ds.$$

$$C'_{L_{fl}} = \frac{L'_{fl}}{\frac{1}{2}\rho V^2 C}$$

IV. EXPERIMENTAL RESULTS

4.1.1 Stationary Square Cylinder

The square cylinder was provided with sixteen pressure taps. The pressure distribution, variation of lift coefficient with angle of attack, and variation of Strouhal number with Reynolds number showed very good agreement with the results obtained by other investigators (15), (20). The recorded results are presented in figures 20, 21 and 22. The Strouhal number was found to be constant at the approximate value of 0.12. At higher Reynolds number the results were considerably scattered yet the average value appeared to be the same. The value is slightly lower than that obtained by Brooks (20).

The fluctuating pressure distribution data were recorded for the angle of attack range of 0° - 17° 30' with Reynolds number held constant at 41,000. The results are presented in Figure 23.

The plot of $C'_{L_{fl}}$ versus angle of attack (Figure 24) shows the maximum value to be 2.4 at an angle of attack of 6° and minimum value of 1.4 at 14°. It is of interest to note that the minimum fluctuating lift coefficient occurs at the angle of attack for which the static lift coefficient is maximum.

Photographs showing pressure oscillations about the square cylinder at zero angle of attack are given in Figure 25. The traces at taps 13 and 14 are purposely reproduced with higher sensitivity (X10, X 2 the normal sensitivity respectively). The

pressure fluctuations are nearly sinusoidal except at the rear of the cylinder. At tap 4 a high frequency signal seems to be superimposed on the fundamental signal while tap 5 shows marked influence of the second harmonic. Decreasing the sweep time of the oscilloscope displayed the amplitude modulation of the pressure oscillations (Figure 26).

The phase study of the oscillating pressure showed that all pressure fluctuations on the same side of the model were in phase while those on the opposite side were 180° out of phase thus indicating that the breaking of a vortex from one side of the model instantaneously affects the pressure distribution on that side.

The wake geometry was also investigated, making use of the designed pressure transducer in the manner explained earlier (section 3.8.3). The longitudinal spacing (h) was found to be 12.13 inches while the lateral spacing (a) was 5.75 inches thus giving an a/h ratio of 0.474.

4.1.2 Oscillating Square Cylinder

The wind velocity was now increased until the model exhibited self excited oscillations. The variation in amplitude of oscillation with velocity leading to two stable limit cycles as reported by Smith (15) was observed. Figure 27 shows plunging oscillations of the model at a wind velocity of 60 feet per second (larger limit cycle).

The comparison of pressure fluctuations at all taps with the square cylinder stationary or oscillating revealed that they were identical. The representative photographs comparing the pressure fluctuations at tap 15 with model stationary and oscillating are shown in Figure 26 and Figure 28.

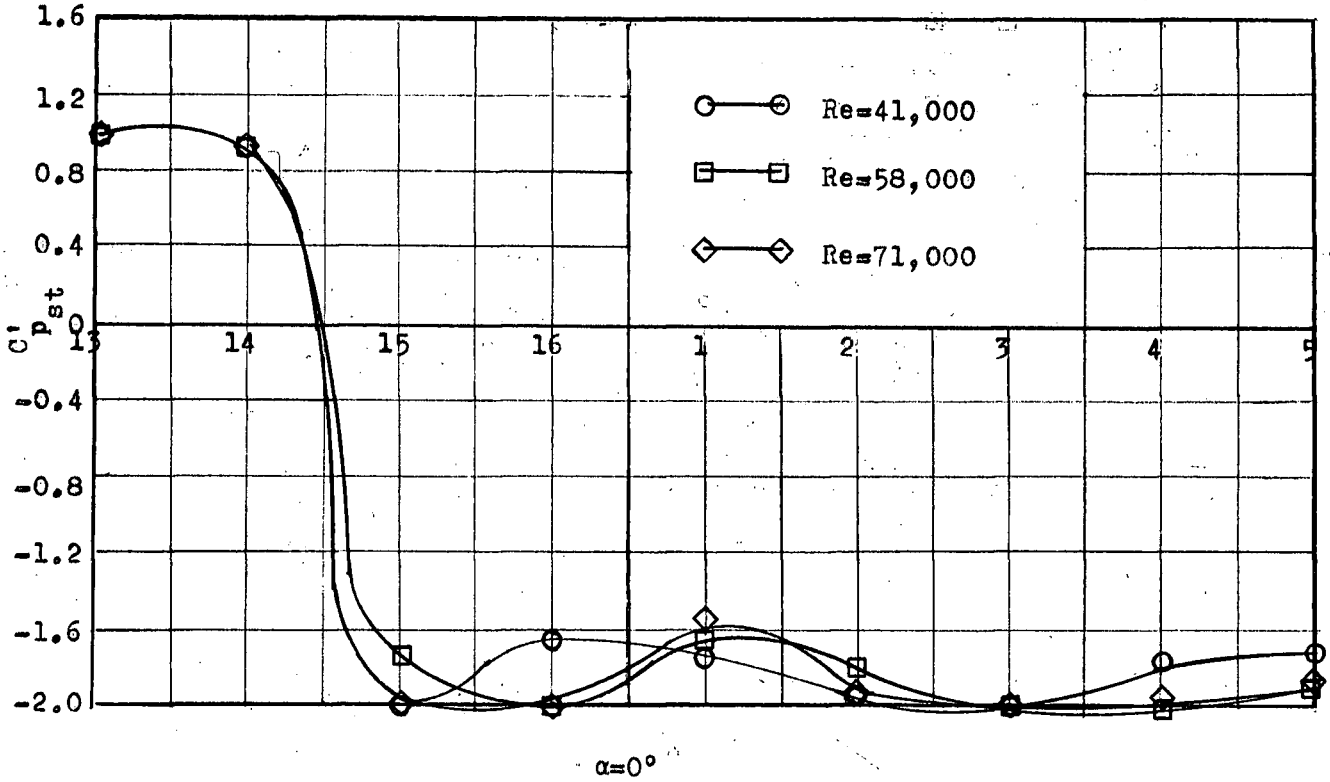

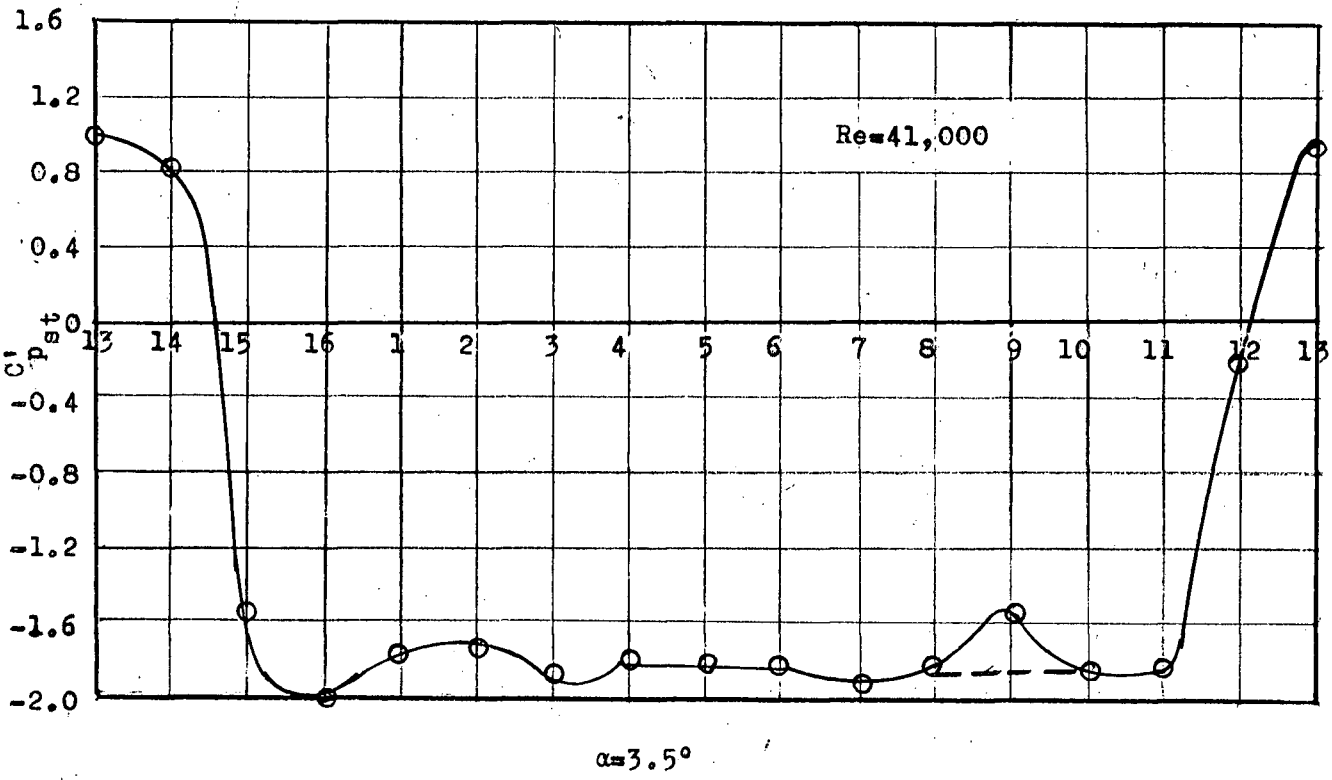

Figure 20. Variation of Static Pressure Distribution With α: Square Cylinder

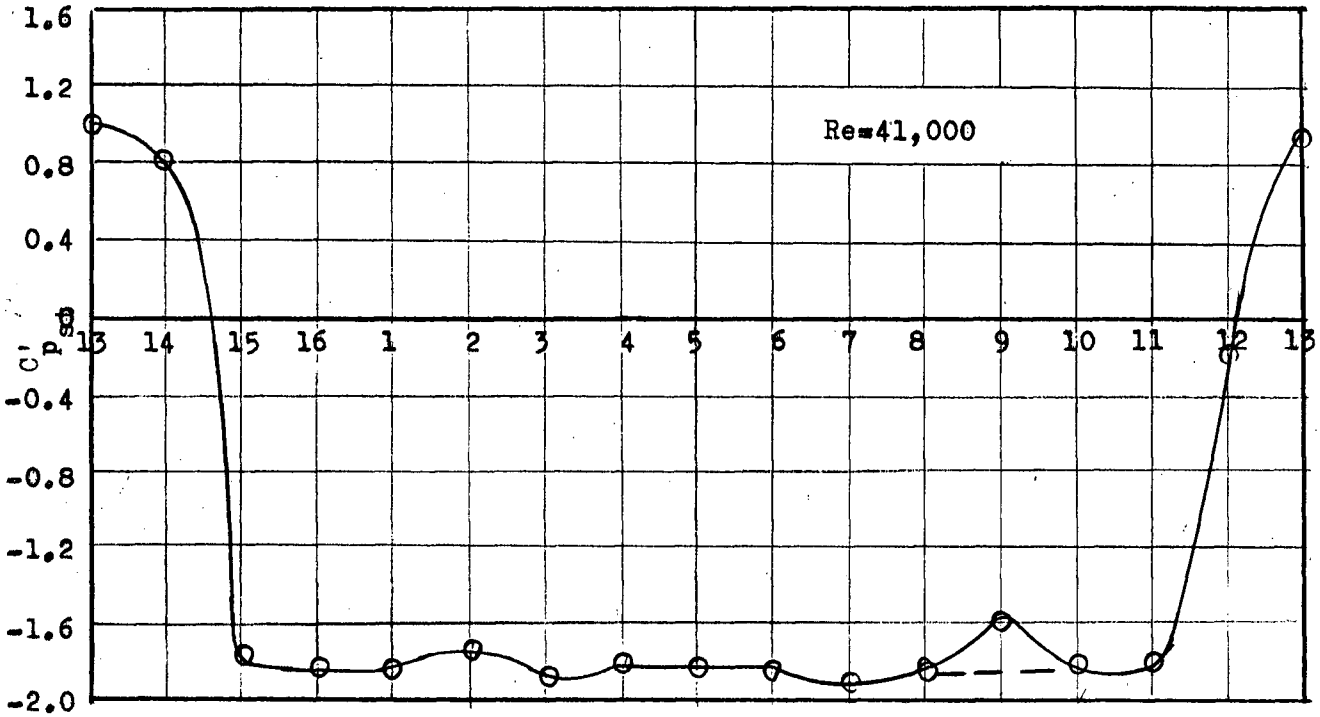

α=7°

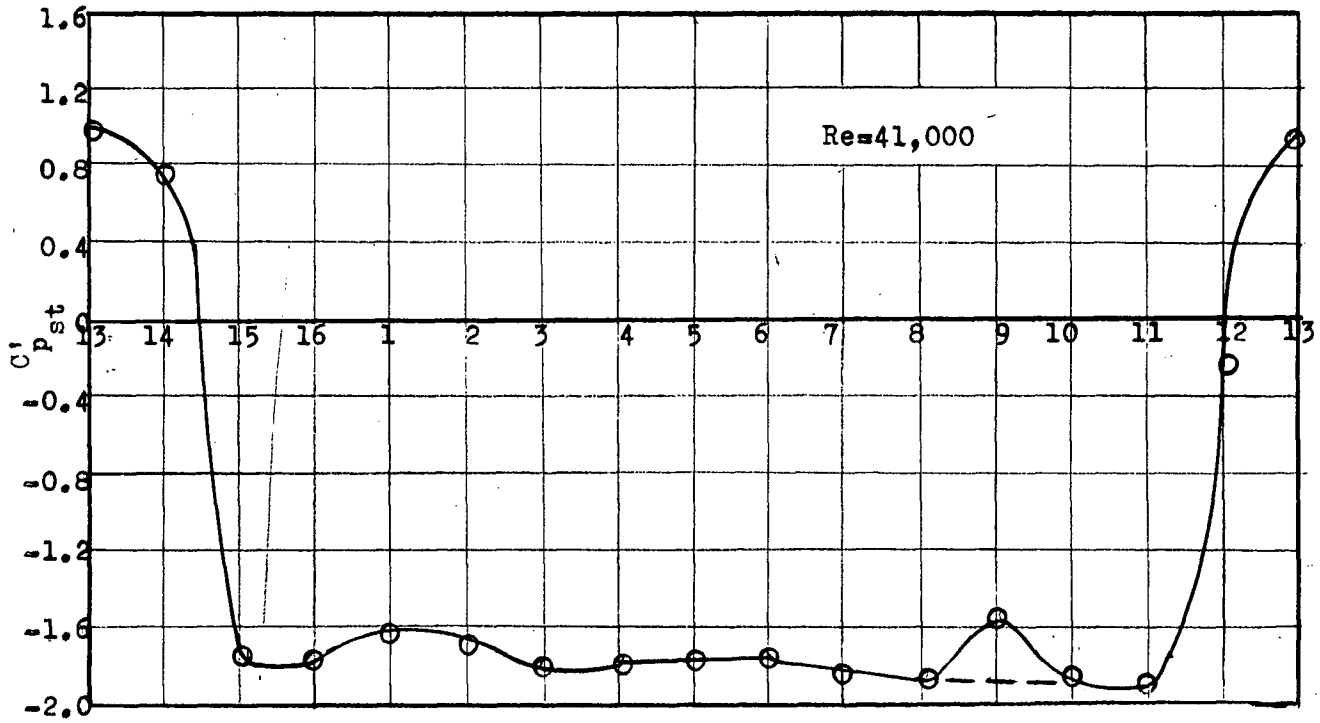

α=10.5°

Figure 20 (cont'd). Variation of Static Pressure Distribution with α: Square Cylinder

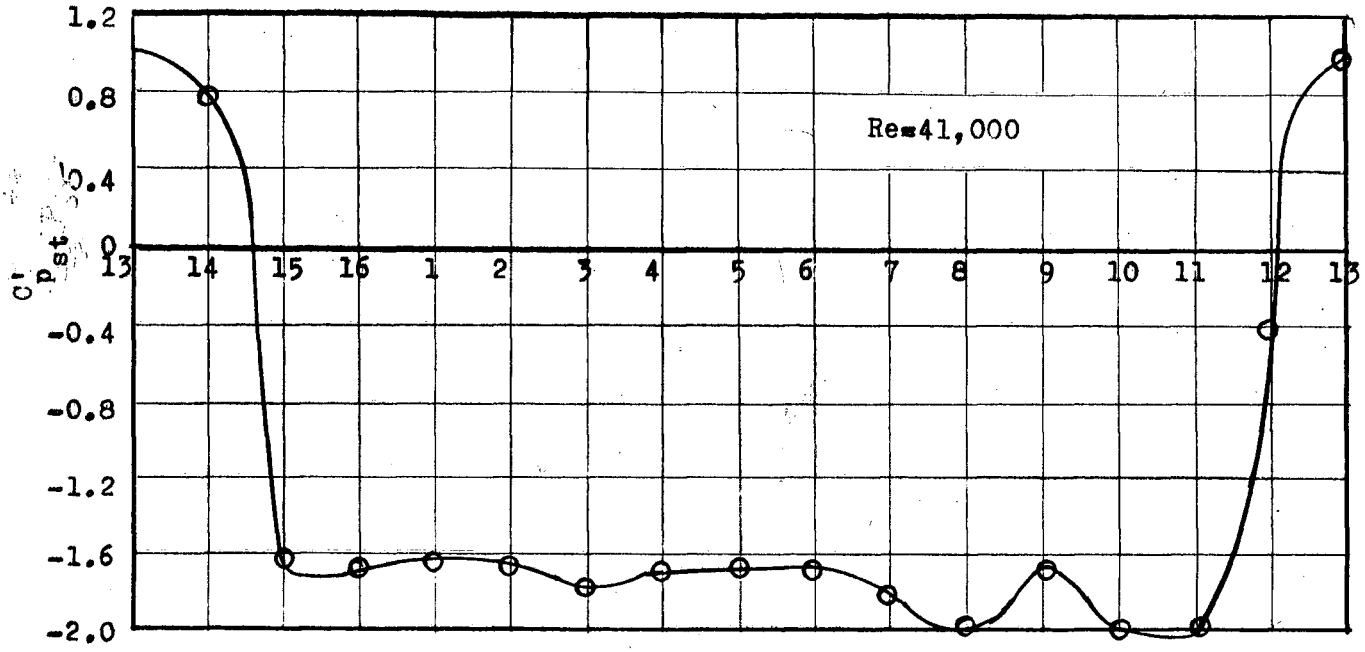

α=14°

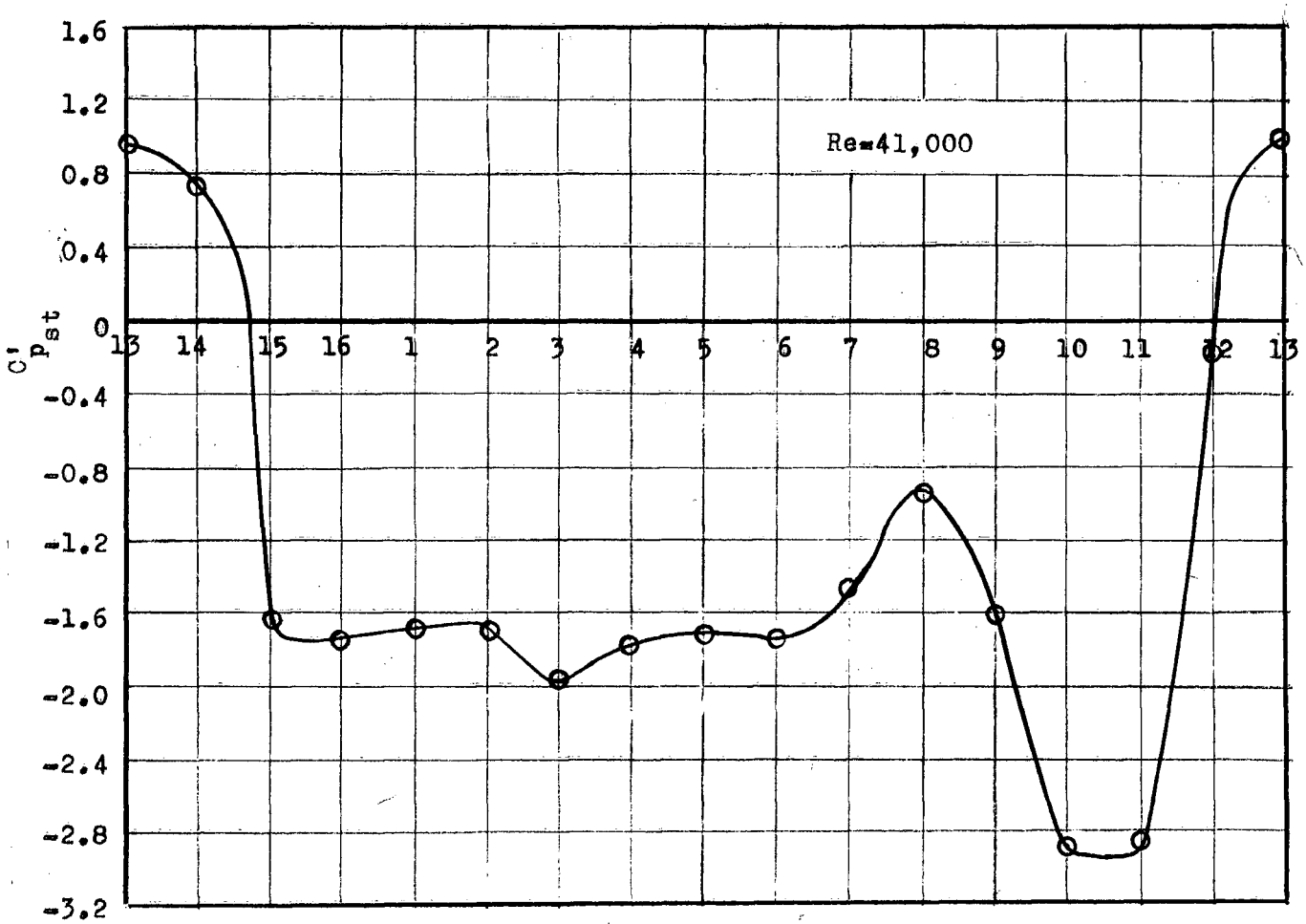

α=17.5°

Figure 20 (cont'd). Variation of Static Pressure Distribution with α: Square Cylinder

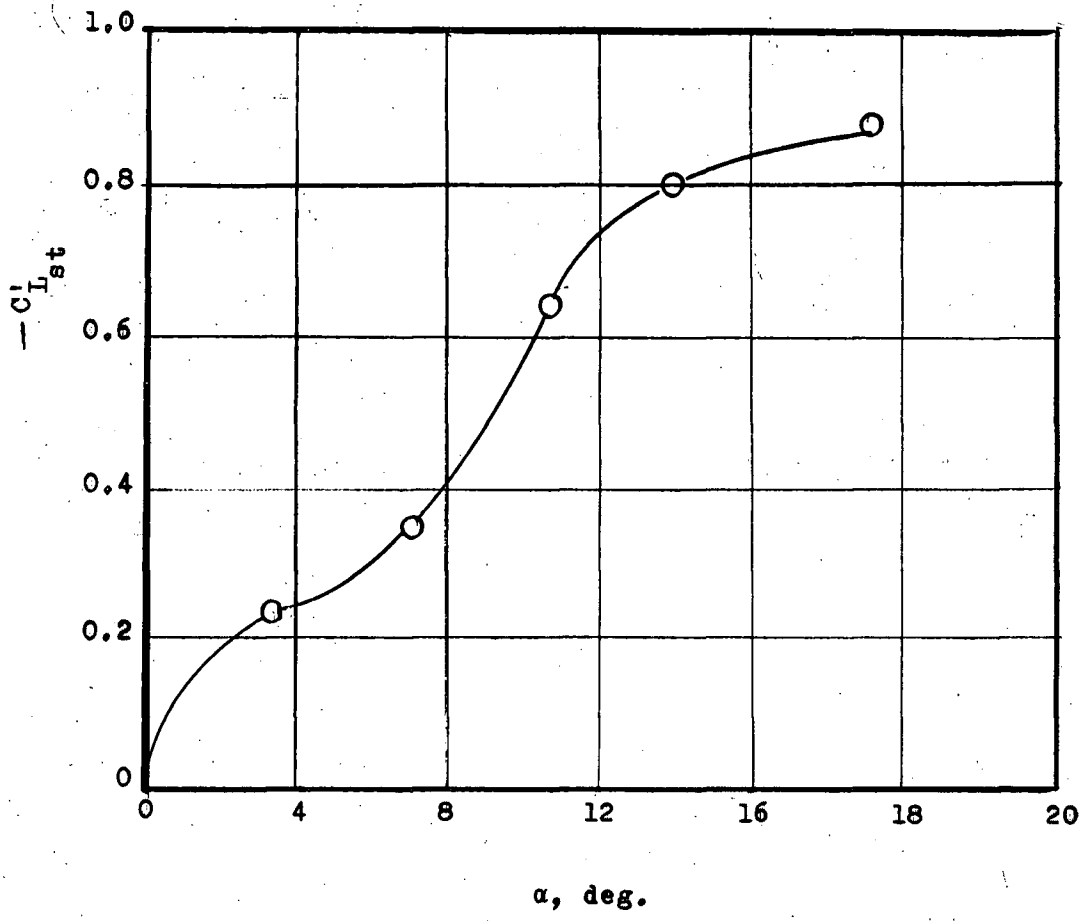

Figure 21. Variation of Static Lift Coefficient with α: Square Cylinder

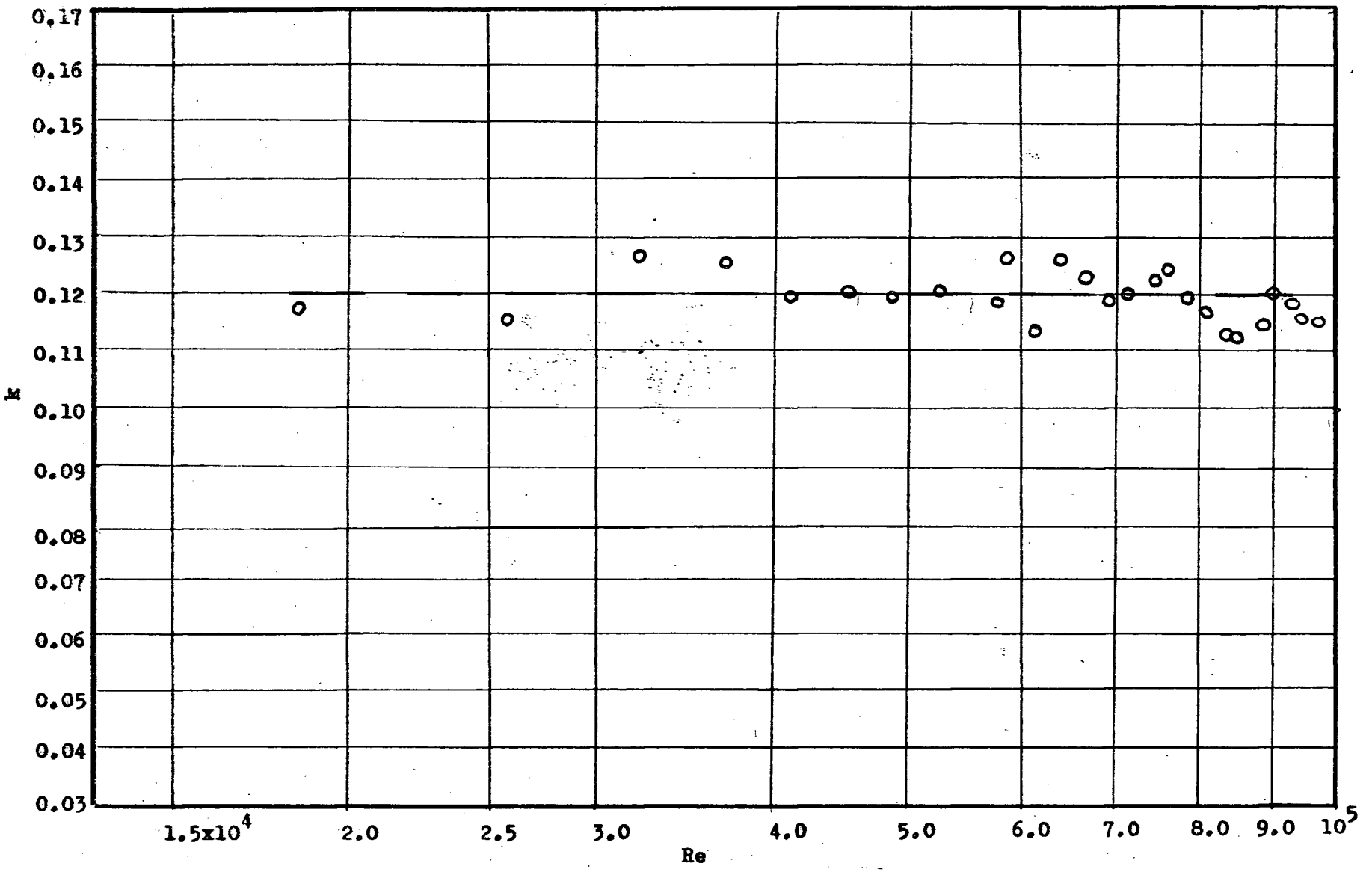

Figure 22. Variation of Strouhal Number with Reynolds Number for Square Cylinder

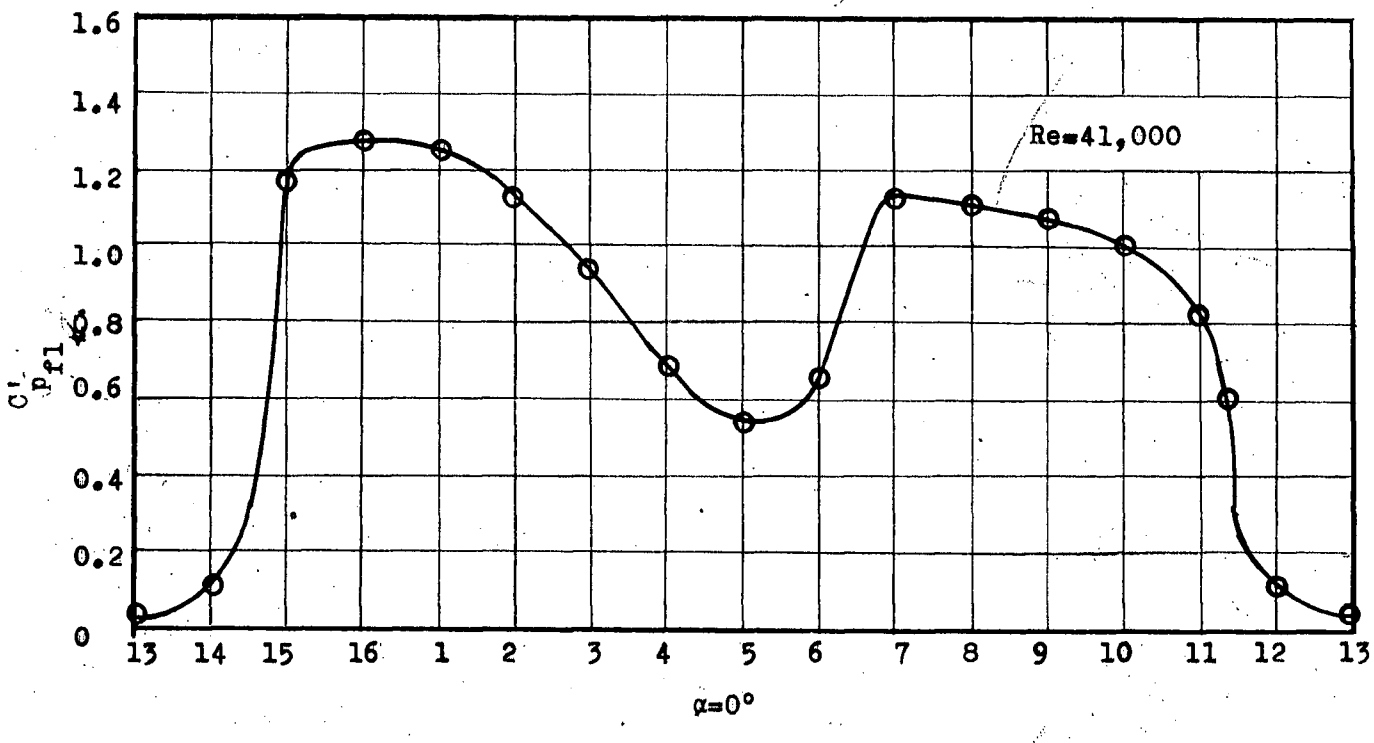

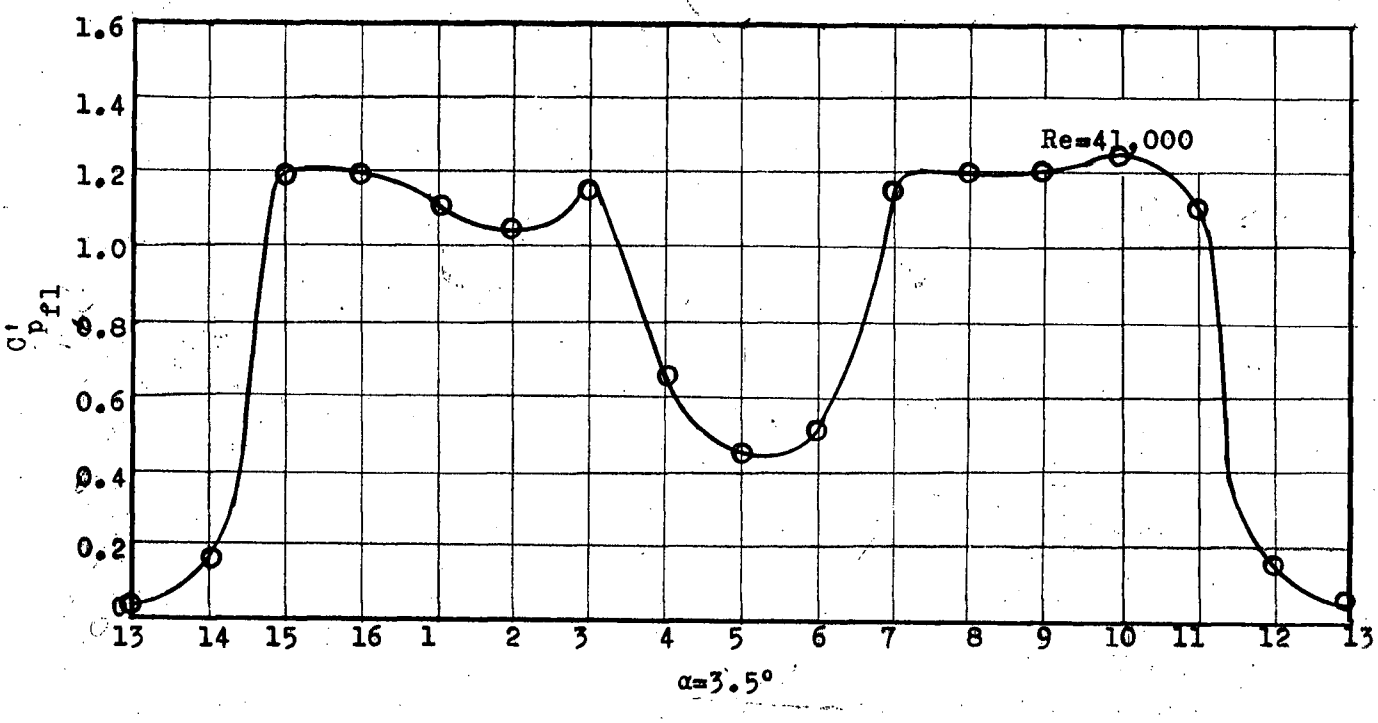

Figure 23. Variation of Fluctuating Pressure Distribution with α: Square Cylinder

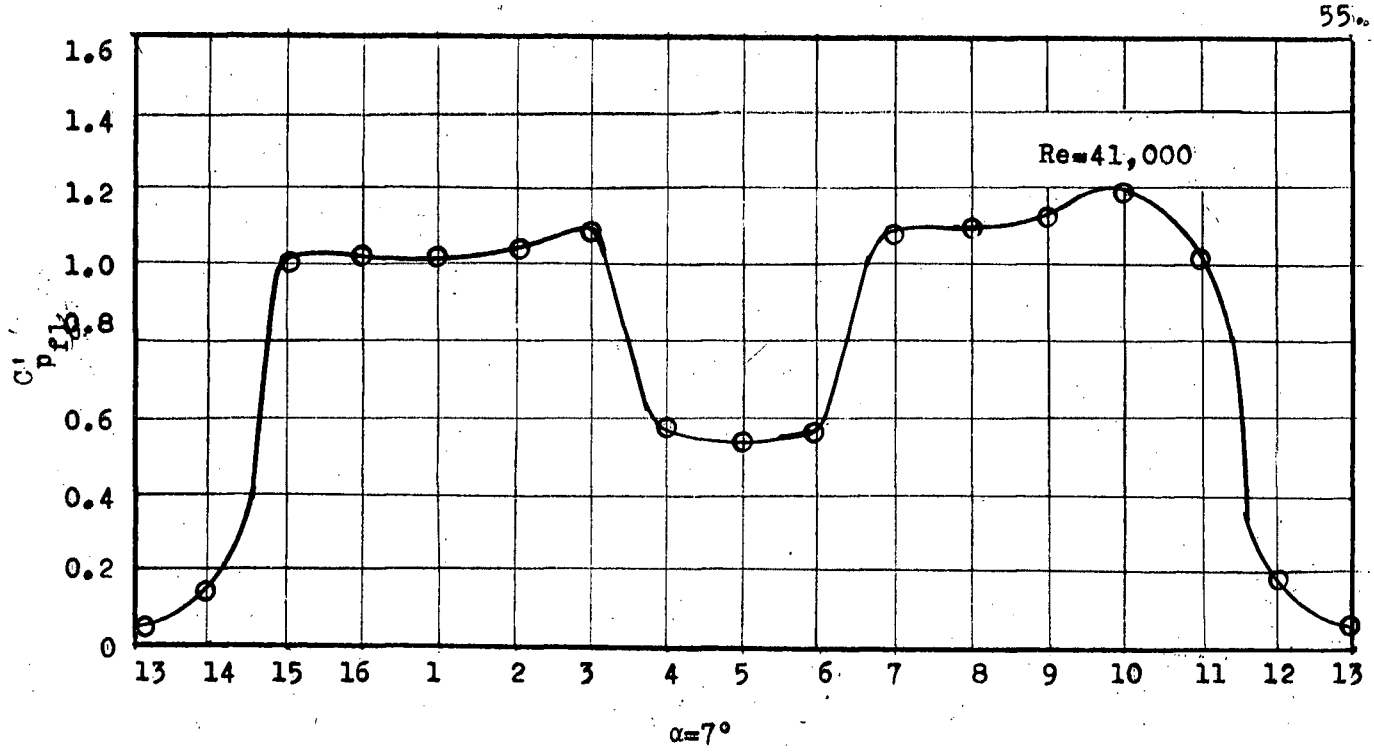

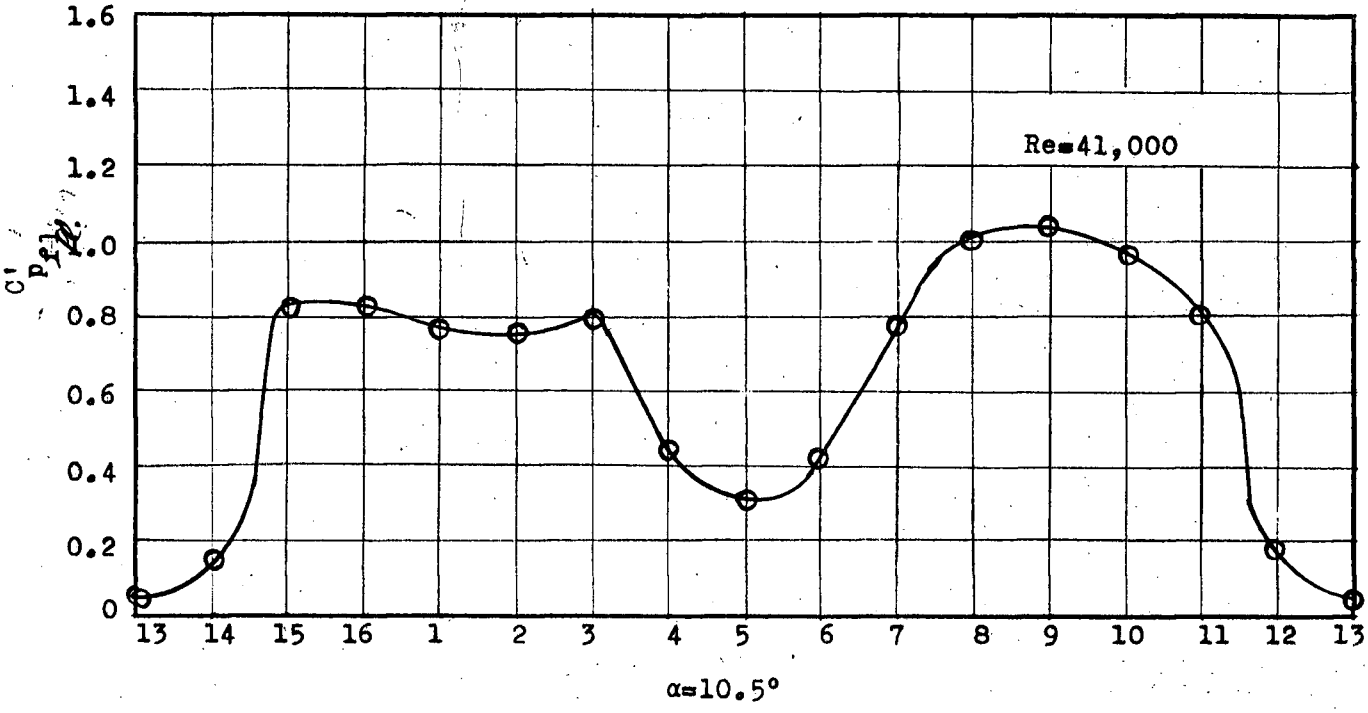

Figure 23 (cont'd). Variation of Fluctuating Pressure Distribution with α: Square Cylinder

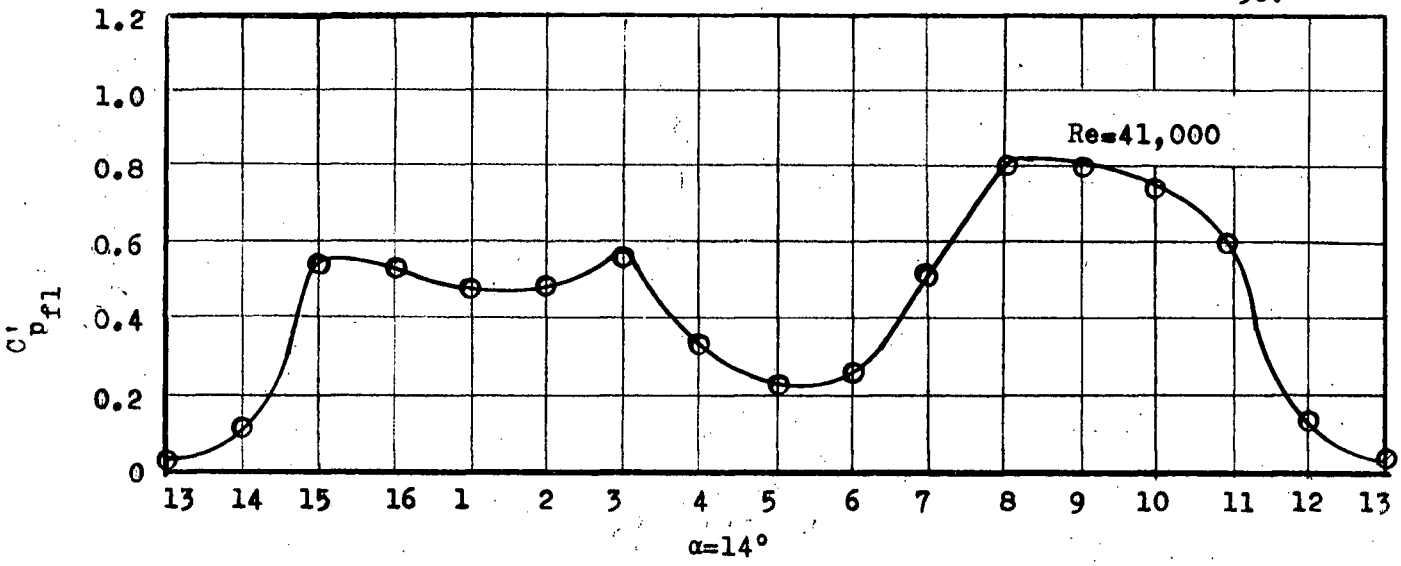

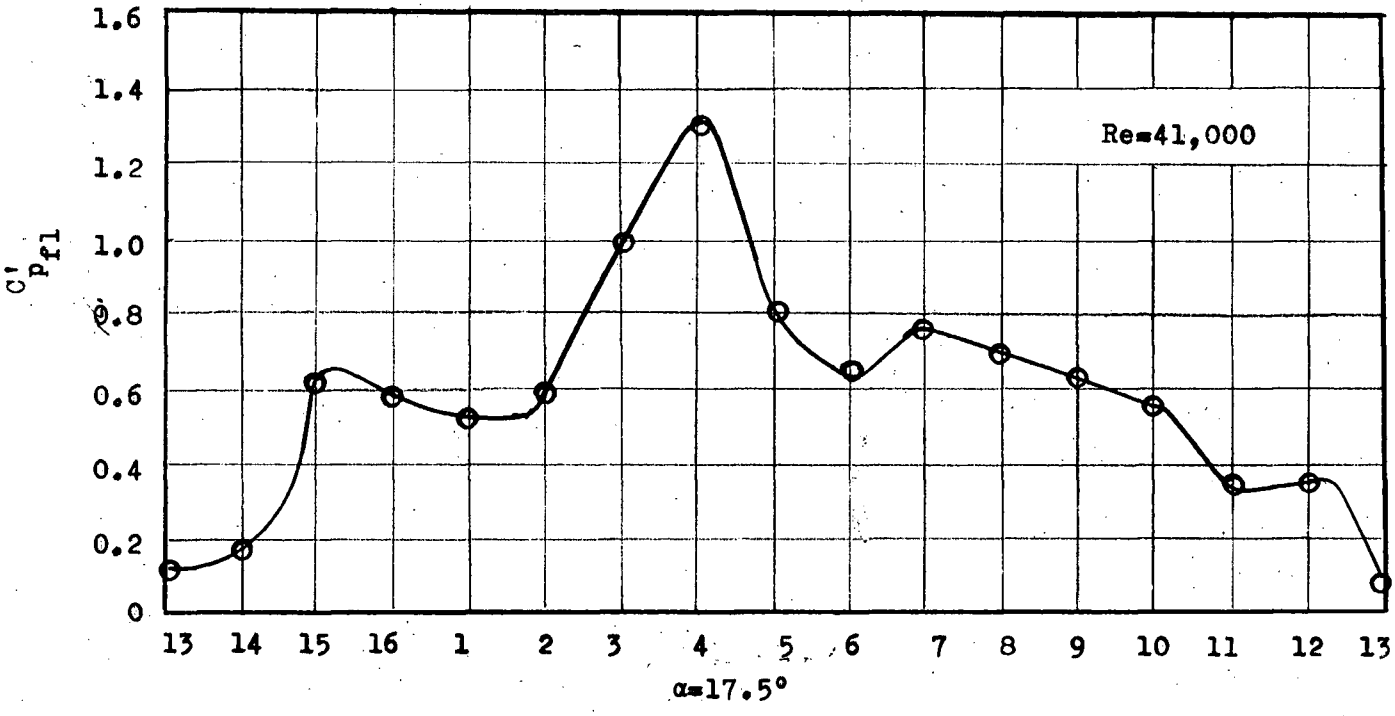

Figure 23 (cont'd). Variation of Fluctuating Pressure Distribution with α: Square Cylinder

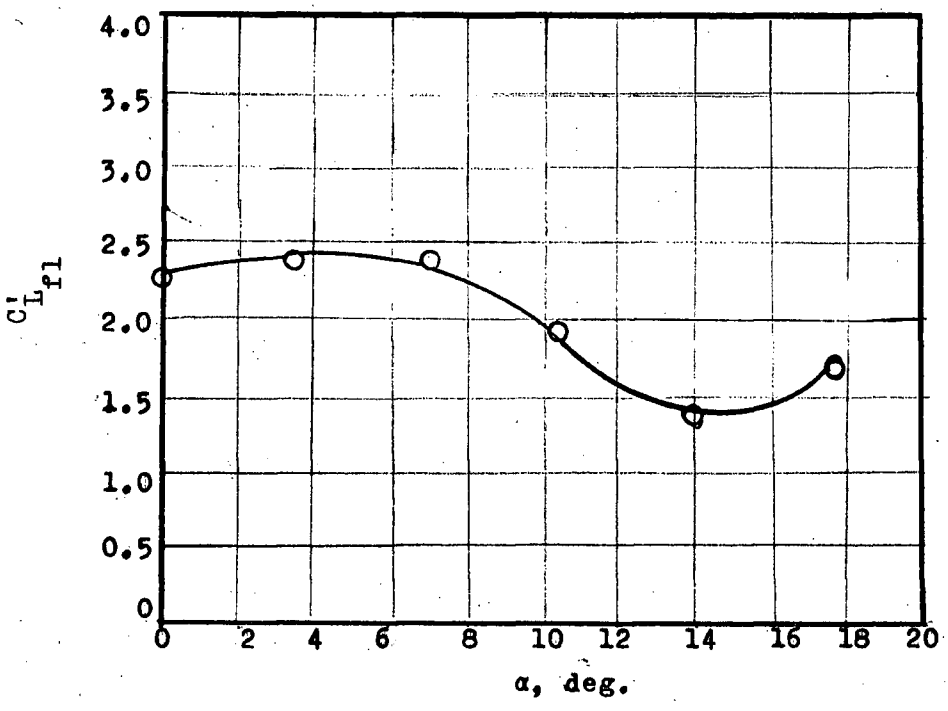

Figure 24. Variation of Fluctuating Lift Coefficient with α: Square Cylinder

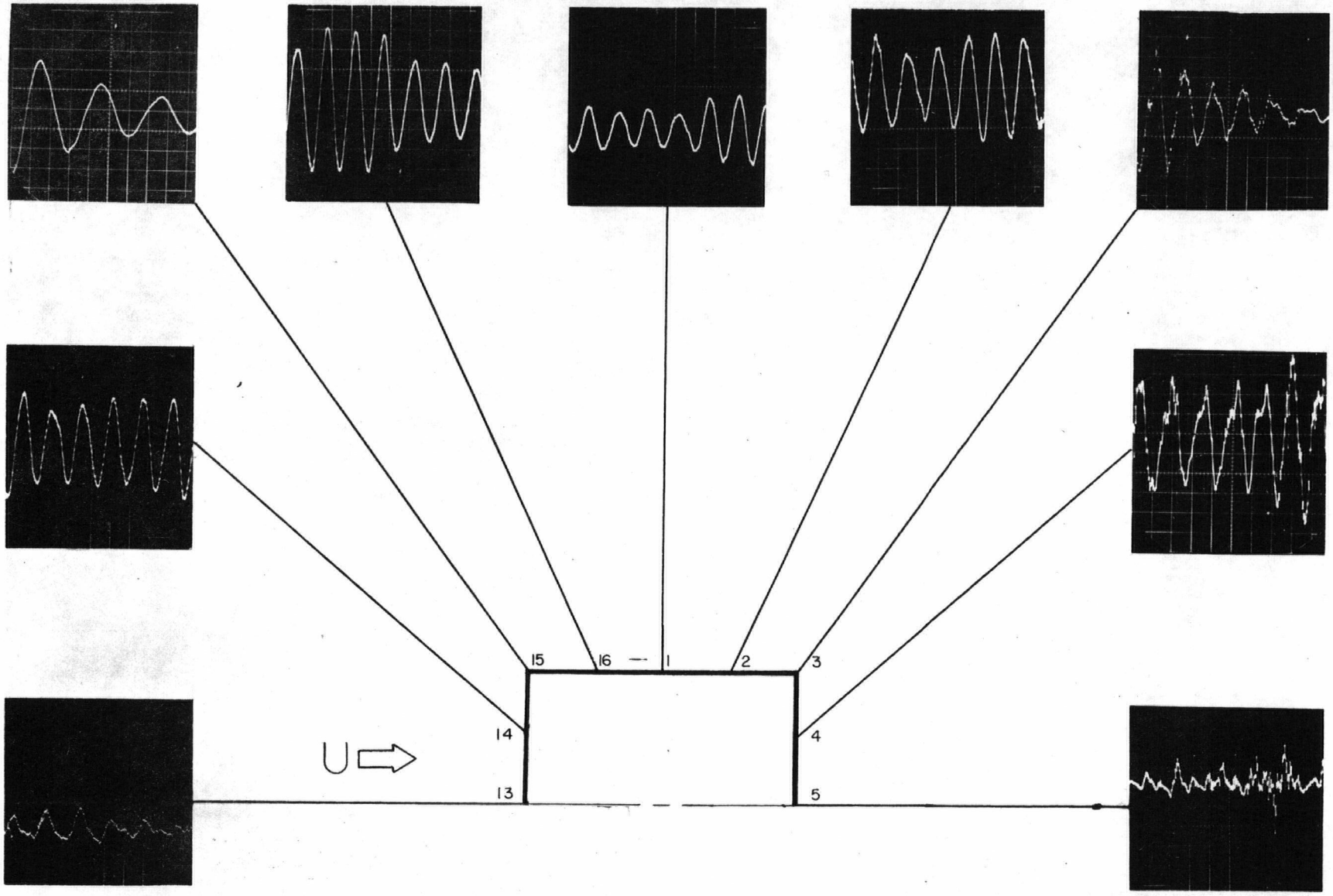

Figure 25. Pressure Oscillations on the Surface of Square Cylinder

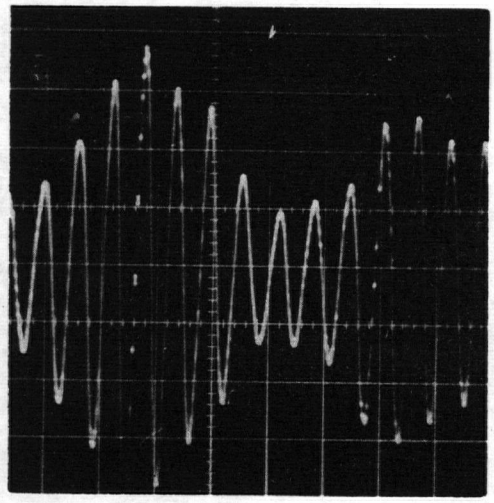

Figure 26. Amplitude Modulations of Pressure Fluctuations on the Surface of Square Cylinder, Tap 15 (Stationary)

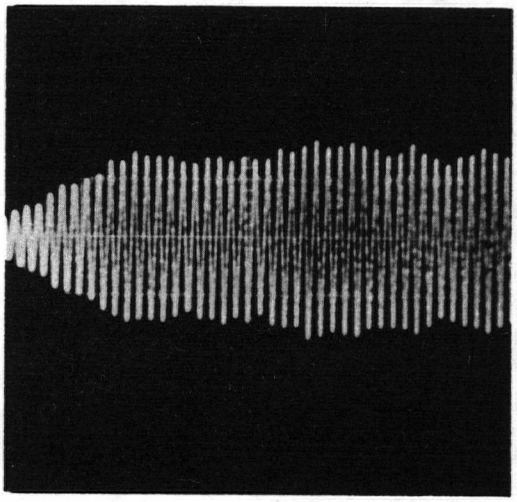

Figure 27. Slowly Varying Amplitude and Frequency of Square Cylinder Motion

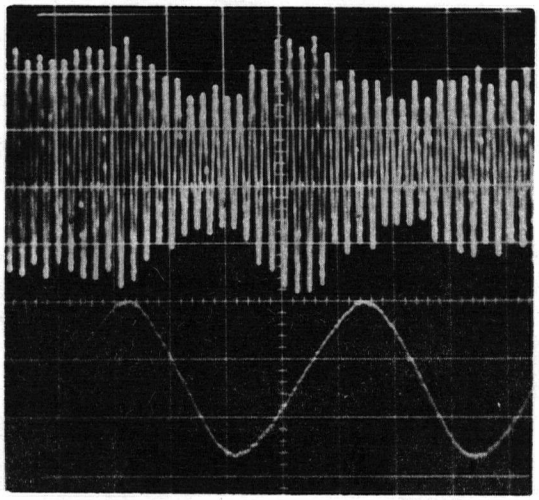

Figure 28. Effect of Motion on Pressure Fluctuations on the Surface of Square Cylinder, Tap 15

4.2.1 Stationary Rectangular Cylinder, AR=2

A rectangular cylinder with AR=2 was tested for static and fluctuating pressure distribution under stationary as well as dynamic conditions. The surface of the cylinder was provided with sixteen pressure taps each connected to the Lambrecht manometer for static pressure measurements and to the designed pressure transducer for fluctuating pressure measurement. The static pressure distribution over a range of angle of attack is presented in Figure 29 while Figure 30 shows variation of lift coefficient with angle of attack. It may be pointed out that the maximum lift coefficient of 0.5 at 10.5° is lower than that obtained for the square cylinder.

The measurements carried out to study variation of Strouhal number with Reynolds number showed it to remain constant at the value of 0.081 as indicated in Figure 31. There was less scatter of data for this case as compared to the square cylinder.

The fluctuating pressure measurements at 0° and 3.5° angle of attack were nearly identical on either side of the centerline of the body as in the case of the square cylinder. At an angle of attack of 14° the surface facing the upstream; i.e. taps 9 and 14 showed signs of turbulence probably due to reattachment of the flow while the opposite face registered sudden rise in fluctuating pressure coefficients (taps 4 and 5). Fluctuating pressure coefficients on the surface of the rectangular cylinder at several angles of attack are shown in Figure 32 while the plot of fluctuating lift coefficient per unit span against

angle of attack is presented in Figure 33.

Photographic representation of the pressure oscillations at various points on the surface of the rectangular cylinder are shown in Figure 34. The photographs are for the model at zero angle of attack with the oscilloscope attenuator maintained at the same sensitivity. Amplitude modulation of the fluctuating pressure in the Reynolds number range of 55,000 to 70,000 is worth pointing out since the modulations did not appear anywhere except in this range. No definite explanation for this can be given here. The phenomenon should be investigated further. Note also the expected double frequency effect at the rear of the cylinder as shown by the photograph for tap 7.

The study of phase relation between the oscillating pressures about the rectangular cylinder showed the taps 1 to 7 and 16 to be in phase while taps 8 to 15 to be 180° out of phase with respect to tap 1.

The wake study revealed the longitudinal and lateral spacing between the consecutive vortices to be 17.3 and 5.5 inches thus giving a/h=0.318. Figure 35 shows the fluctuating pressure traces produced by the probe located 17.3 inches behind the model and that existing at tap 1. The two signals are apparently in phase.

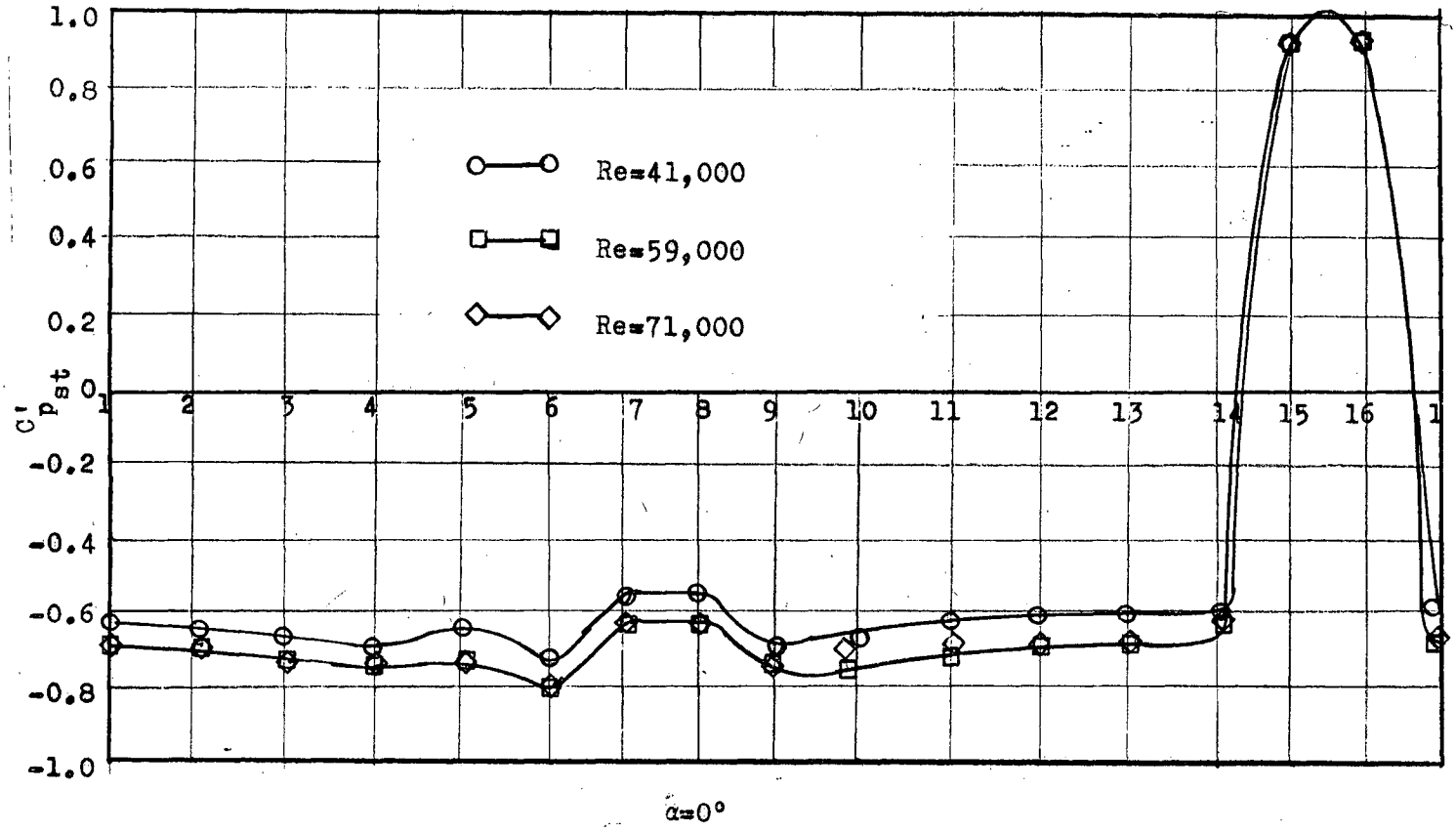

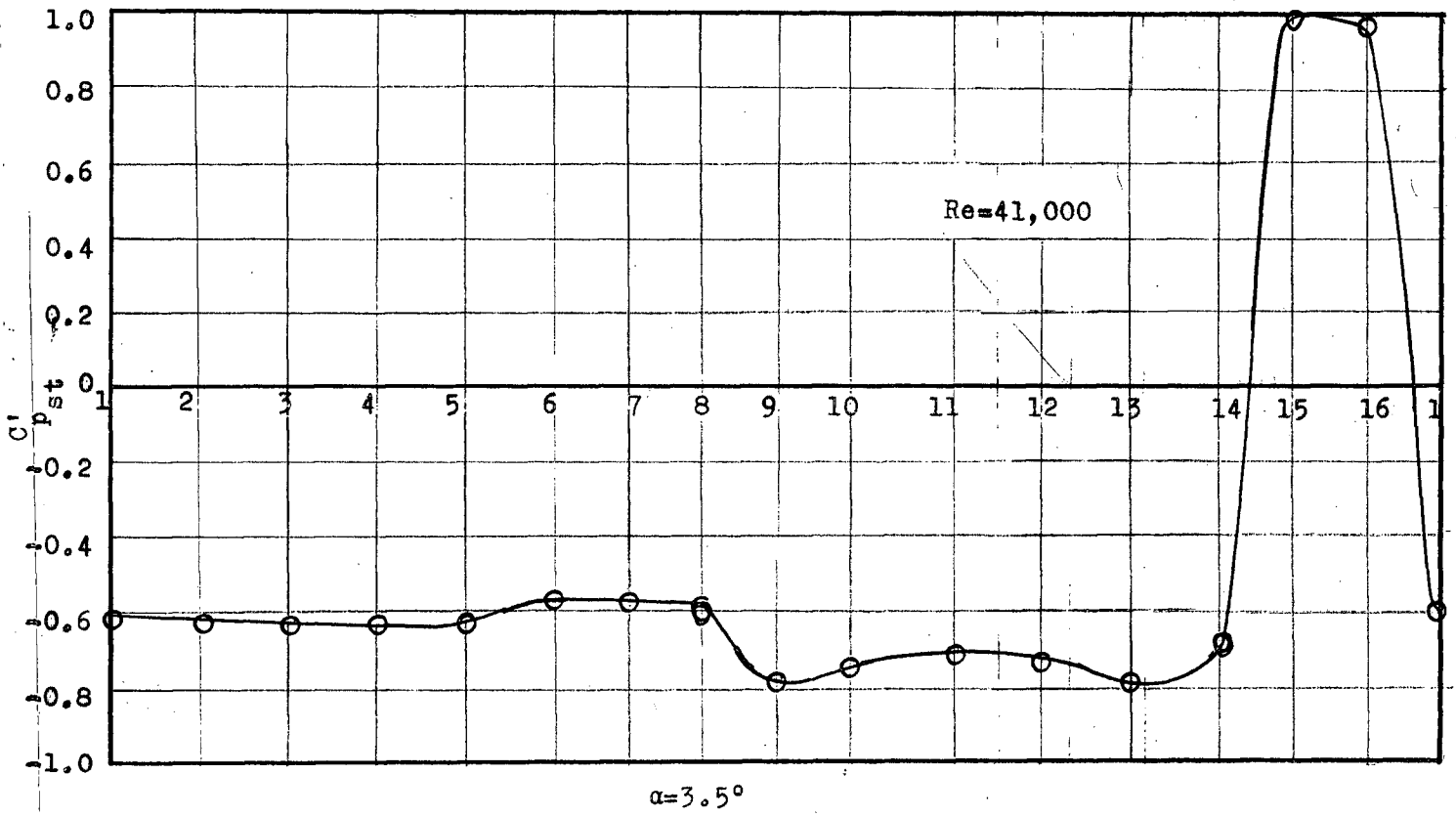

Figure 29. Variation of Static Pressure Distribution with α: Rectangular Cylinder AR =2

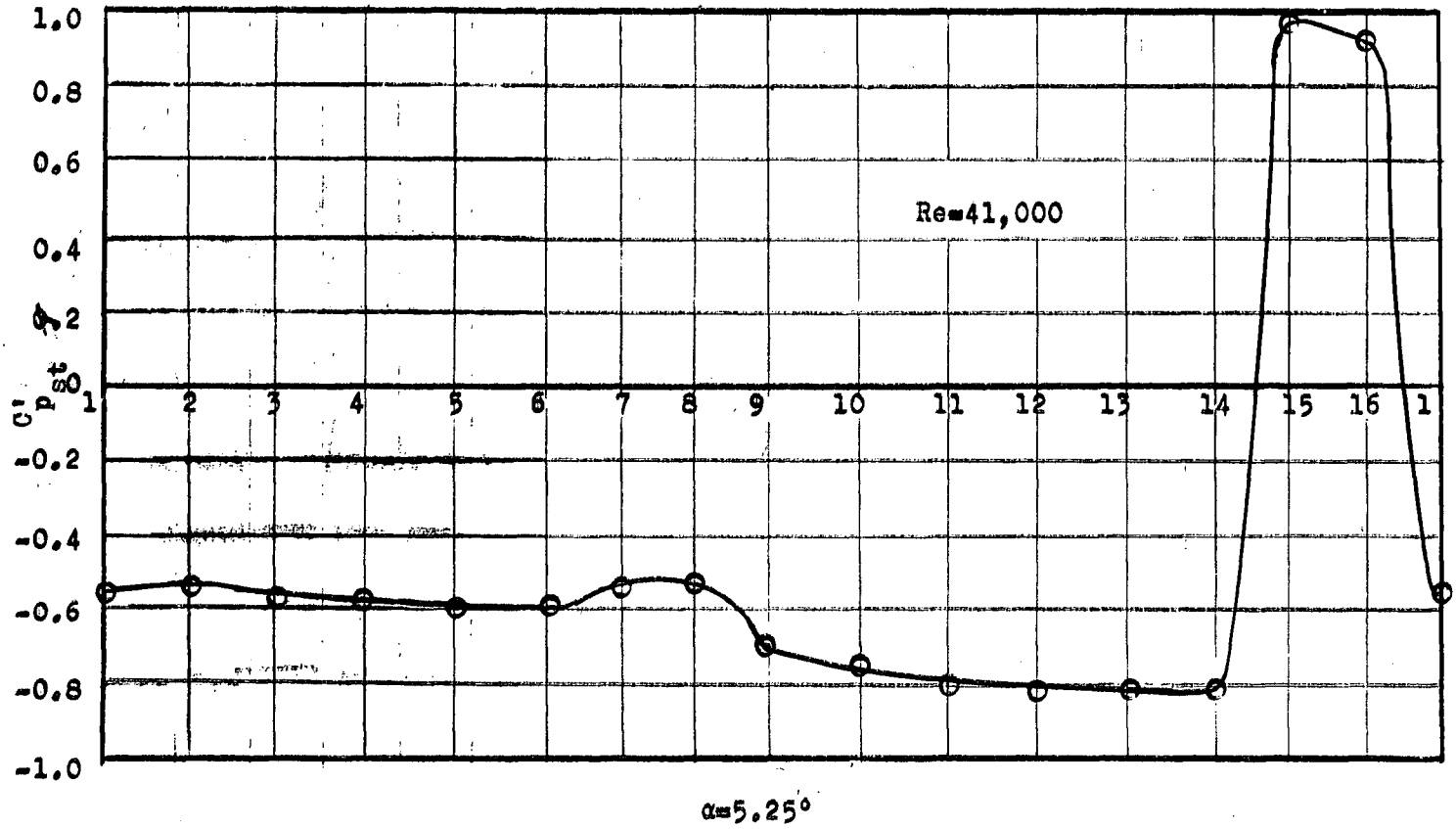

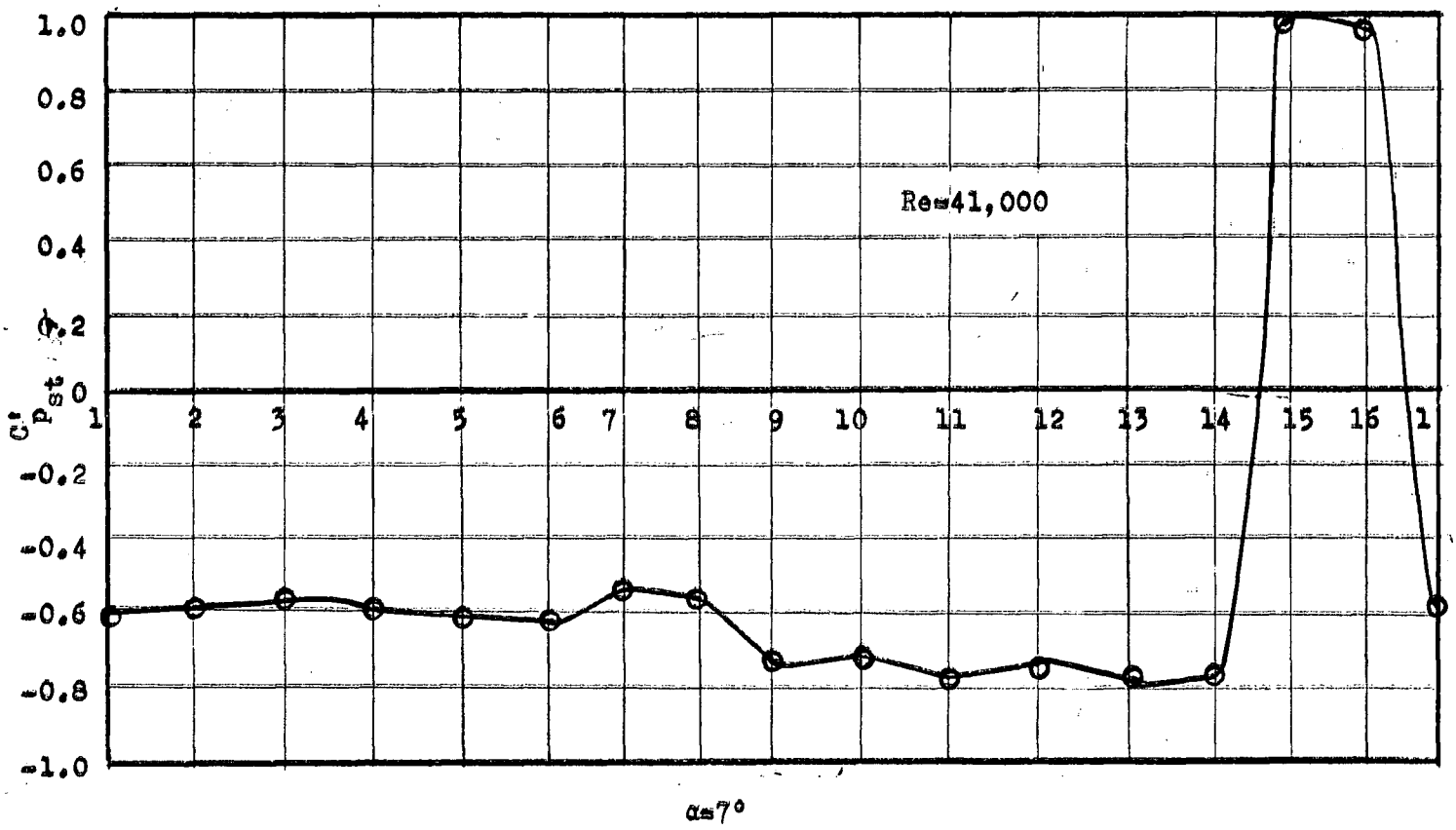

Figure 29 (cont'd). Variation of Static Pressure Distribution with α: Rectangular Cylinder AR=2

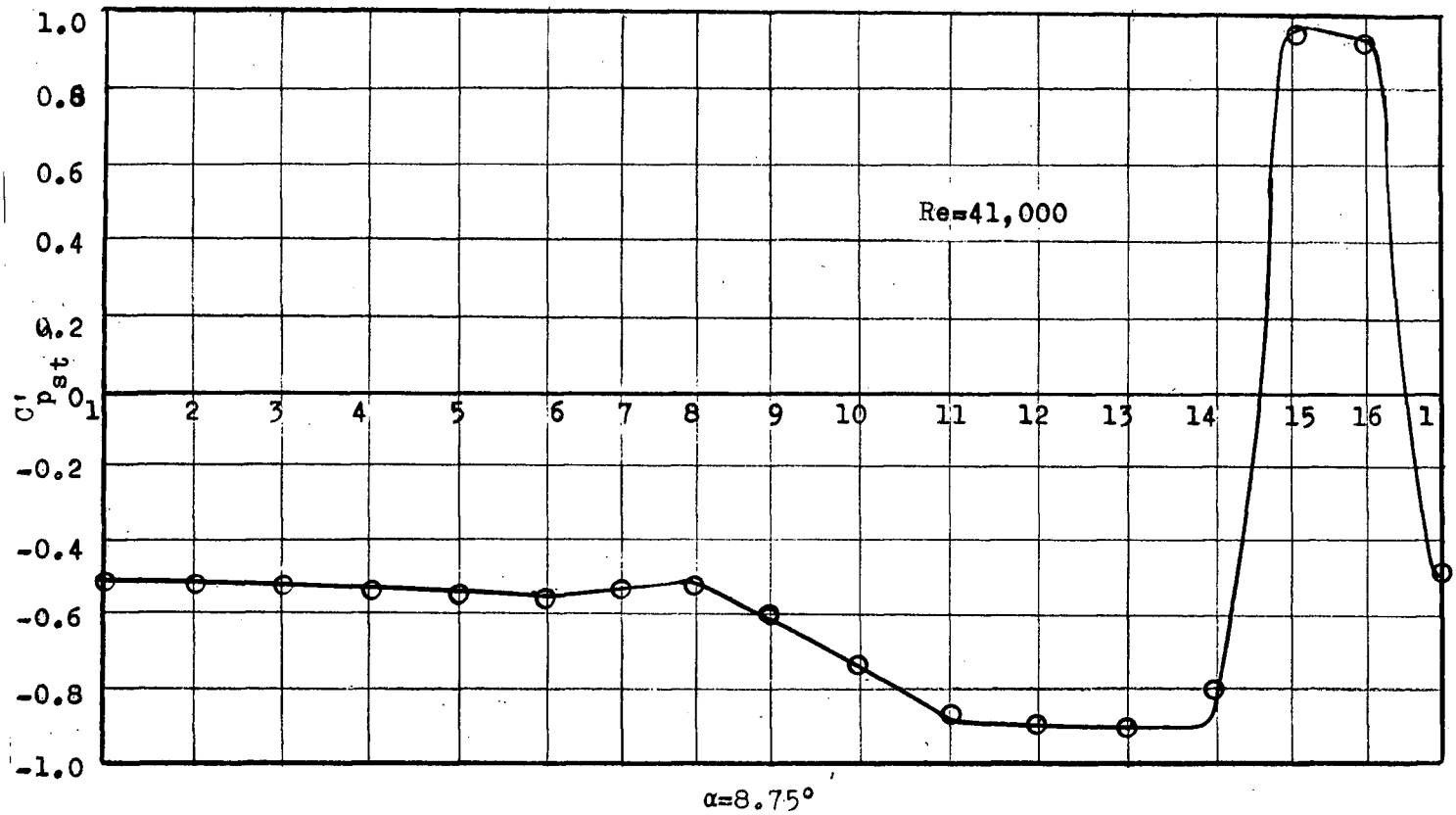

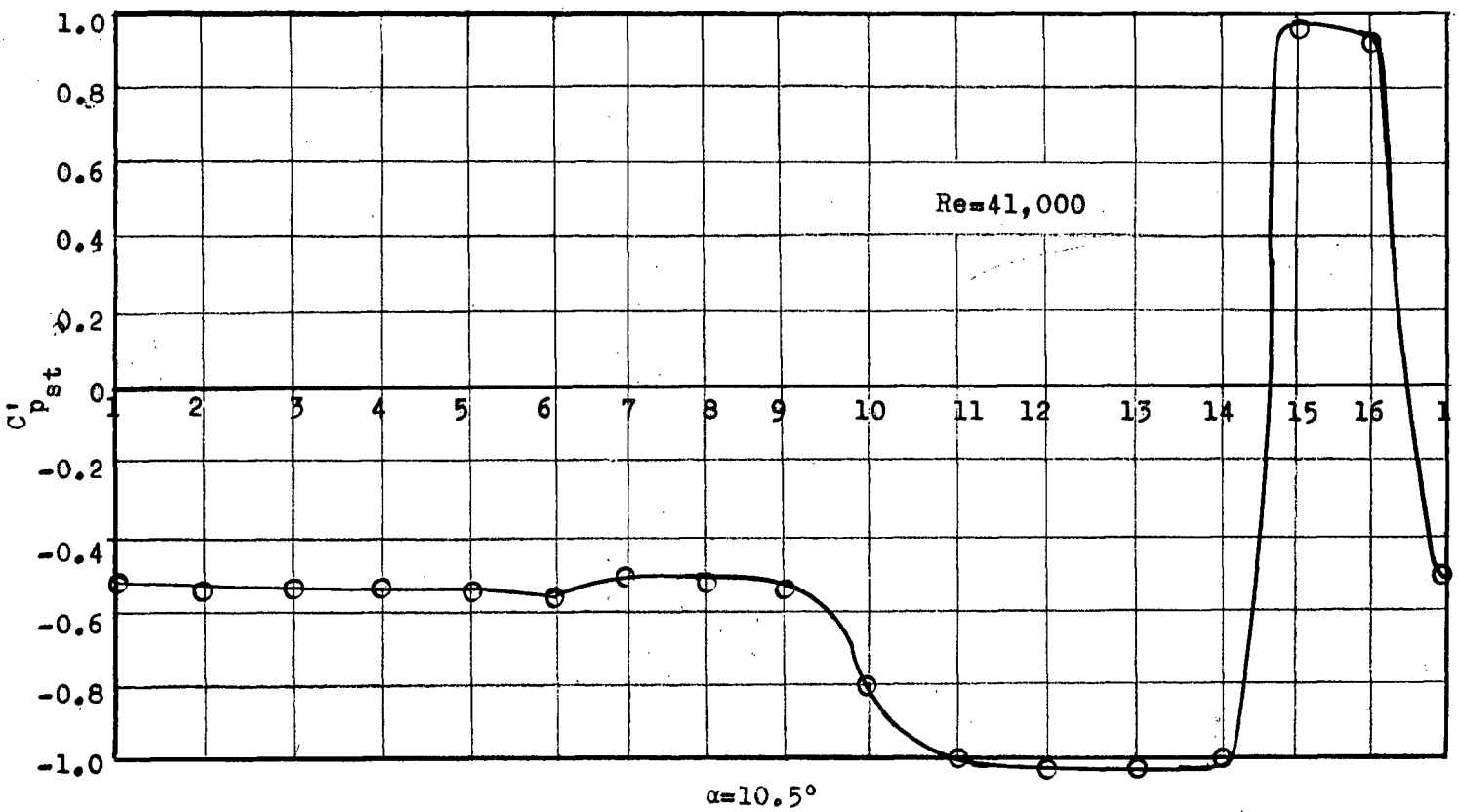

Figure 29 (cont'd). Variation of Static Pressure Distribution with α: Rectangular Cylinder AR =2

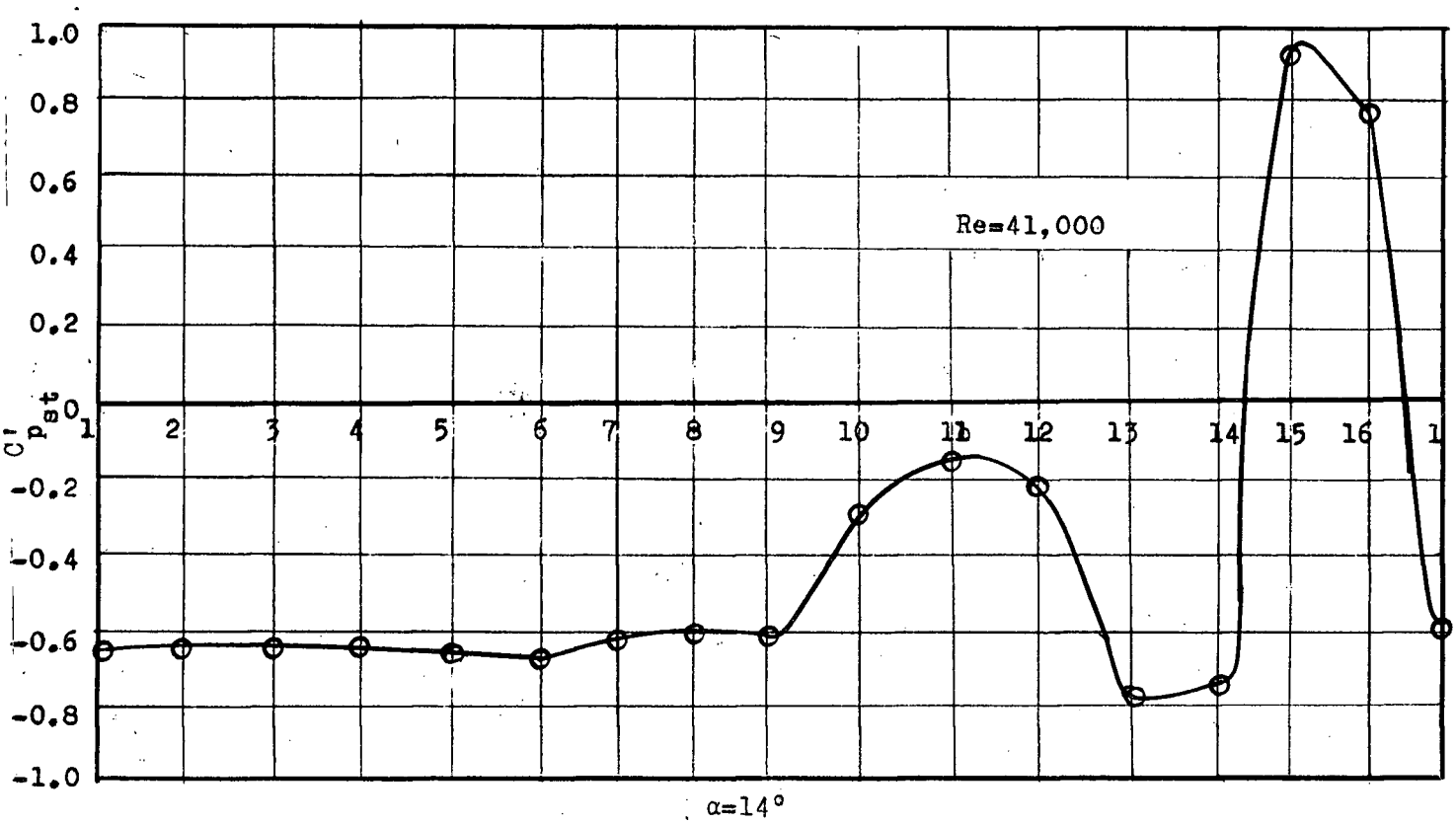

Figure 29 (cont'd). Variation of Static Pressure Distribution with α: Rectangular Cylinder AR=2

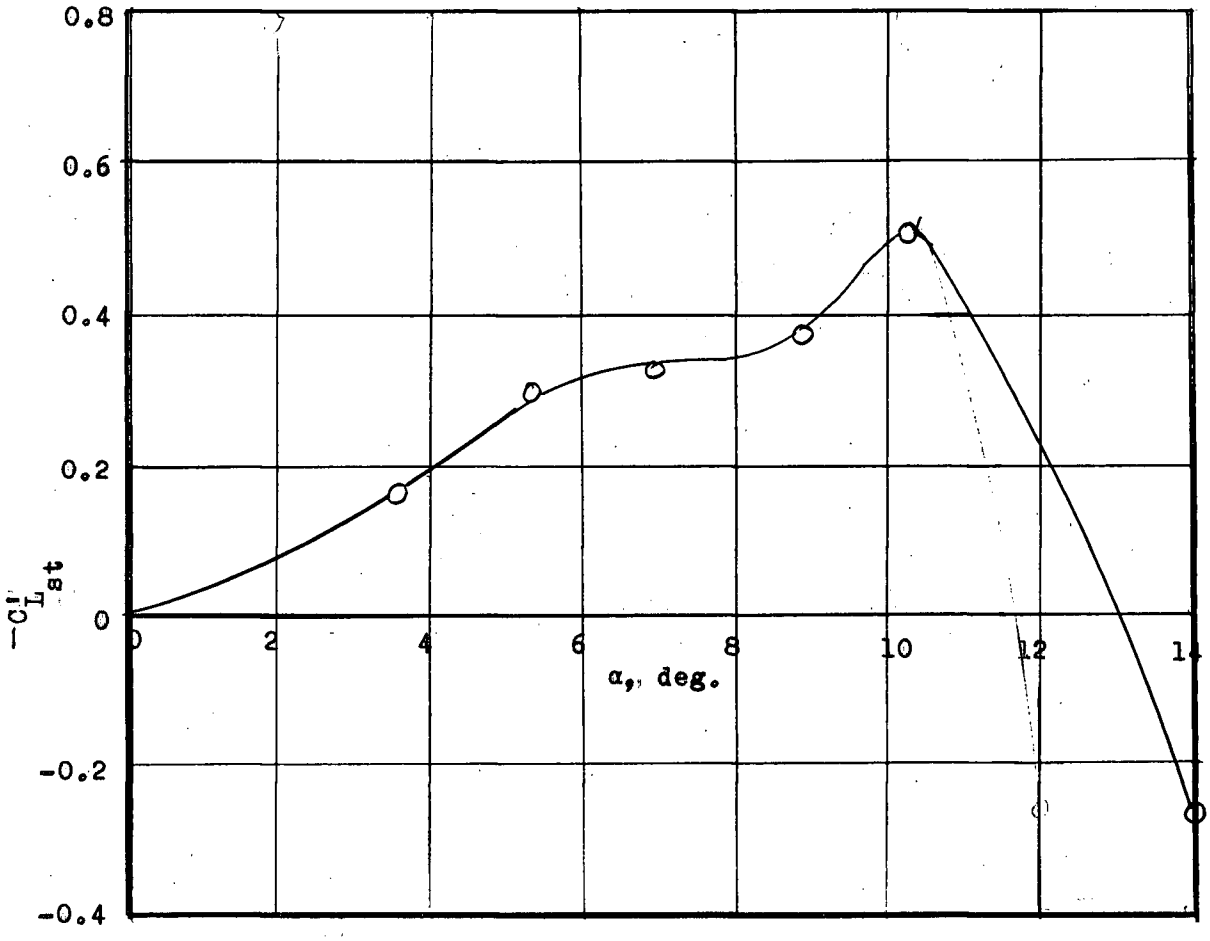

Figure 30. Variation of Static Lift Coefficient with α: Rectangular Cylinder AR =2

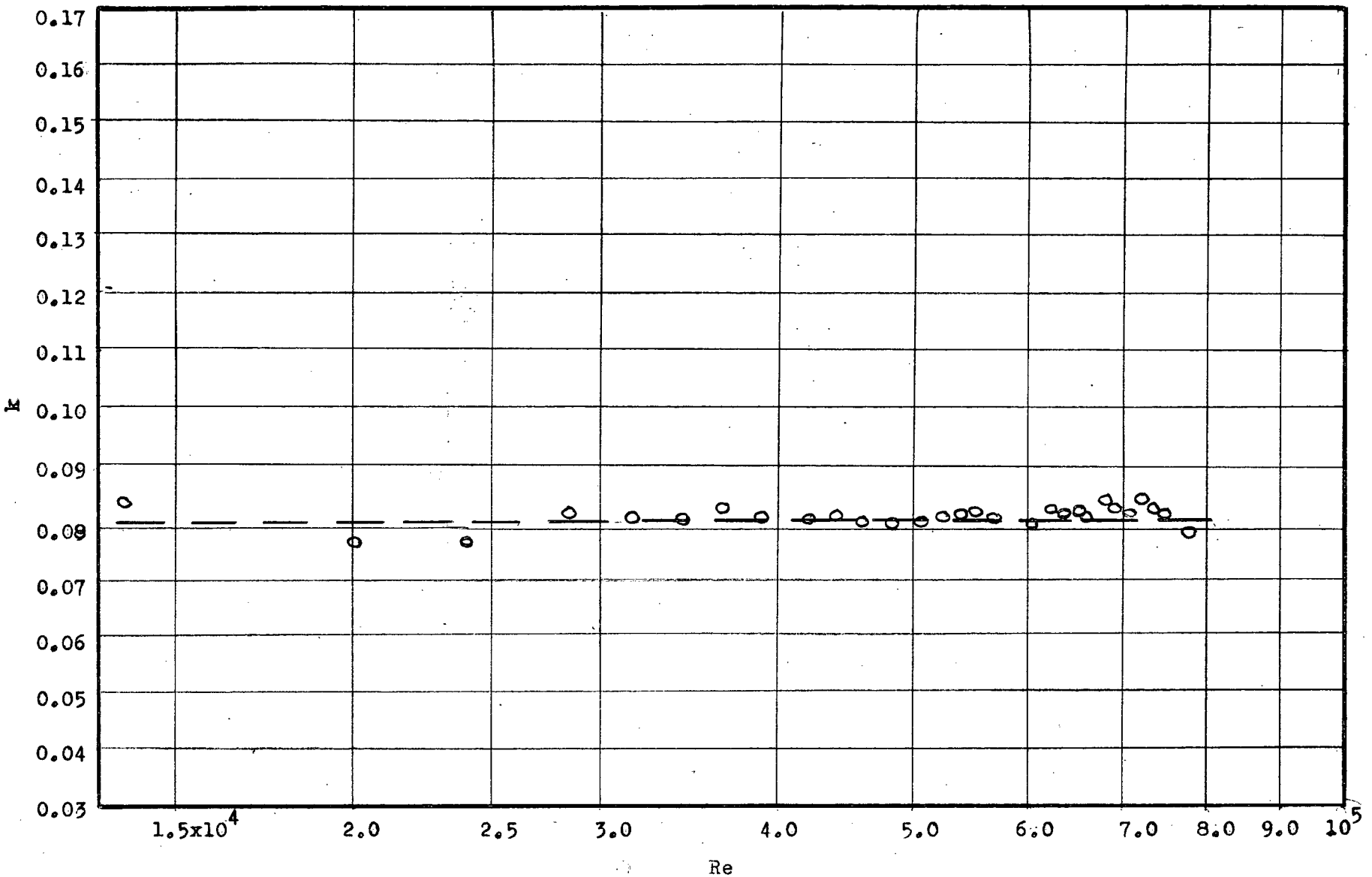

Figure 31. Variation of Strouhal Number with Reynolds Number for Rectangular Cylinder AR = 2

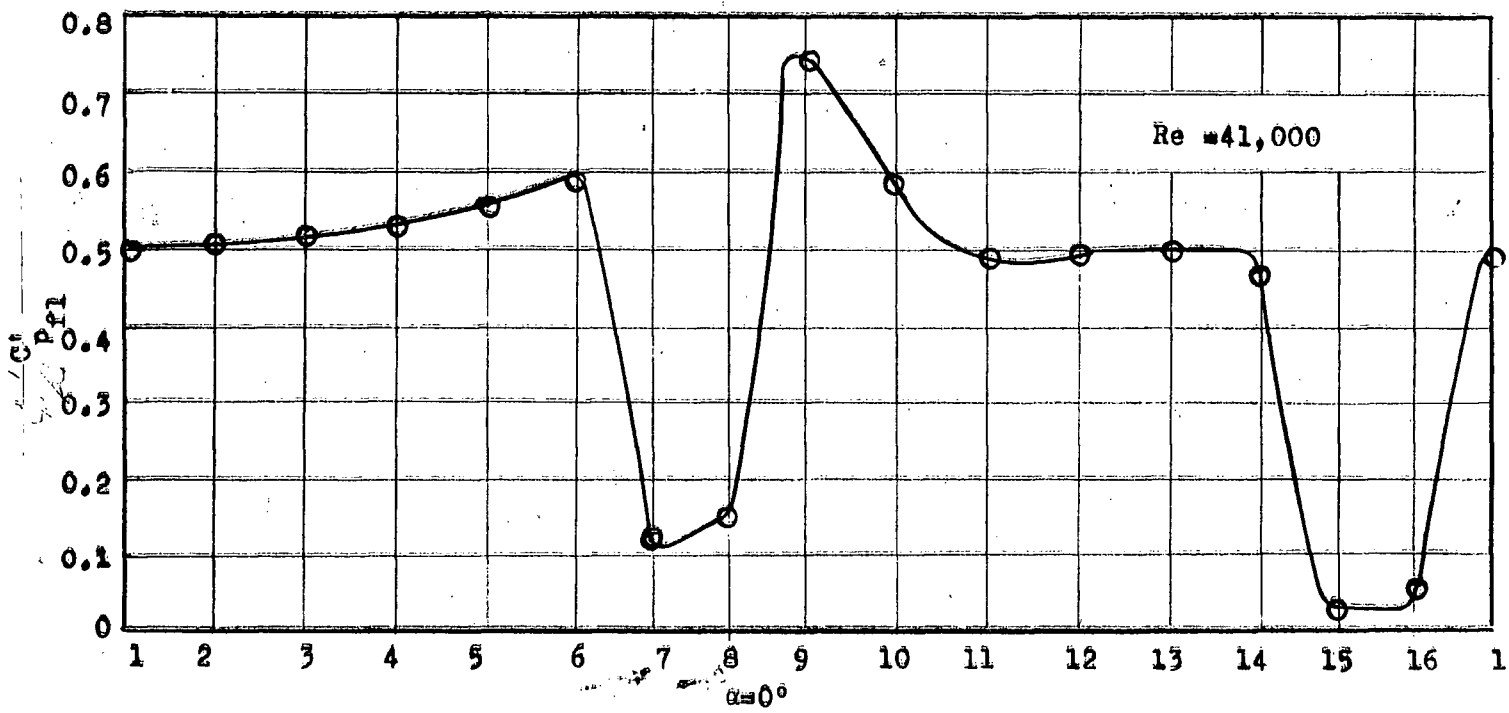

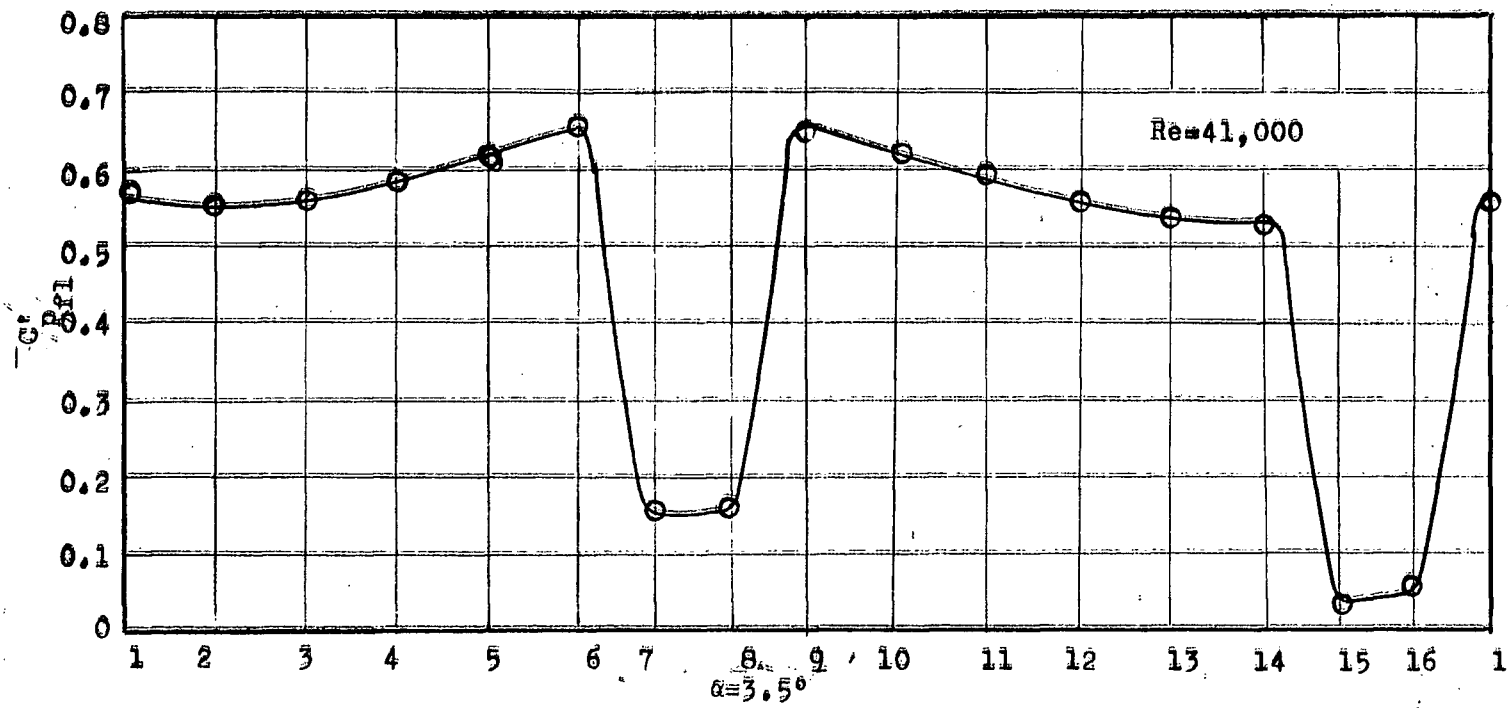

Figure 32. Variation of Fluctuating Pressure Distribution with α: Rectangular Cylinder $\bar{A}$ =2

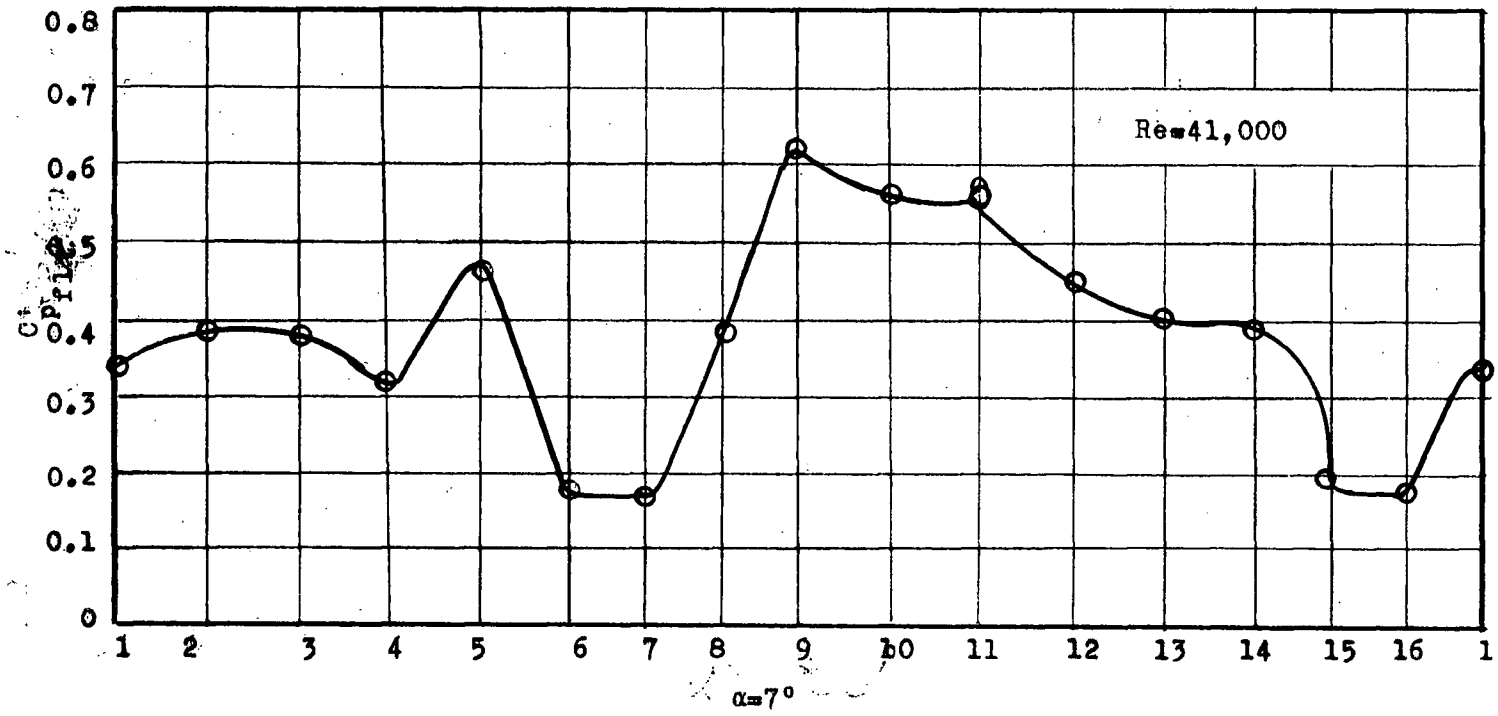

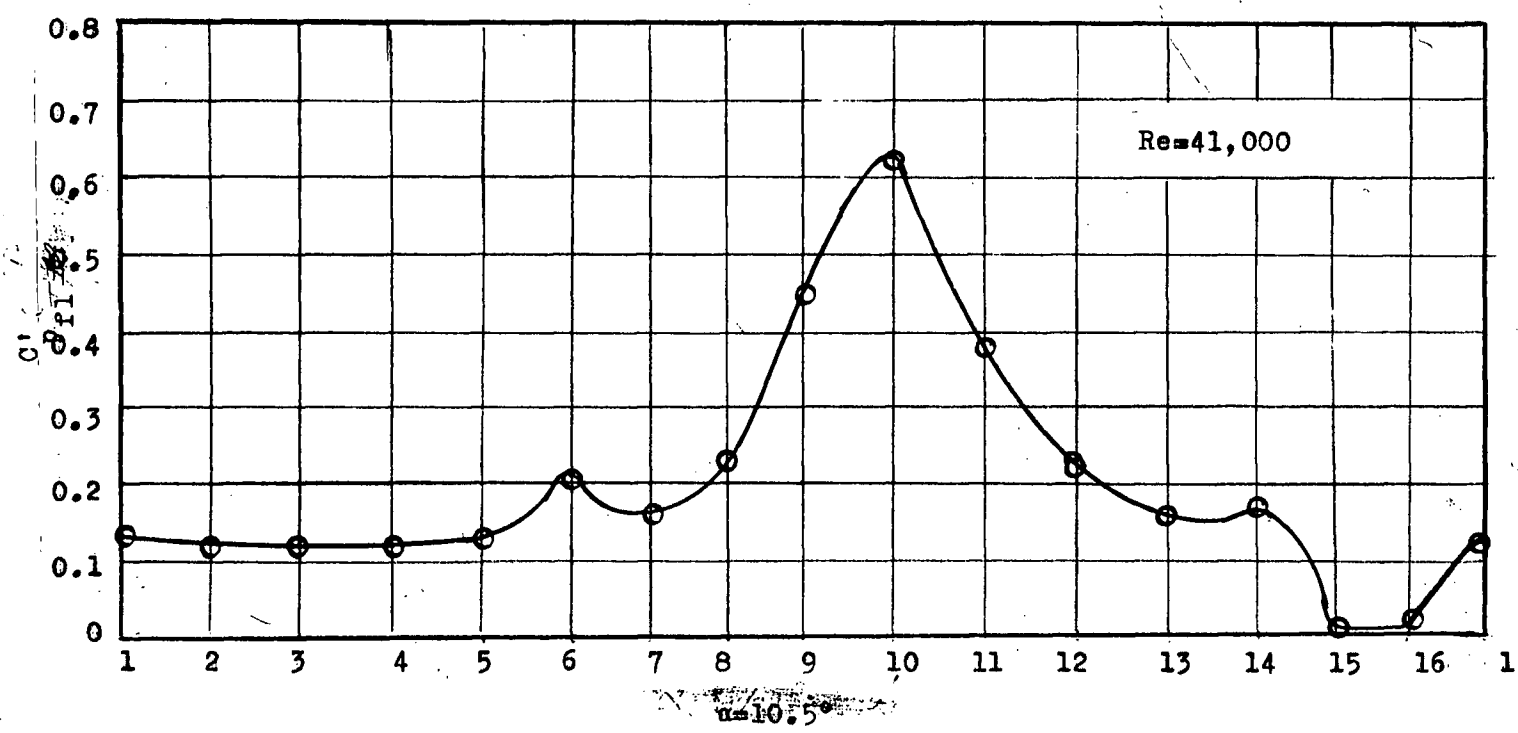

Figure 32 (cont'd). Variation of Fluctuating Pressure Distribution with α: Rectangular Cylinder AR=2

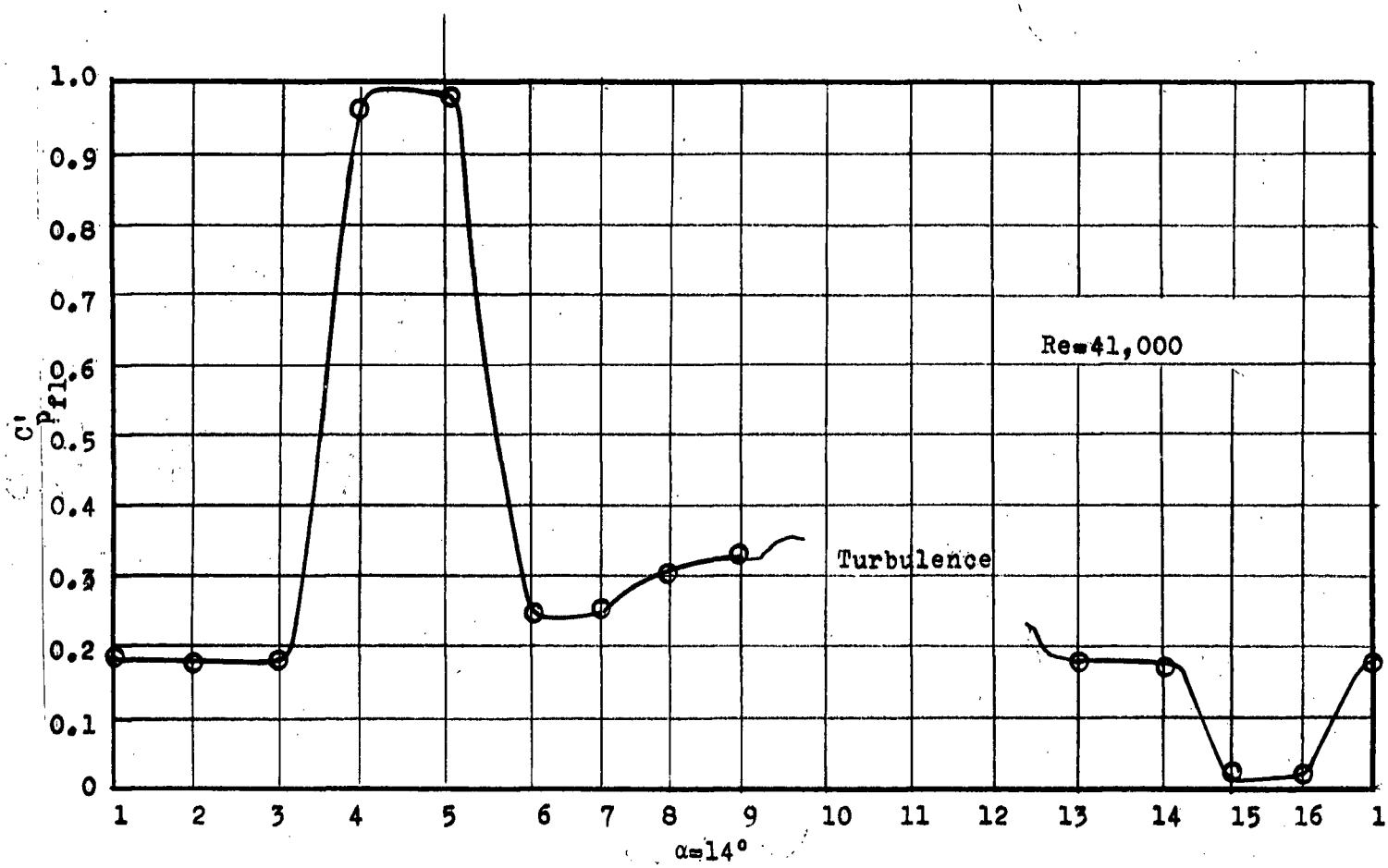

Figure 32 (cont'd). Variation of Fluctuating Pressure Distribution with α: Rectangular Cylinder AR =2

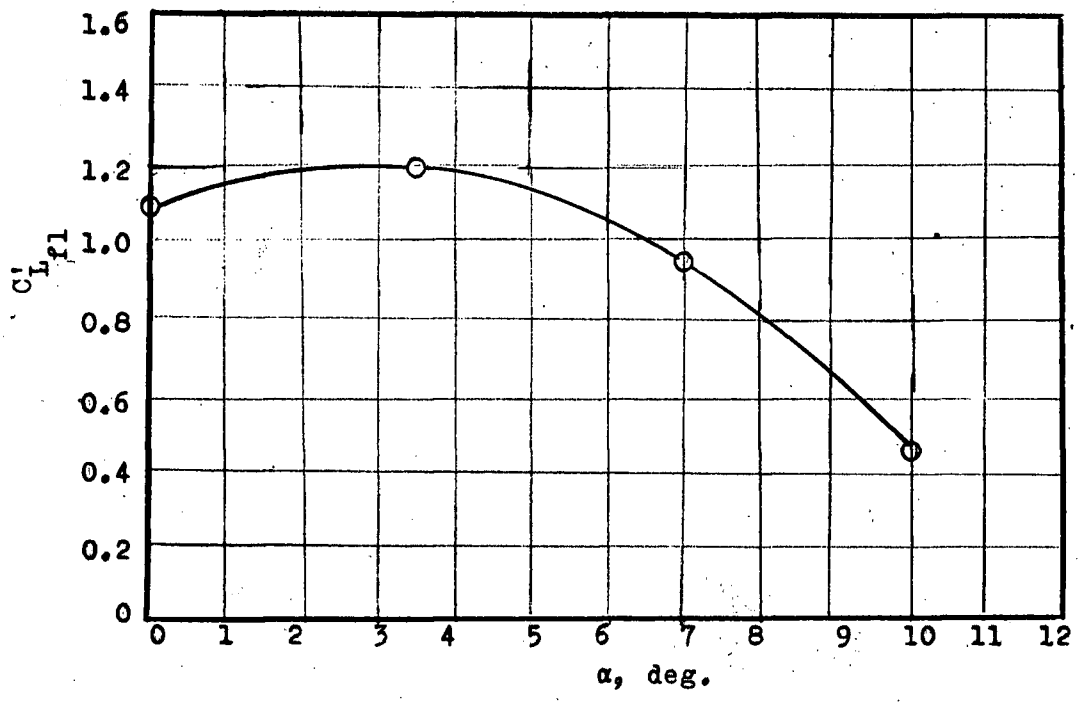

Figure 33. Variation of Fluctuating Lift Coefficient with α: Rectangular Cylinder AR=2

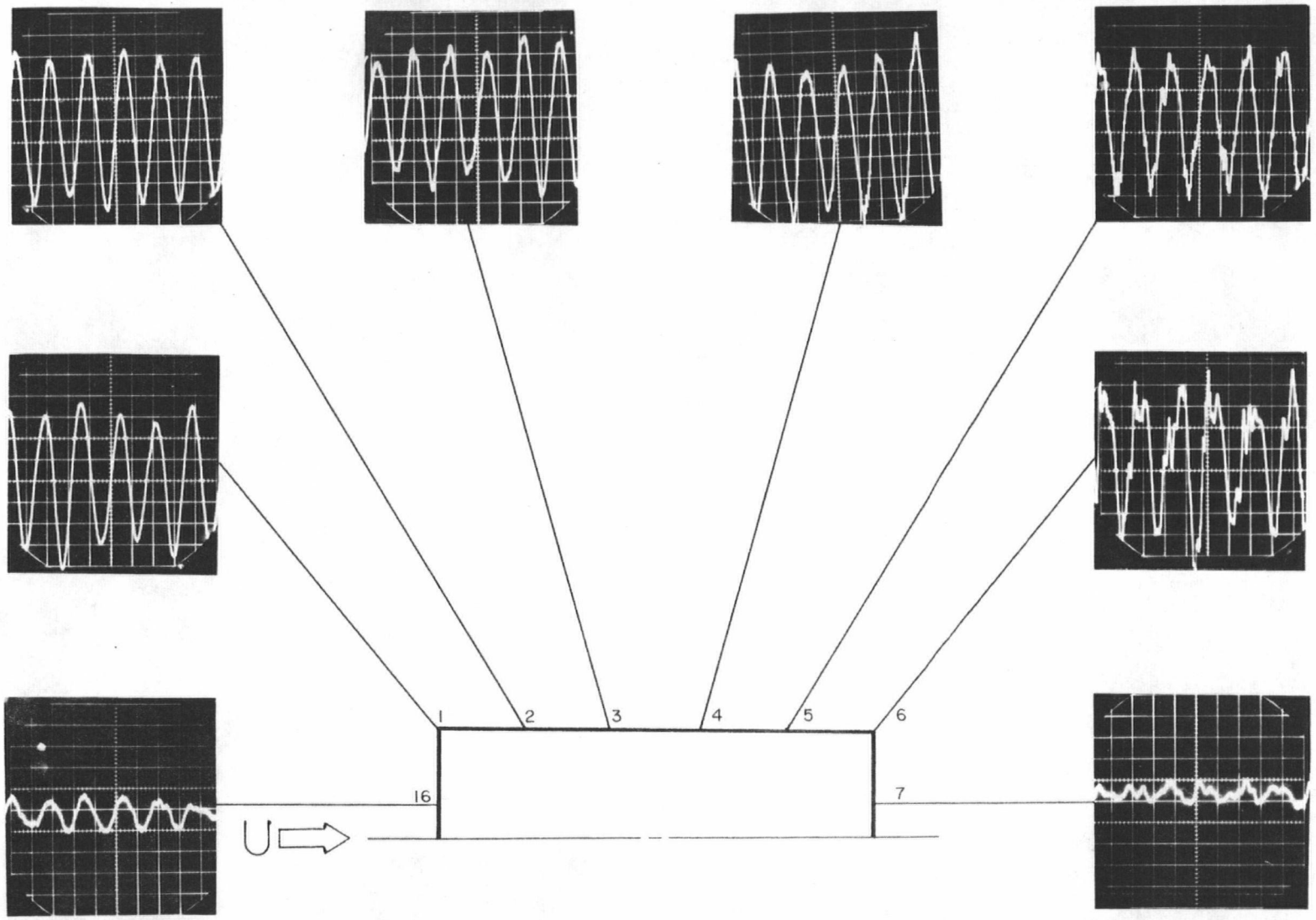

Figure 34. Pressure Oscillations on the Surface of Rectangular Cylinder AR = 2

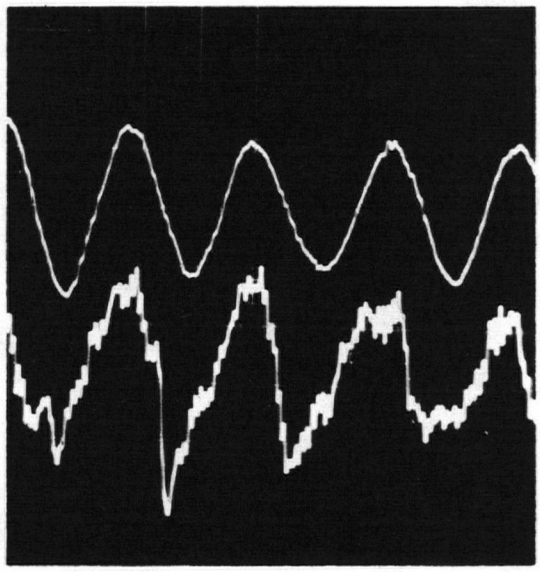

Figure 35. Pressure Fluctuations as Recorded by Probe and Tap 1, Rectangular Cylinder AR =2, Probe 17.3 inches downstream of the Model

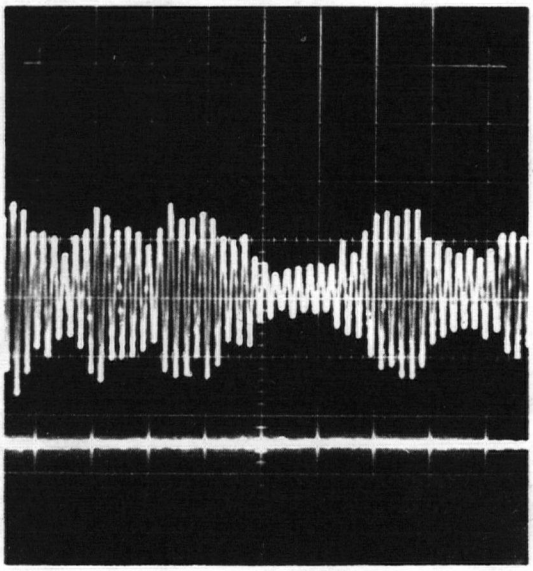

a. No Motion, Sweep Time 50ms/cm.

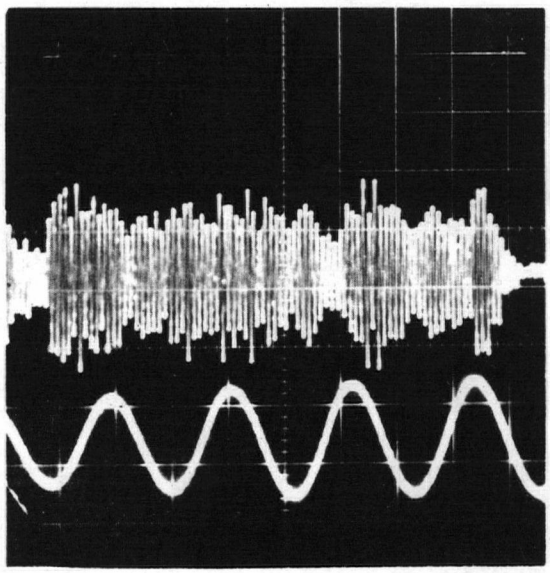

b. Motion, Sweep Time 100ms/cm

Figure 36. Effect of Motion on Pressure Fluctuations on the Surface of Rectangular Cylinder AR =2

4.2.2 Oscillating Rectangular Cylinder, AR=2

Next the wind speed was gradually increased until the model exhibited self excited oscillations. The oscillating pressure at all taps on the surface of the model was found to be identical to the corresponding pressure under stationary conditions. This is shown for a representative pressure tap in Figure 36.

4.2.3 Stationary Rectangular Cylinder, AR=1/2

As a matter of curiosity the previous model; i.e. rectangular cylinder with AR=2, was rotated through 90° to give a rectangular cylinder with AR= 1/2. The model in this position represented a body with greater bluffness thus giving large drag particularly at higher angle of attack and speed. The insufficient stiffness of the model caused it to deflect under the influence of drag hence the tests were limited to zero angle of attack.

The static and fluctuating pressure distributions for this case are presented in Figure 37. The large fluctuations in pressure on the top, bottom and rear face with relatively small values on the upstream face are worth pointing out. Note also the comparatively large value of $C'_{L_{fl}} = 4.8$ with reference to the narrow side, and $C'_{L_{fl}} = 2.4$ with reference to the broad side.

The variation of Strouhal number with Reynolds number is shown in Figure 38. The results are quite scattered primarily due to the fact that the oscillating pressure fluctuations

were generally unorganized showing a large amplitude modulation effect.

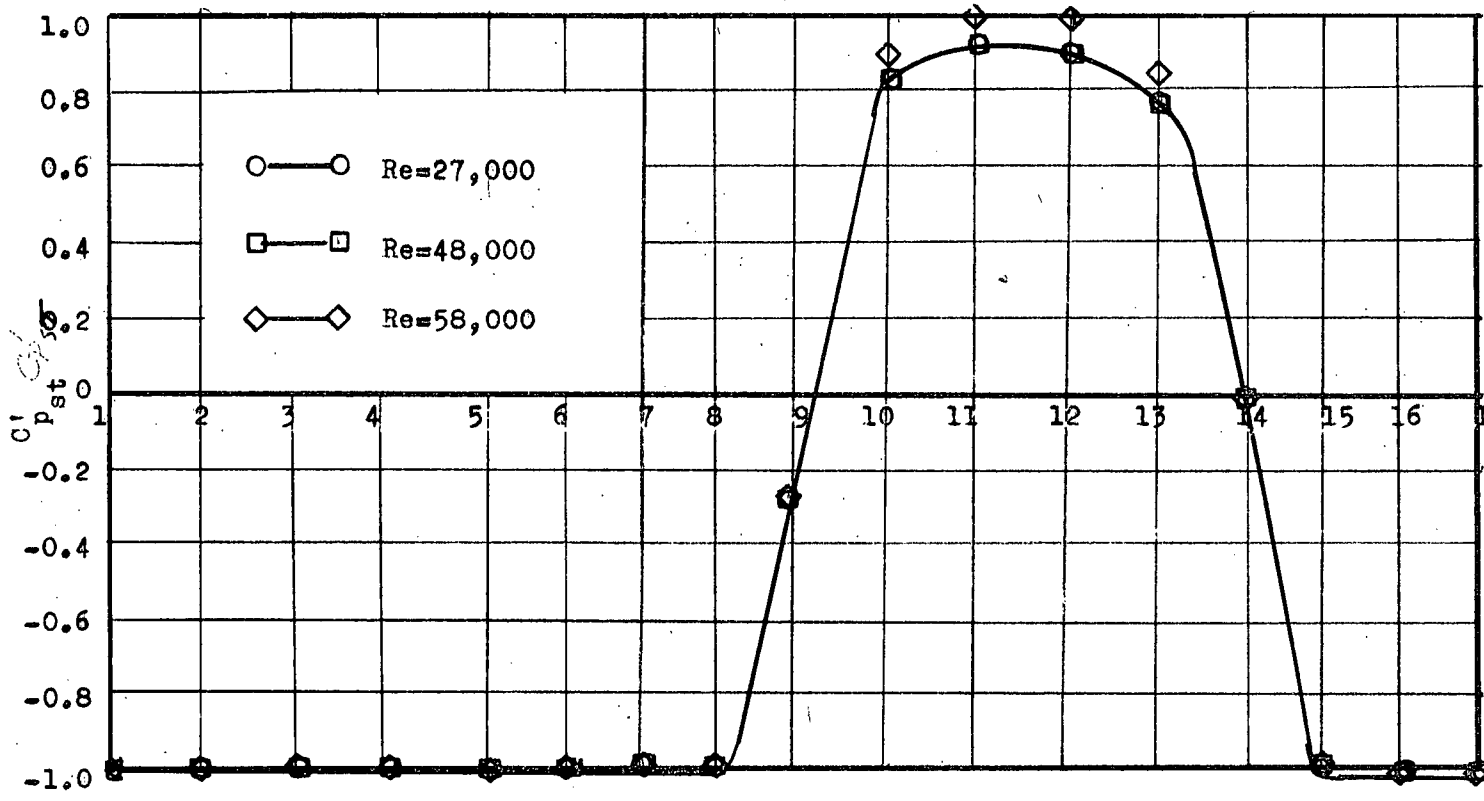

Figure 37a. Static Pressure Distribution Over Rectangular Cylinder AR = 1/2

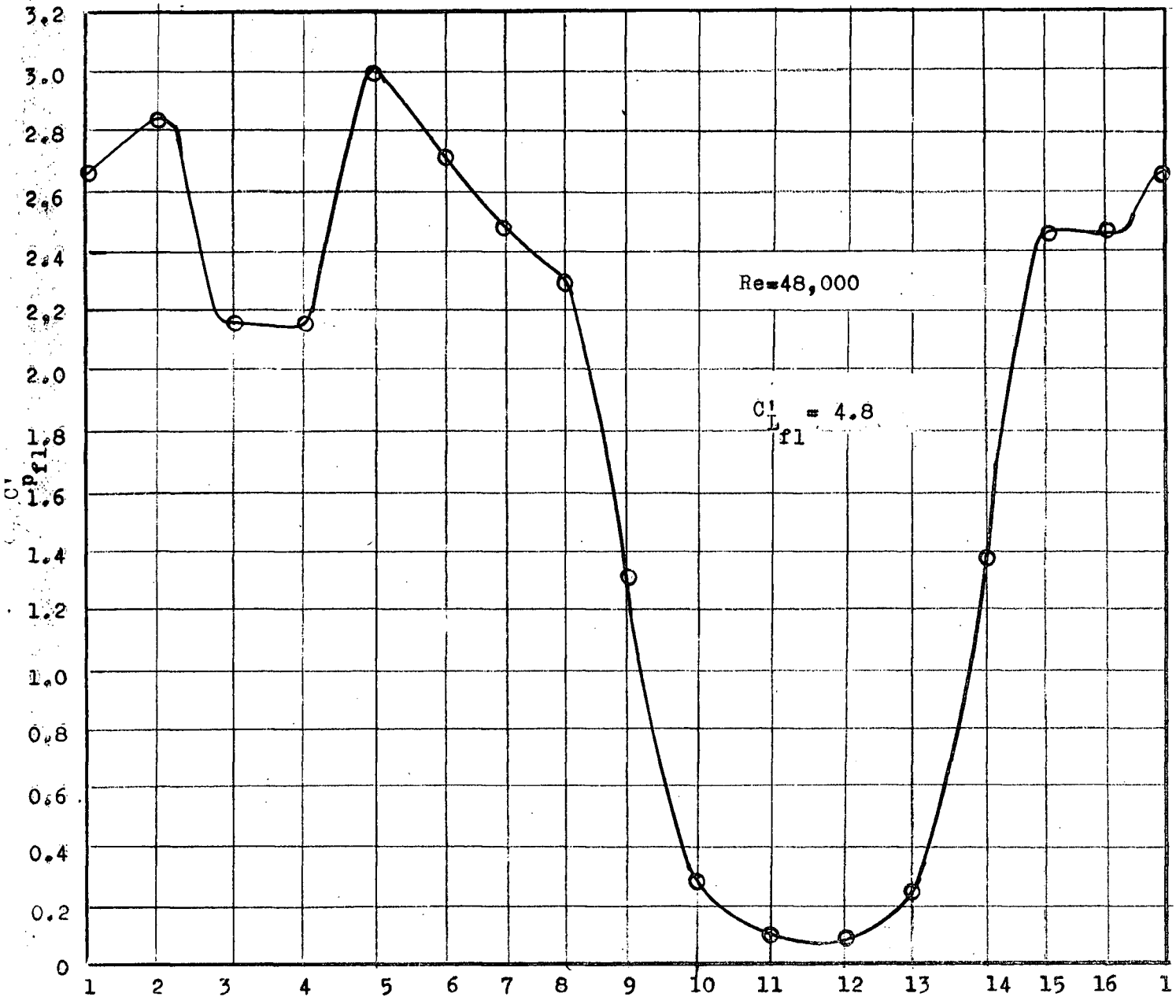

Figure 37b. Fluctuating Pressure Distribution Over Rectangular Cylinder AR=1/2

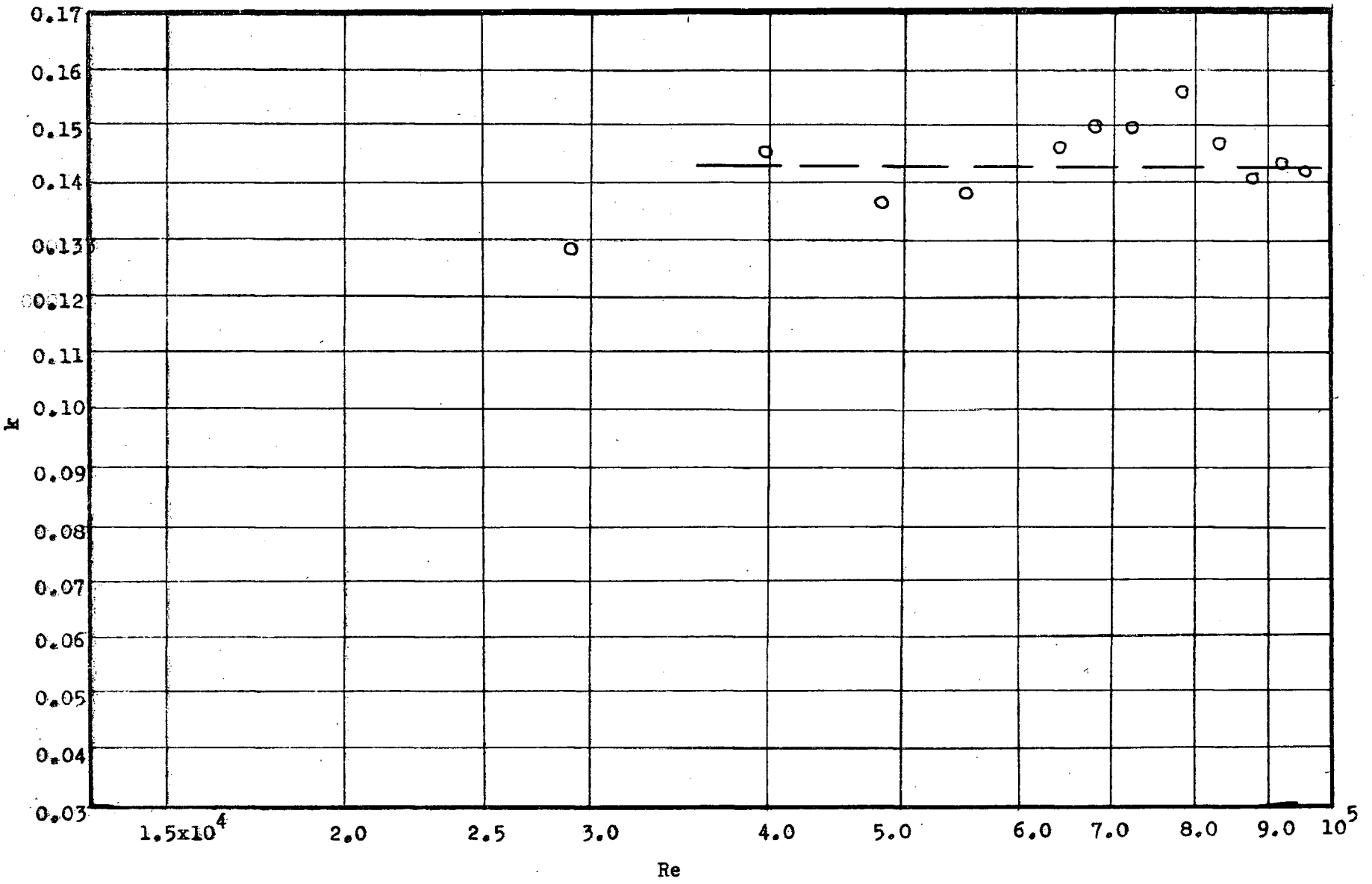

Figure 38. Variation of Strouhal Number with Reynolds Number for Rectangular Cylinder AR = 1/2

4.3.1 Stationary Circular Cylinder

The static pressure distribution around a circular cylinder is well known yet for completeness its measurement was carried out at three different values of Reynolds number (Figure 39).

The measurement of Strouhal number as a function of Reynolds number gave results which were scattered around the curve obtained by Relf and Simmons (21), and as shown in Figure 40.

The measurement of fluctuating pressure distribution around a stationary circular cylinder was carried out by McGregor (11) making use of a microphone as mentioned earlier. His results served as a guide in checking the calibration accuracy of the designed transducer. The dynamic pressure distribution shown in Figure 41 agreed quite well with that obtained by McGregor. The variation of $C'_{p_{fl}} \sin\theta$ with θ was plotted (Figure 42) to evaluate the integral $\int_0^{\pi} C'_{p_{fl}} \sin\theta \, d\theta$ The resultant fluctuating lift coefficient per unit span was $C'_{L_{fl}} = 0.60$ which is comparable to that obtained by McGregor ($C'_{L_{fl}} = 0.58$, Re=53,000).

The pressure fluctuations on the surface of the circular cylinder are shown photographically in Figure 43. The second harmonic effect appears to be quite prominent at pressure tap 7. The amplitude modulation of the pressure oscillations was found to be more random than that for the square cylinder as

shown in Figure 44.

The survey of phase between the oscillating pressures revealed taps 2 to 7 to be in phase and taps 8 to 12 to be 180° out of phase. Figure 45a portrays the signals of the pressure oscillations on one side of the cylinder to be in phase and Figure 45b show 180° phase shift for the pressure signals originating from the opposite side.

The effectiveness of the pressure transducer as a wake survey instrument was substantiated by applying it to the study of wake geometry behind the circular cylinder and comparing the results with theoretically established values. The wake survey probe operating in conjunction with the pressure transducer gave longitudinal spacing of 9.7 inches and lateral spacing of 2.8 inches between the adjacent vortices, thus giving the ratio $a/h = 0.29$. This is slightly higher than the theoretically established value of 0.281. Figure 46 compares the pressure fluctuations sensed by the probe located 9.7 inches downstream from the center of the model with those occurring at pressure tap 4. The two responses are apparently in phase. The dominance of the second harmonic fluctuations along the centerline of the wake is shown in Figure 47 where the upper and lower traces represent the output from tap 4 and the probe located in the center of the wake respectively.

4.3.2 Oscillating Circular Cylinder

The critical wind speed causing self excited oscillations of the circular cylinder was observed to be 26 feet per second. Obviously this was not the vortex excited oscillation which should occur at the wind velocity of 4.9 feet per second. The oscillations therefore were attributed to imperfections in model construction or end effects.

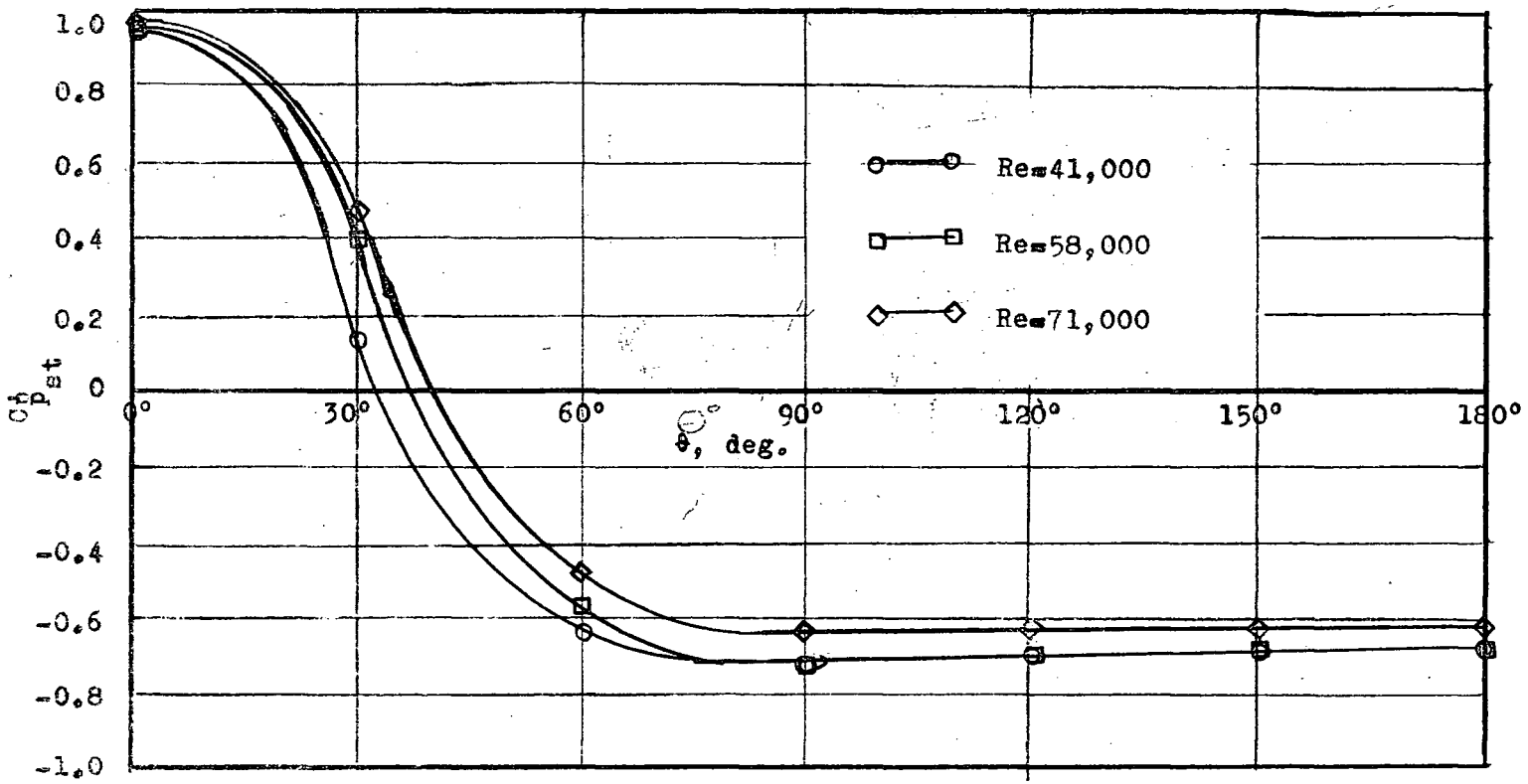

Figure 39. Static Pressure Distribution: Circular Cylinder

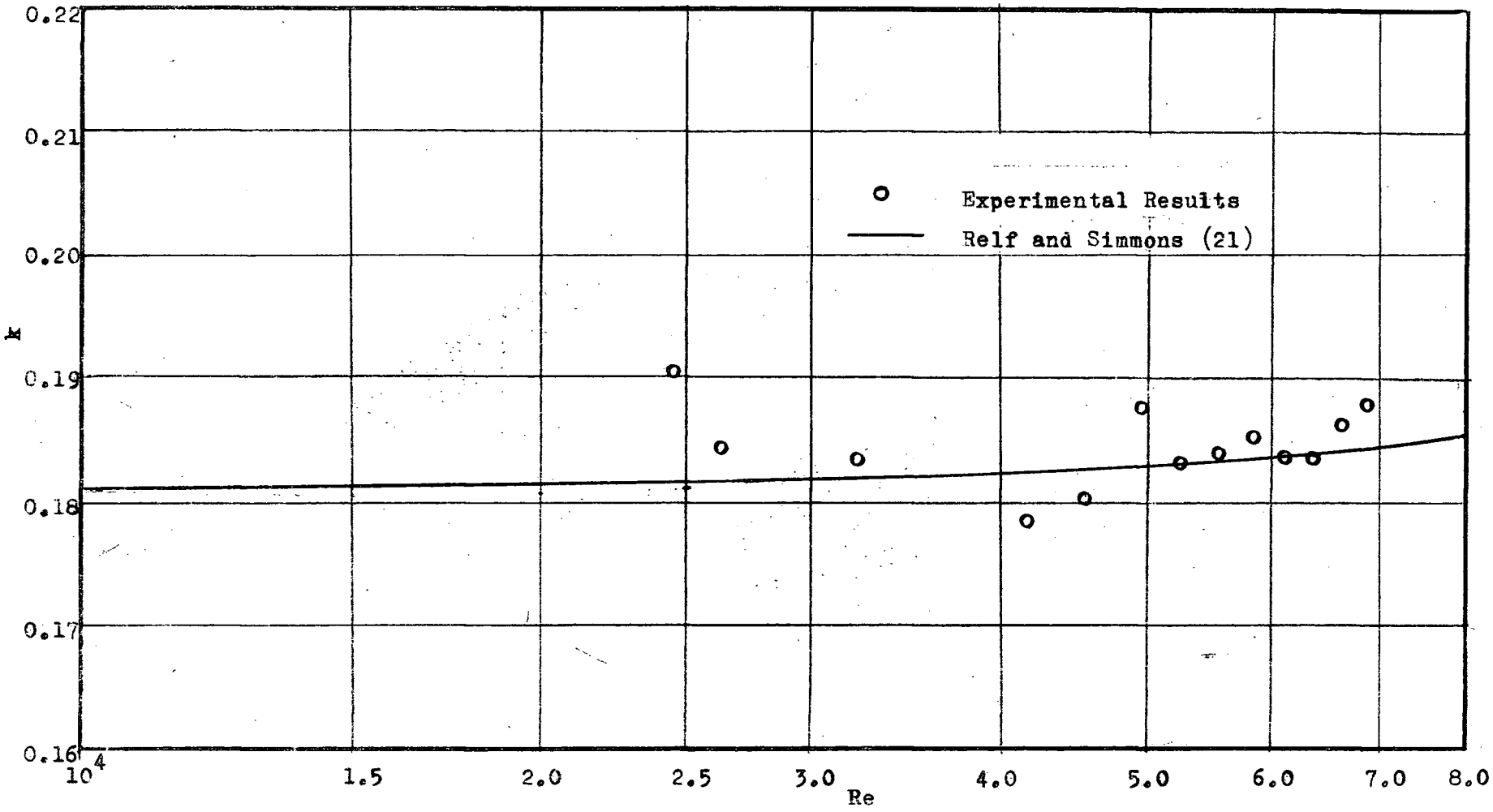

Figure 40. Variation of Strouhal Number with Reynolds's Number: Circular Cylinder

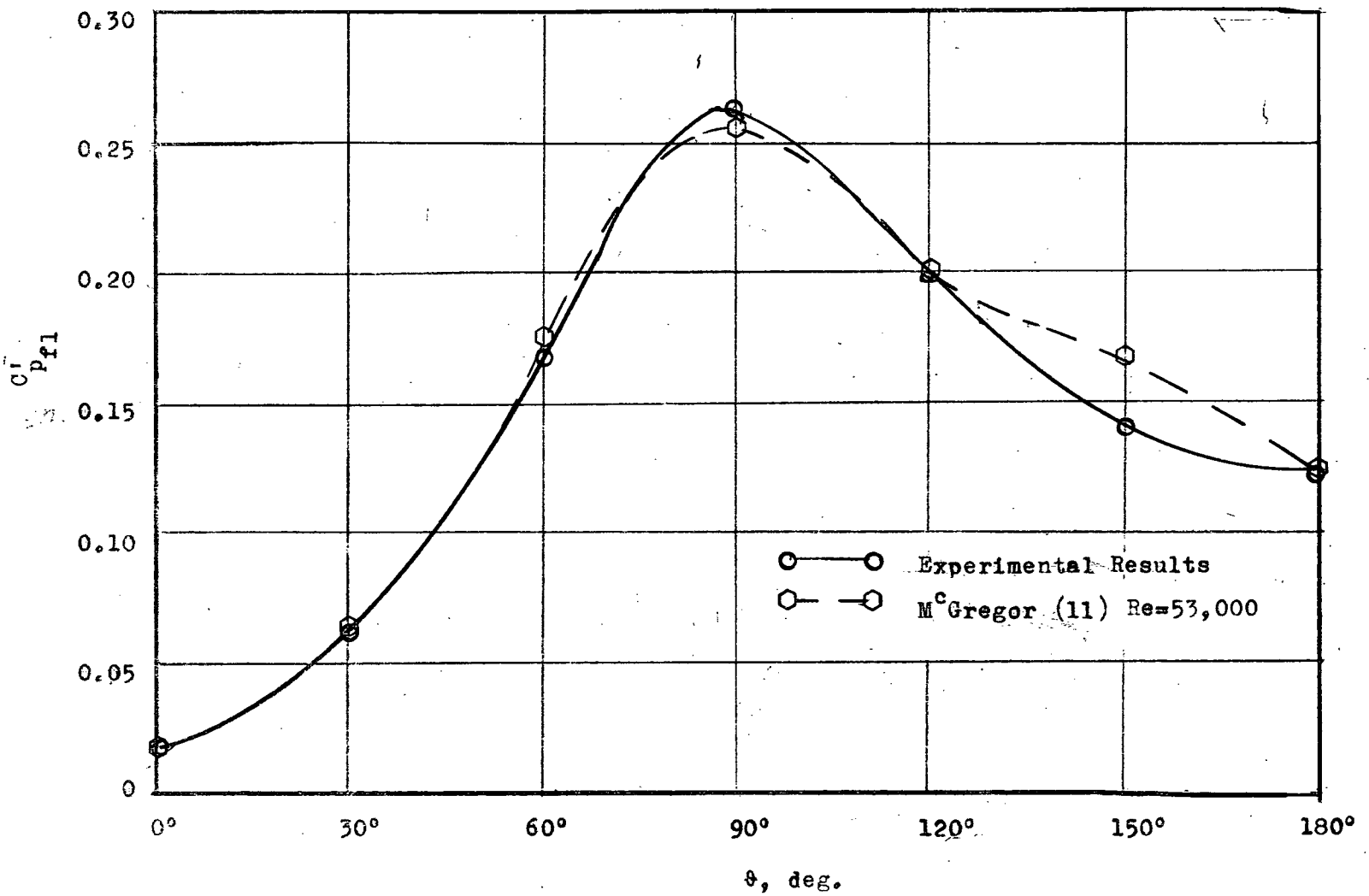

Figure 41. Fluctuating Pressure Distribution: Circular Cylinder

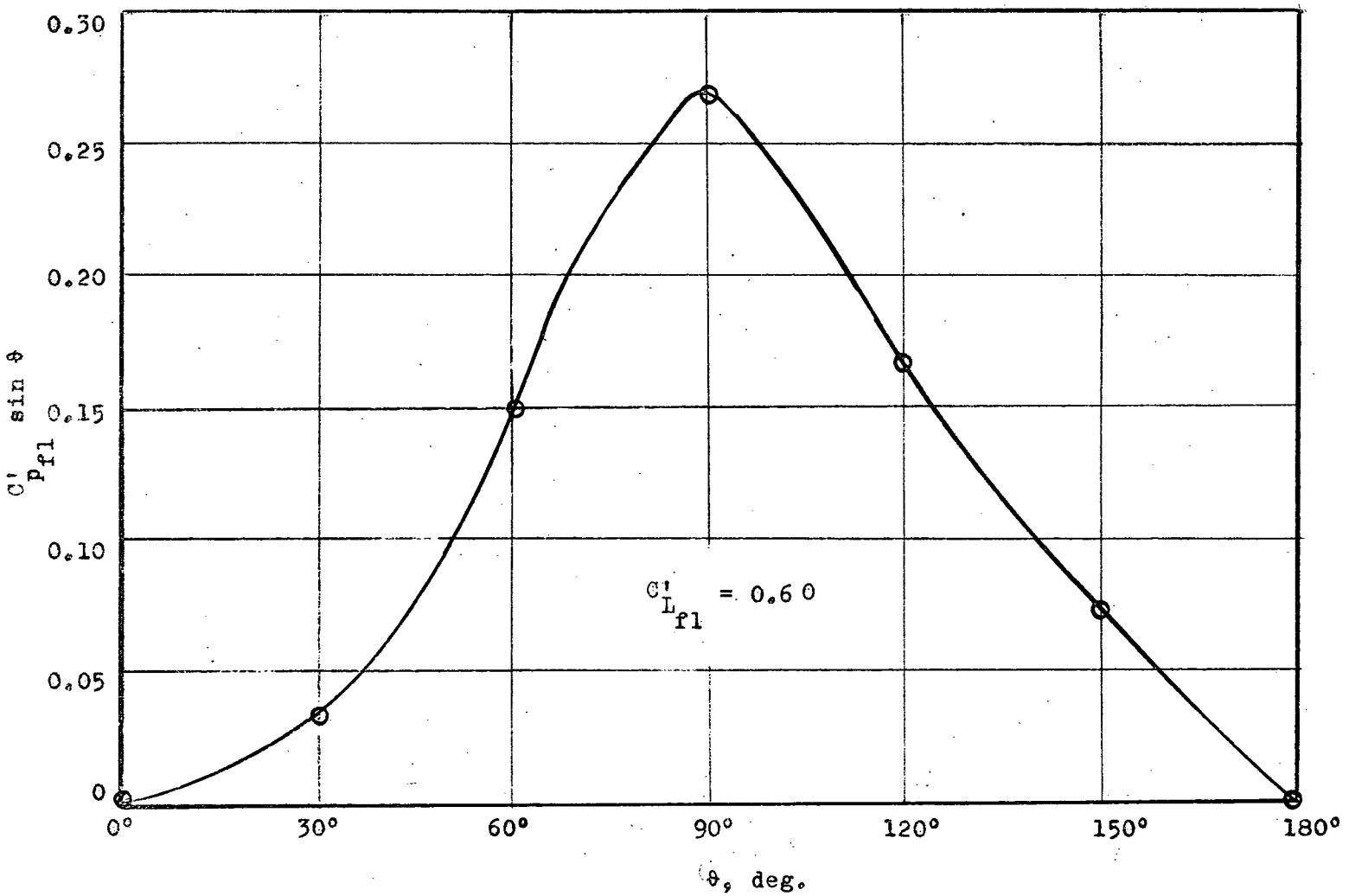

Figure 42. $C'_{p_{fl}}$ sin ϑ versus ϑ for Circular Cylinder

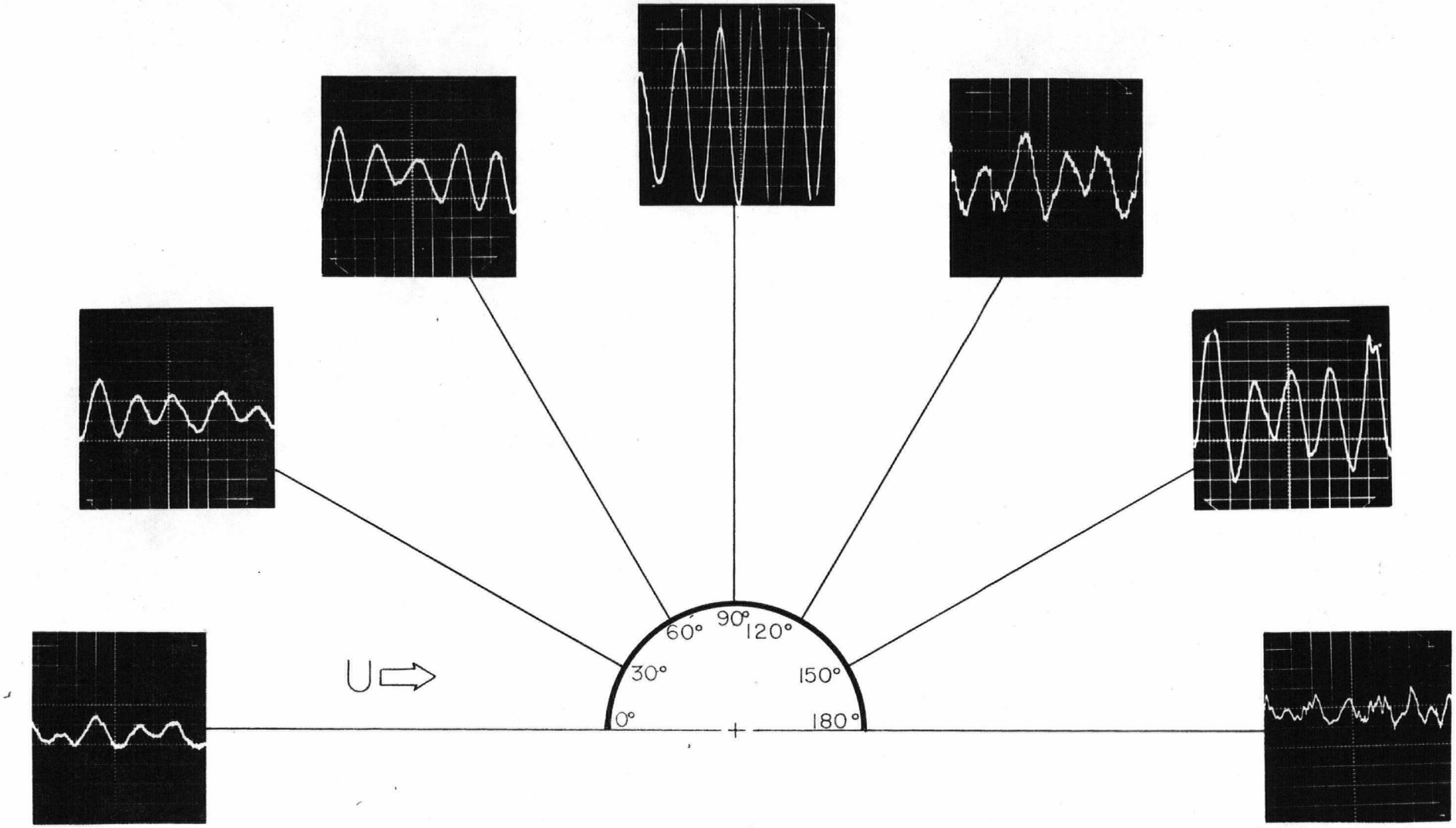

Figure 43. Pressure Oscillations on the Surface of Circular Cylinder

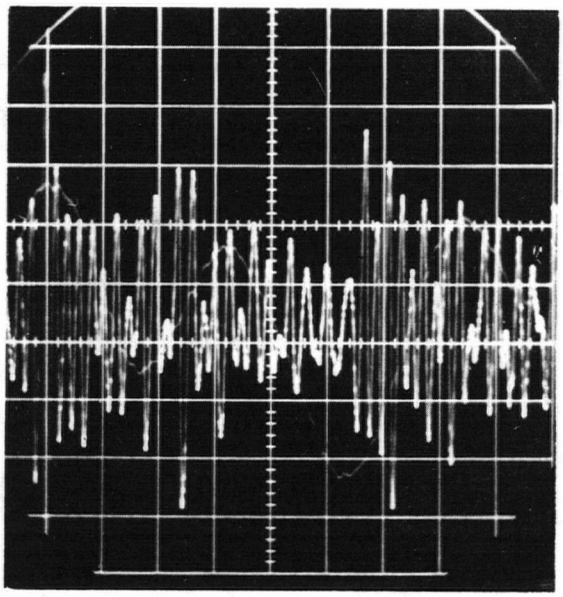

Figure 44. Amplitude Modulations of Pressure Oscillations over Circular Cylinder

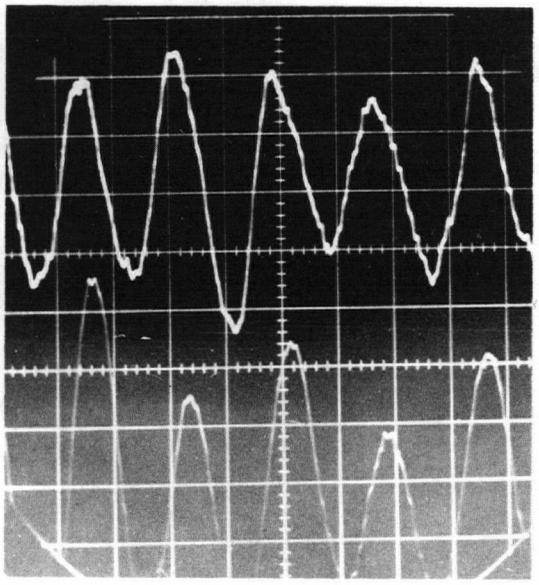

a. Same Side, Taps 2 and 6

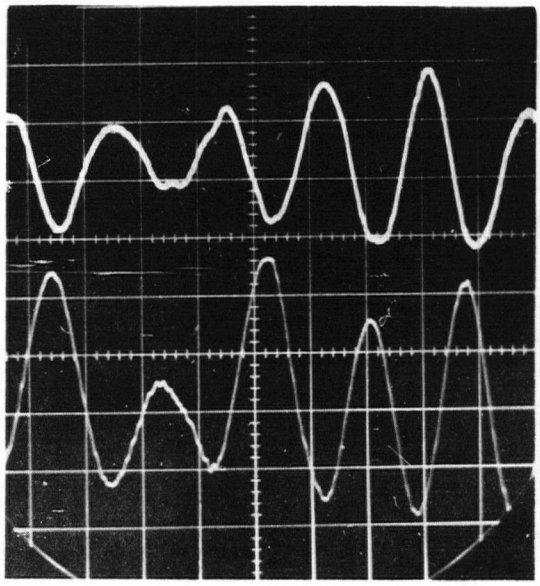

b. Opposite Side, Taps 4 and 10

Figure 45. Variation of Phase on the Surface of the Circular Cylinder

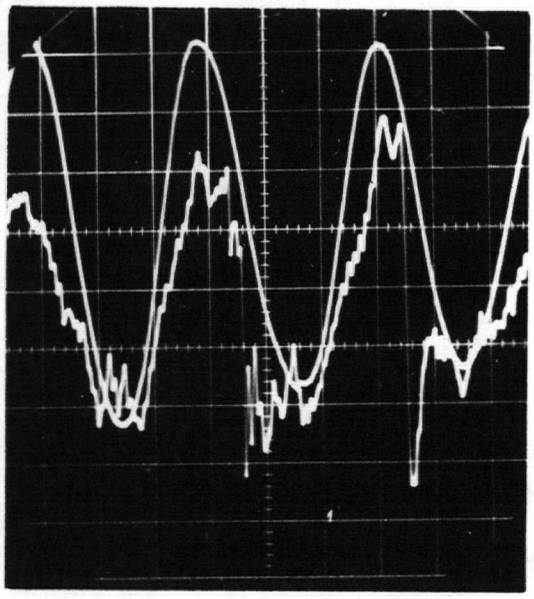

Figure 46. Pressure Fluctuations as Recorded by Probe and Tap 4, Circular Cylinder, Probe 9.7 inches Downstream of the Model

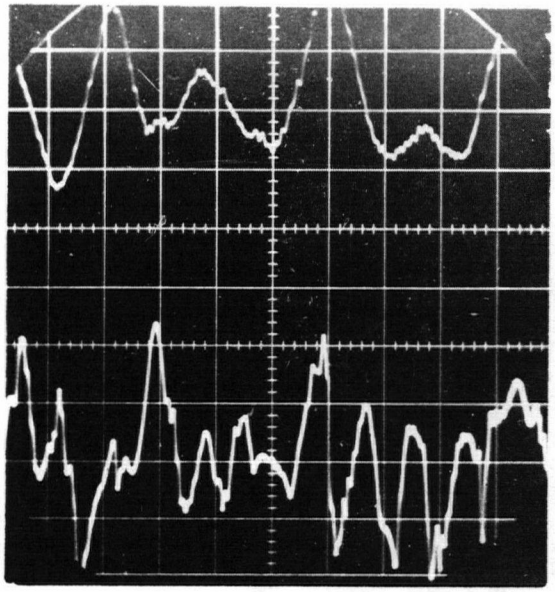

Figure 47. Double Frequency Effect at the Center of Wake of Circular Cylinder

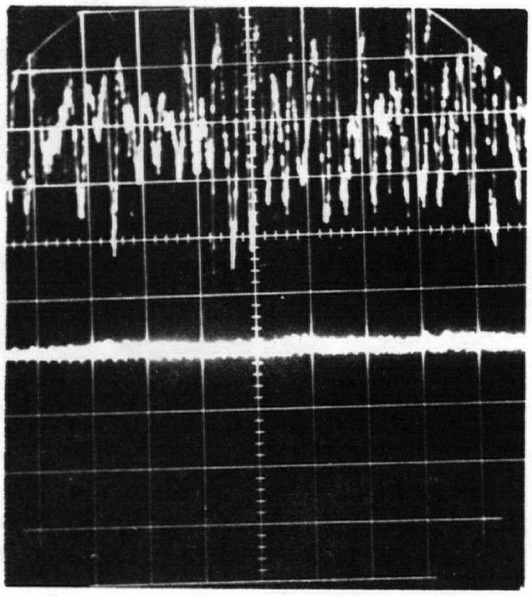

a. No Motion

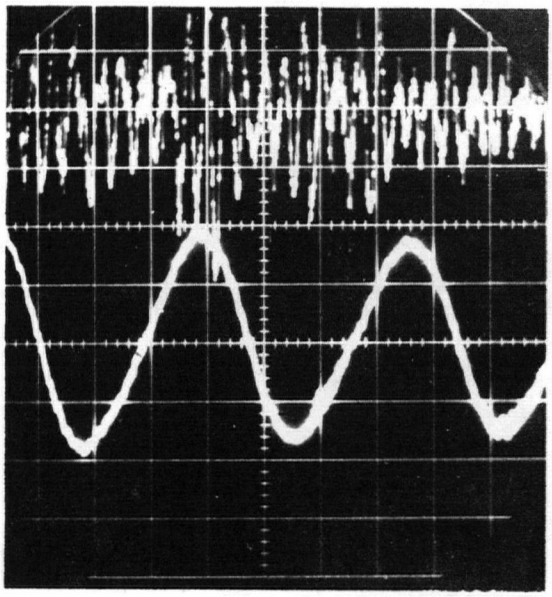

b. Motion

Figure 48. Pressure Fluctuations on the Surface of Circular Cylinder as Affected by its Motion

4.4.1 Stationary Elliptic Cylinder ($\bar{a}$=3 inches e=0.985)

Static pressure measurements on the surface of the elliptic cylinder were carried out over a wide range of angle of attack as shown in Figure 49. The static lift coefficient as function of α is presented in Figure 50.

The pressure fluctuations were not observed until an angle of attack of 9.5°. From this point on to the angle of attack of 28.5° the pressure fluctuations though present were not well defined. But beyond 28.5° the pressure variations were observed to be quite regular. Photographs of the pressure oscillation on the surface of the elliptic cylinder are given in Figure 51. Figure 52 shows the variation in fluctuating pressure coefficient on the surface of the cylinder for several values of α. Fluctuating lift coefficient as a function of angle of attack is presented in Figure 53.

The study of phase difference between fluctuating pressures at different positions on the surface of the elliptic cylinder at angles of attack of 28°, 38° and 48° showed taps 1 to 5 in phase, tap 6 out of phase by 90° and taps 7 to 12 out of phase by 180° all with respect to tap 1.

At an angle of attack of 57° the phases of the pressure oscillations with respect to tap 1 were found to be as follows: taps 1 to 5 in phase, tap 6 lagging by 45°, tap 8 lagging by 135°, tap 9 to 12 lagging by 180°. At pressure tap 7 phase difference fluctuated randomly between 0° and 180°.

The measurement of variation in Strouhal number with Reynolds number at different angles of attack gave readings which were quite scattered as shown in Figure 54.

The study of the nature of the wake revealed the longitudinal distance between the vortices of 17.6 inches and the lateral spacing of 4.5 inches. This test was conducted only at an angle of attack of 30°.

The study of static pressure distribution showed the presence of large twisting moment for angles of attack other than zero. This led the elliptic cylinder to exhibit pure divergence under the condition of stiffness and damping present in the system. This made measurement of fluctuating pressure under dynamic conditions of the model impossible.

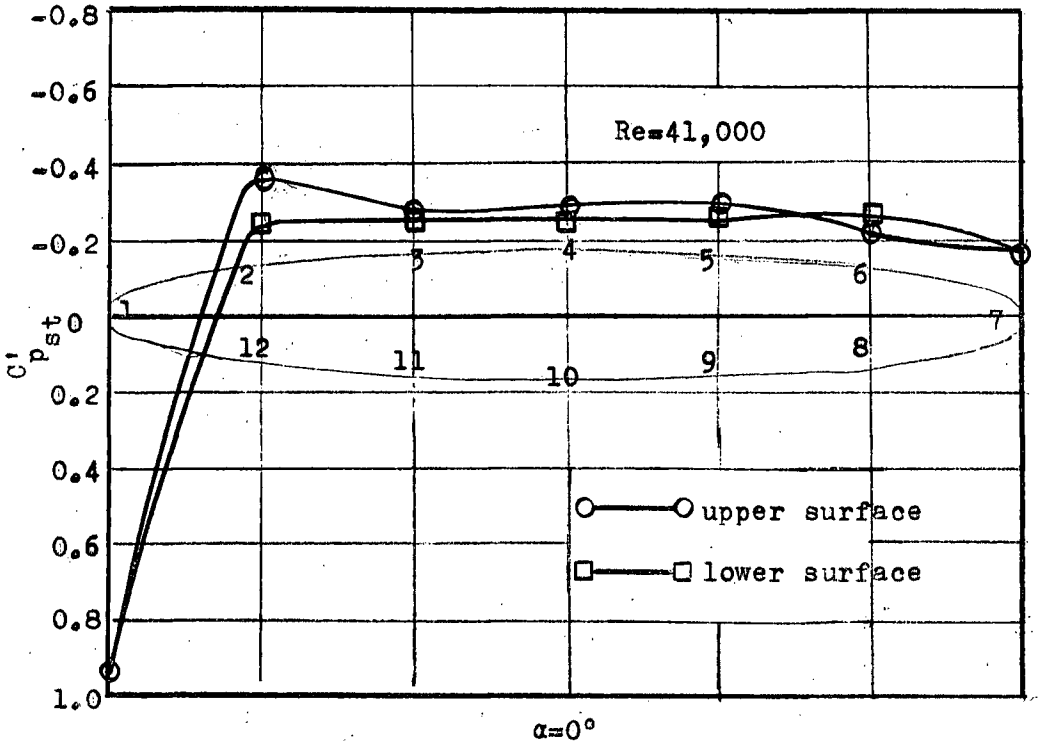

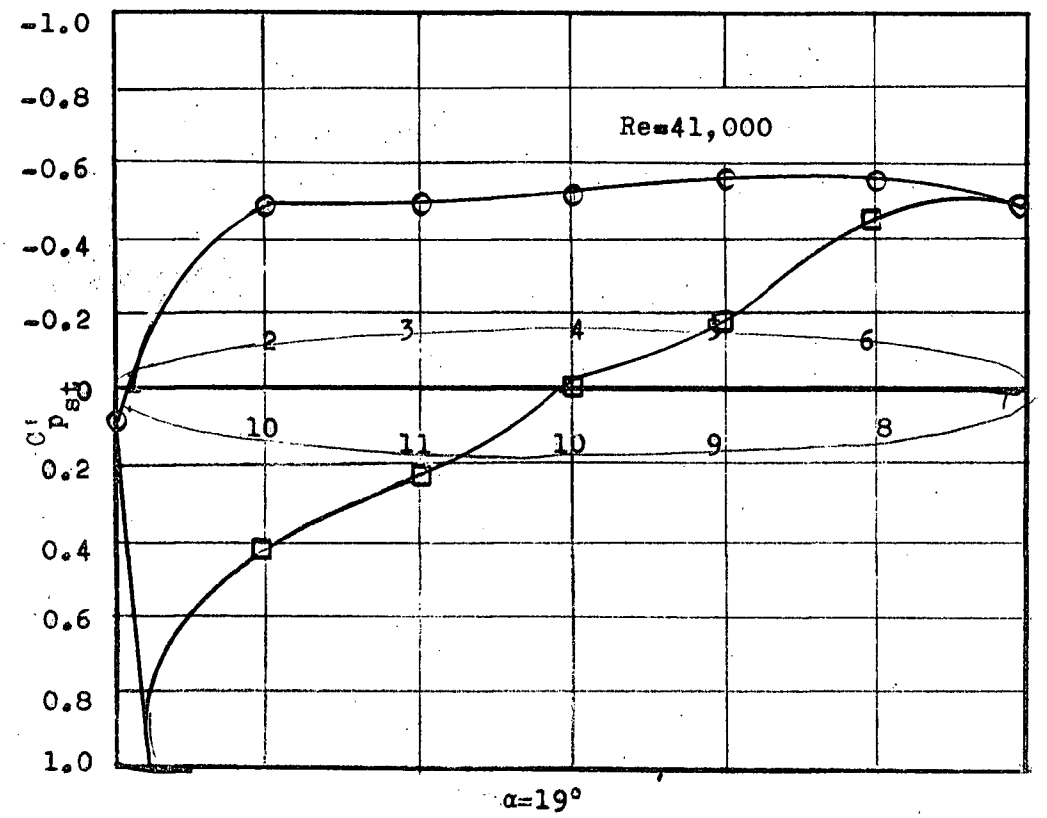

Figure 49. Variation of Static Pressure Distribution with α: Elliptic Cylinder

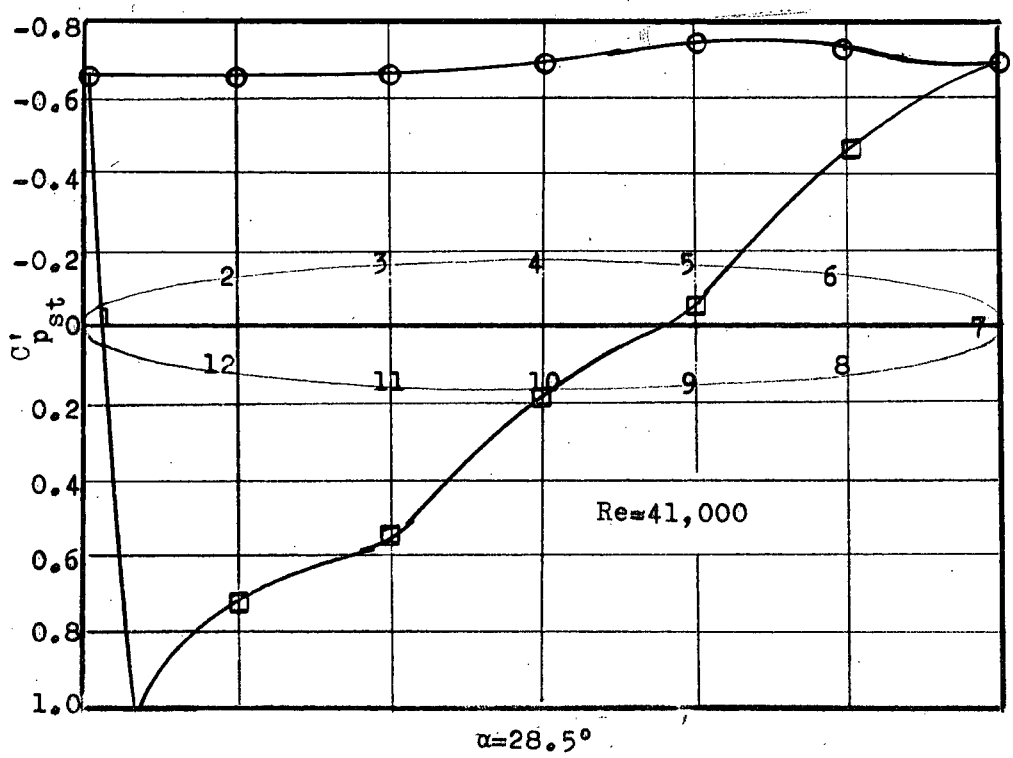

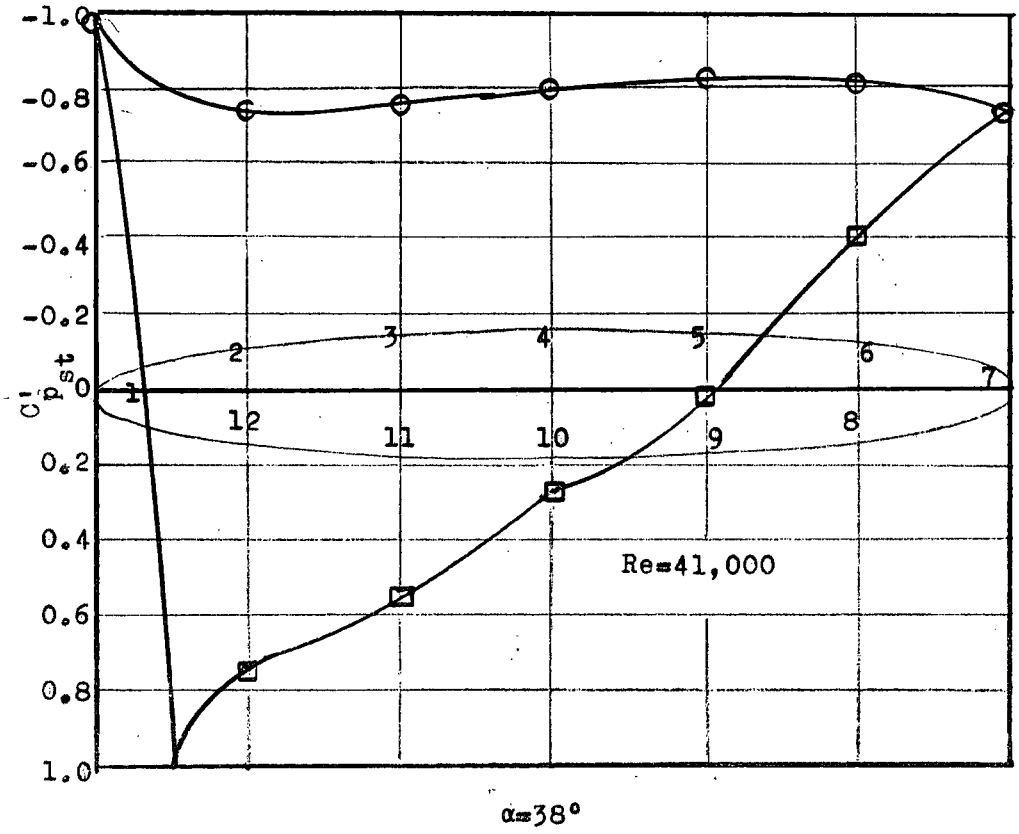

Figure 49 (cont'd). Variation of Static Pressure Distribution with α: Elliptic Cylinder

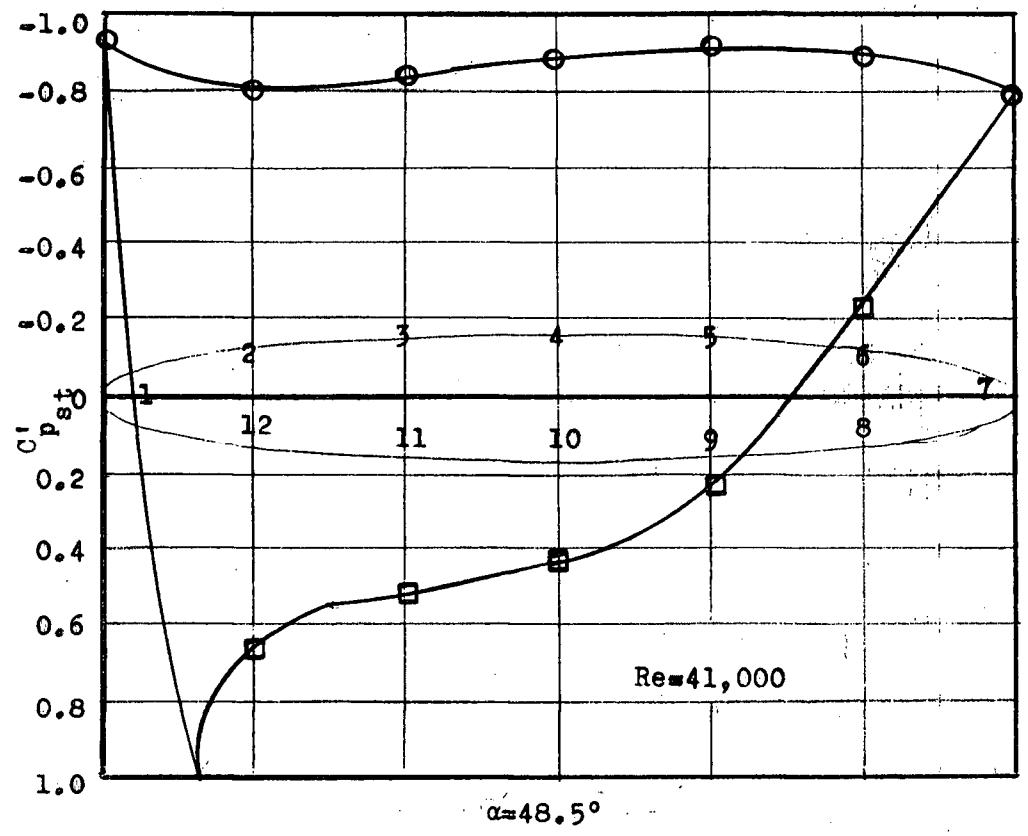

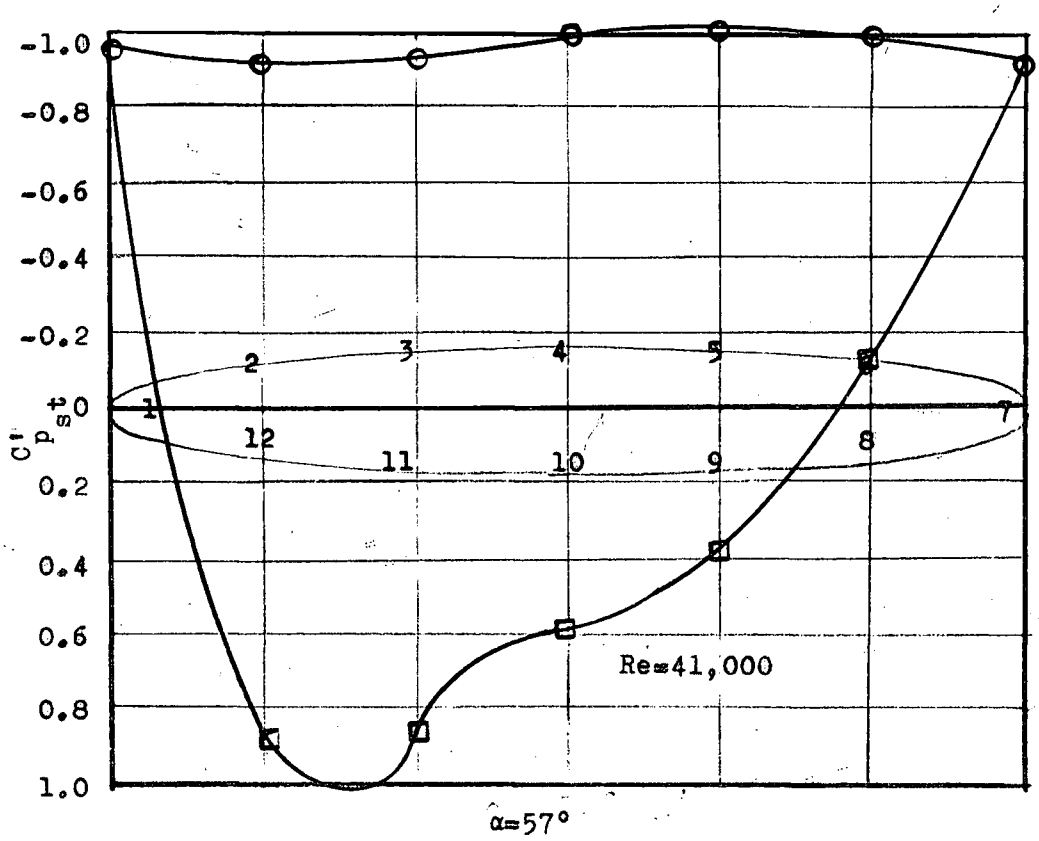

Figure 49 (cont'd). Variation of Static Pressure Distribution with α: Elliptic Cylinder

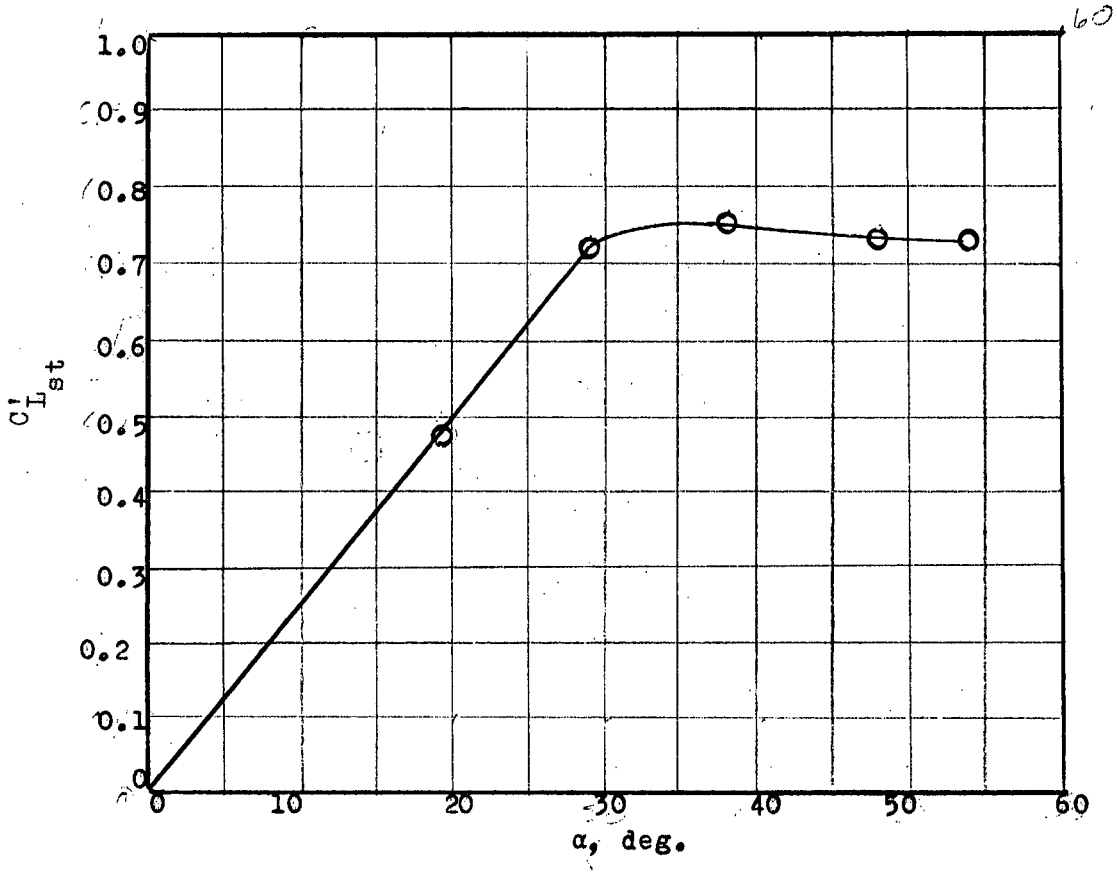

Figure 50. Variation of Static Lift Coefficient with α: Elliptic Cylinder

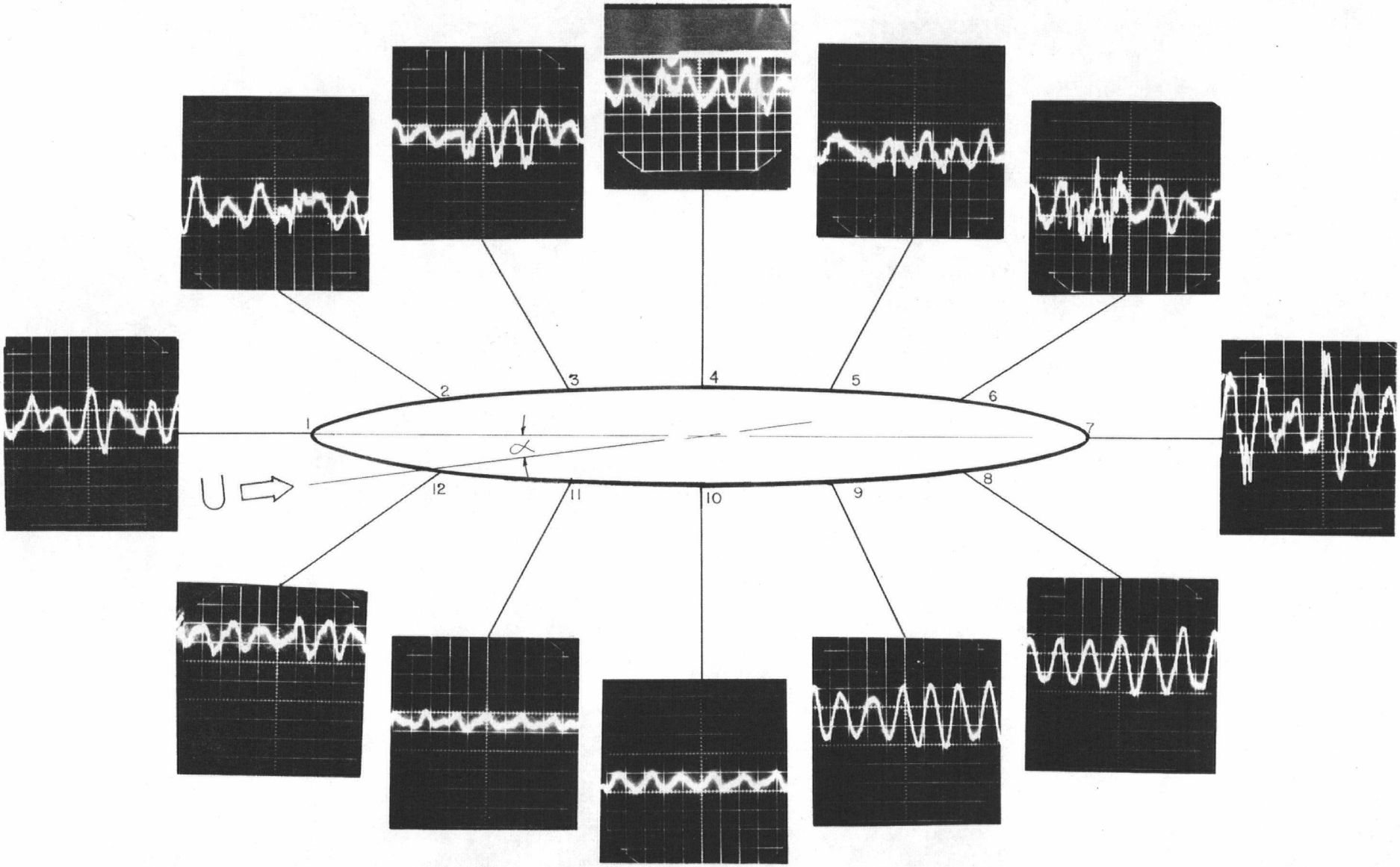

Figure 51. Pressure Oscillations on the Surface of Elliptic Cylinder

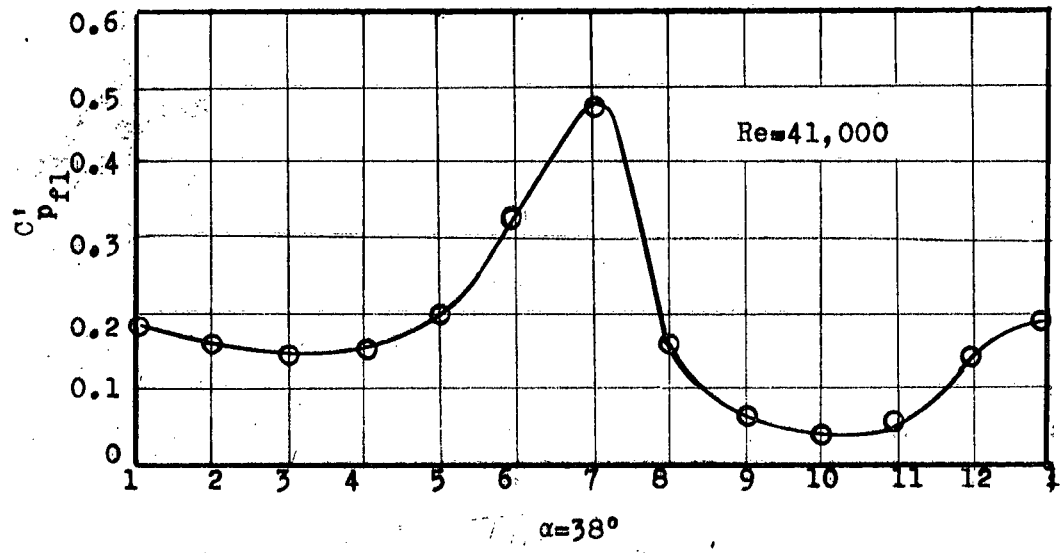

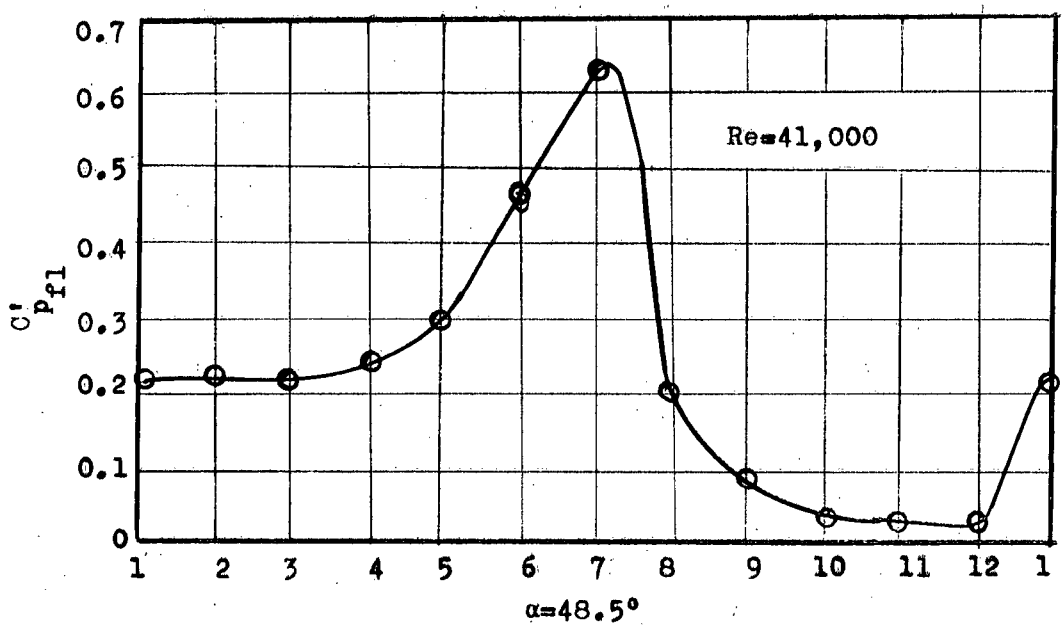

Figure 52. Variation of Fluctuating Pressure Distribution with α: Elliptic Cylinder

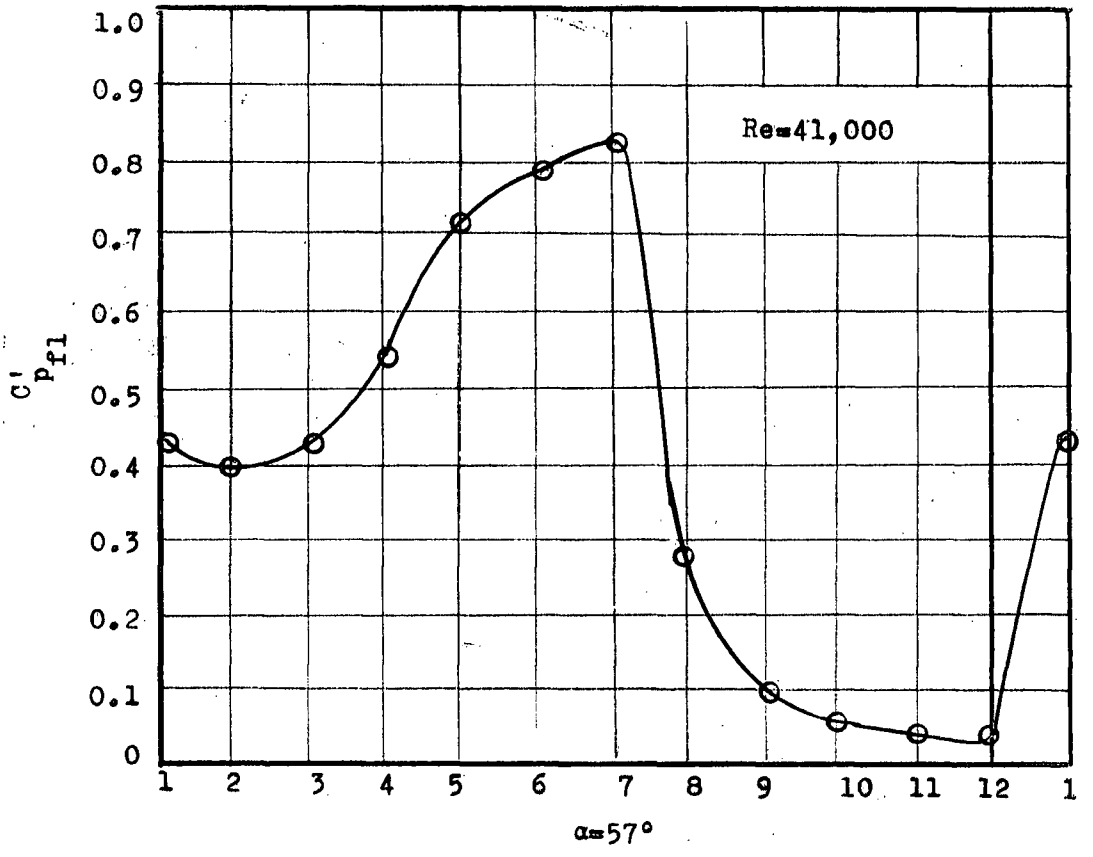

Figure 52 (cont'd). Variation of Fluctuating Pressure Distribution with α: Elliptic Cylinder

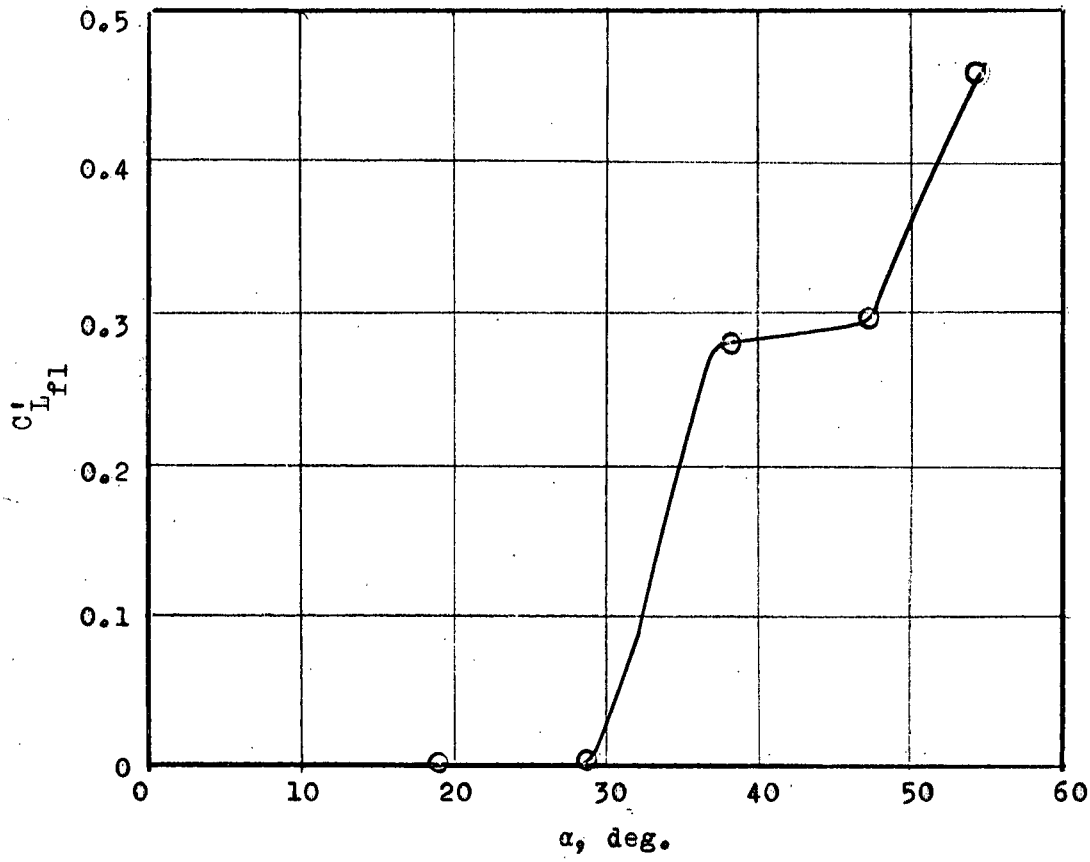

Figure 53. Variation of Fluctuating Lift Coefficient with α: Elliptic Cylinder

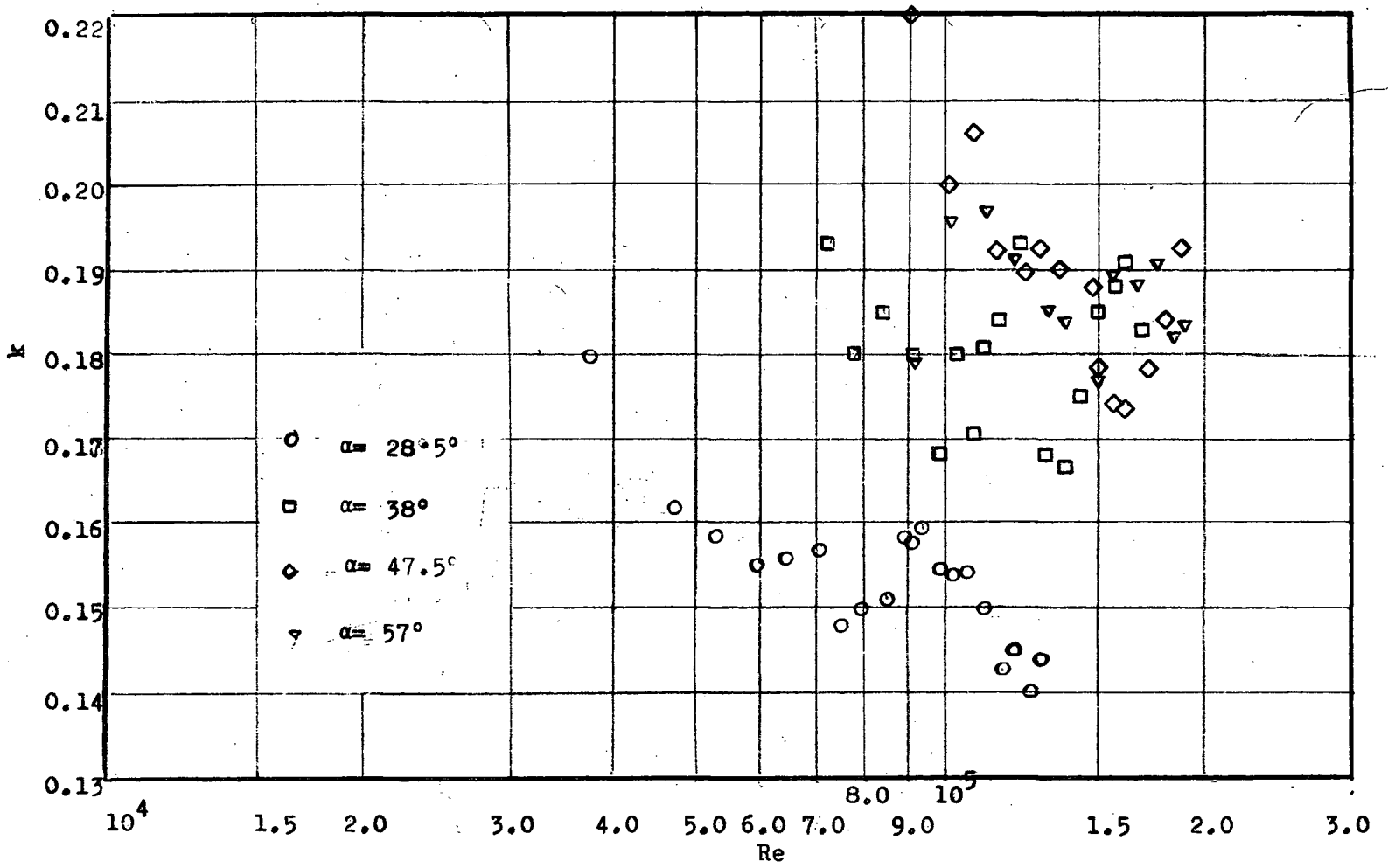

Figure 54. Variation of Strouhal Number with Reynolds Number : Elliptic Cylinder

4.5.1 Stationary and Oscillating Airfoil

The airfoil section used being standard NACA 4412, it was not necessary to measure static pressure distribution around its surface. When tested from 0° to 35° angle of attack it did not show existence of any fluctuating pressure. The critical flutter speed of the airfoil was found to be 32 feet per second. The small value of velocity was due to absence of any external damping except that provided by the airbearings. The stiffness of the system in plunging and torsion is indicated by its natural frequencies in those degrees of freedom which were 5.3 and 5.6 cycles per second respectively. Figure 55 shows the time record of plunging and torsional displacement of the model during aeroelastic oscillations. The Lissajous figure representing the phase difference between the two degrees of freedom is shown in Figure 56. Under this oscillating condition the airfoil did exhibit fluctuating pressure on its surface. Figure 57 shows the oscillating pressure at a representative point (tap 3) together with the plunging and torsional motion of the model. Figure 58 surveys the oscillating pressure at the surface of the model.

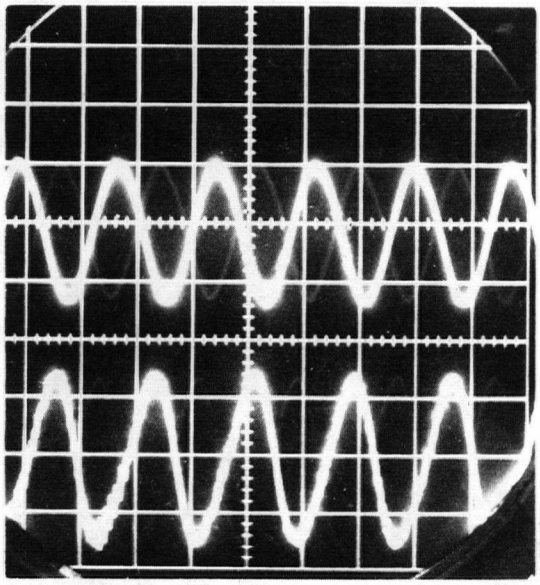

Figure 55. Self Excited Motion of the Airfoil

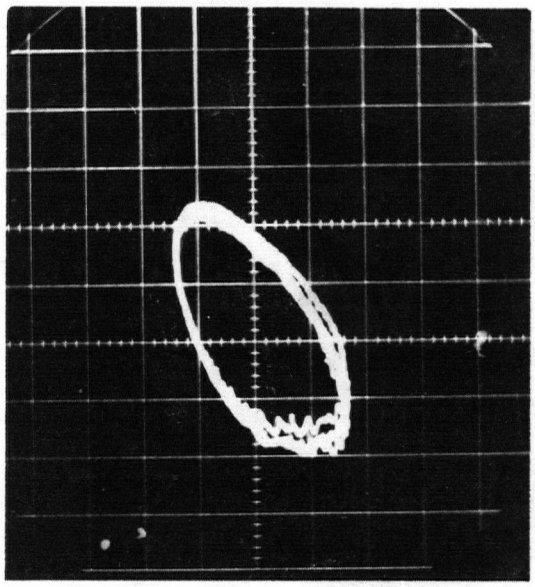

Figure 56. Lissajous Figure During Self Excited Motion of the Airfoil

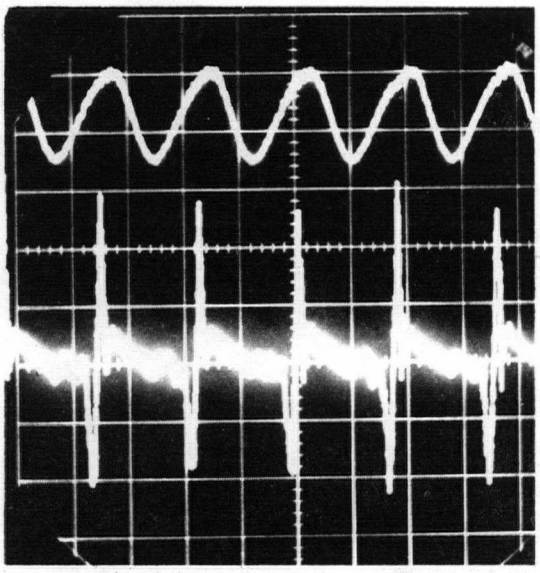

Figure 57a. Lateral

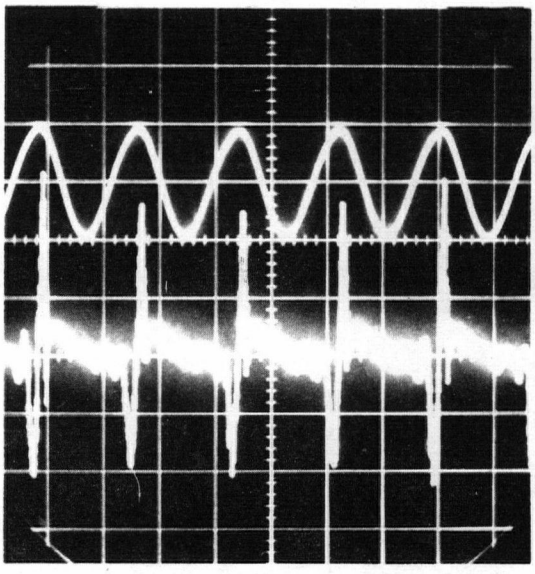

Figure 57b. Torsion

Figure 57. Pressure fluctuations at tap 3 with Lateral and Torsional Displacement of the Airfoil

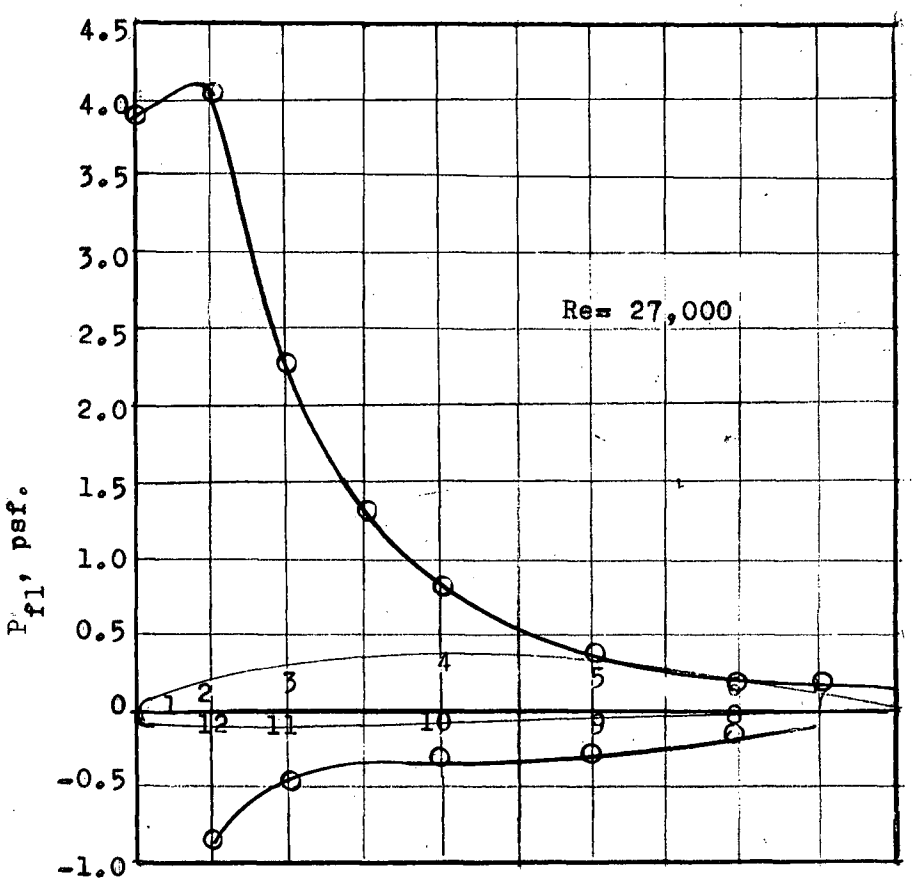

Figure 58. Oscillating Pressures on the Surface of Airfoil Undergoin Flutter

V. DISCUSSION OF RESULTS AND CONCLUDING REMARKS

(a) It was interesting to observe the oscillating lift coefficient decrease with reduction in the bluffness of the body. For example at zero angle of attack the rectangular cylinder with its broad side upstream ($AR = 1/2$) had a fluctuating lift coefficient of 4.6 referred to the face parallel to the flow. As the body size was reduced to a square cylinder the lift coefficient dropped to 2.4. With further streamlining of the body into a rectangular cylinder with $AR = 2$ the oscillating lift coefficient showed further decrease to 1.2 referred to the face parallel to the flow while for circular cylinder it was only 0.60. Further streamlining of the body from circular cylinder into elliptic cylinder and then into airfoil showed no pressure fluctuation at all at zero angle of attack. This reduction in $C'_{L_{fl}}$ with streamlining of the body is schematically shown in Figure 59. It is also of interest to note that $C'_{L_{fl}}$ is constant for the rectangular cylinders if it is referred to the face perpendicular to the flow.

(b) For square and rectangular cylinders as well as for the elliptic cylinder at large angles of attack the magnitude of fluctuating lift coefficient was observed to be minimum at the points where static lift coefficient was maximum.

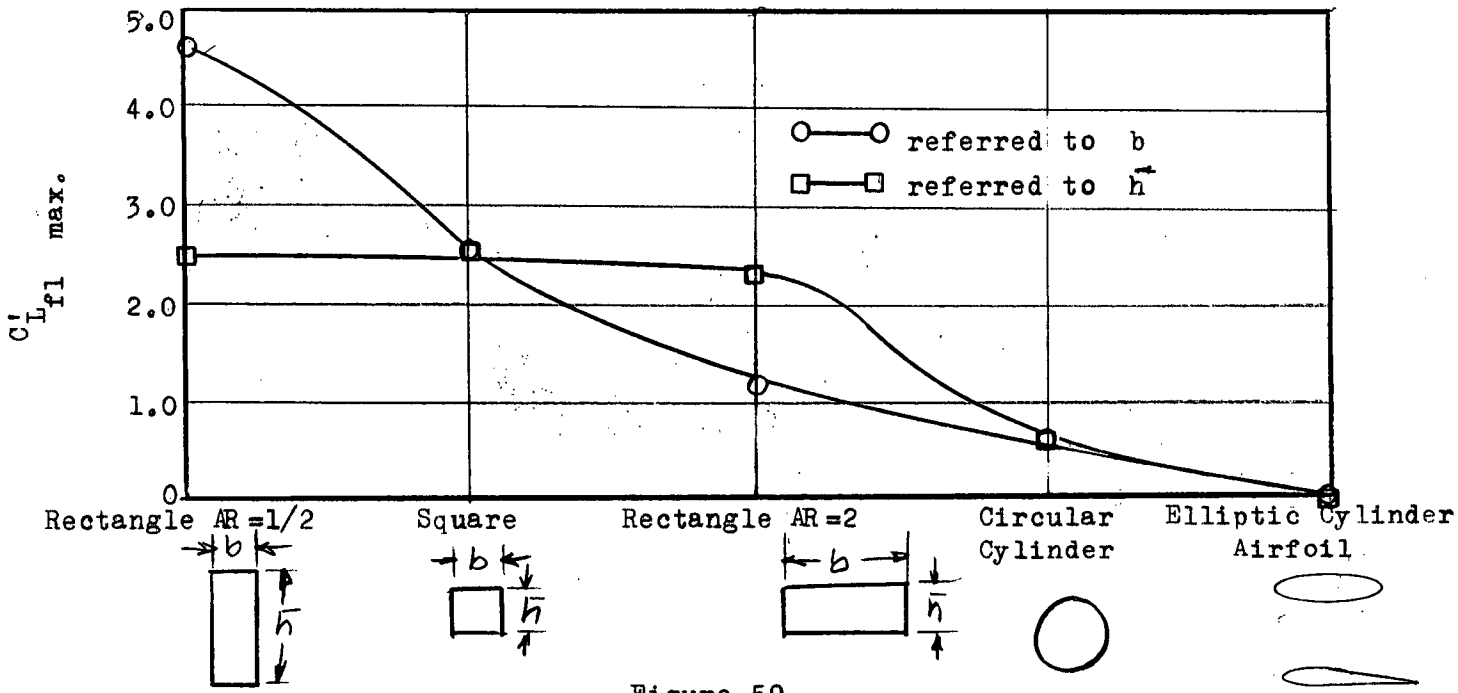

Figure 59.

(c) For bodies with sharp leading edge providing well defined separation e.g. the rectangular cylinders, fluctuating pressure and lift coefficients were observed to be considerably larger than the corresponding static values, while for the circular cylinder, elliptic cylinder and airfoil the fluctuating coefficients were found to be smaller than their static counterpart.

(d) Due to the model and model mounting system design, vortex excited oscillations of the bodies were not possible. Other unbalancing forces produced the self-excited motions which, particularly for a bluff body, does not seem to affect either the frequency of the shedding vortices or the fluctuating pressure.

(e) Probably the most significant outcome of the project was the development of a transducer capable of measuring acoustic level pressure fluctuations over a wide range of frequency. The capability of the device to serve as a wake survey instrument further enhances its usefulness.

RECOMMENDATION FOR FUTURE INVESTIGATION

1. Although the pressure transducer was found to be quite adequate for the present set of experiments, further refinement in its construction and calibration would make it a more useful unit.
2. Usefulness of the transducer as a wake survey unit was described before. For precise measurement of wake geometry, a mechanical device capable of providing motion to the probe, in three-dimension is necessary.
3. Measurement of fluctuating pressure and wake geometry should be undertaken for a rectangular cylinder of AR = 1/2 over a range of angles of attack for completeness of investigation.
4. Dynamic results were not obtained in the case of elliptic cylinder as it exhibited pure divergence. Use of higher stiffness and/or damping should correct this tendency and provide self-excited oscillating motion of the body.
5. In the investigation presented here, the wake measurements were carried out for stationary condition of the model. Corresponding measurements during dynamic condition of the model should also be undertaken.
6. Study of pressure fluctuations and wake during vortex excited motion of the body should be of interest.
7. Similar study of I-section, T-section, channel and angle section, dumbbell shaped body, etc., should prove useful.
8. Study of fluctuating pressure, wake geometry and aeroelastic instability of a body when located in the wake generated by another body should be of importance in VTOL design.

BIBLIOGRAPHY

1. Duncan, W.J., Ellis, D.L., Smyth, E., "First Report on the General Investigation of Tail Buffeting," Br. ARC R&M 1457, 1933.

2. Van de Vooren, A.I., and Bugh, H., "Spontaneous Oscillations of an Aerofoil due to Instability of Laminar Boundary Layer," Natl. Luchvaartlab. Amsterdam, Rept. F96, 1951.

3. Mendelson, A., "Aerodynamic Hysteresis as Factor in Critical Flutter Speed of Compressor Blades at Stalling Conditions," J. Aeronaut. Sci., 1949.

4. Sisto, F., "Stall Flutter in Cascades," J. Aeronaut. Sci., 1953.

5. Stüder, H.L., "Experimental Study of Wing Flutter," Brit. Translation ARC 2777, 1946.

6. Kármán, Th. von., "Flüssigkeits u. Luftwiderstand," Physik Z. 13, 1911.

7. Kármán, Th. von., "Flüssigkeits u. Luftwiderstand," Nachr. Ges. Wiss., Göttingen, 547, 1913.

8. Cometta, C., "An Investigation of the Unsteady Flow Pattern in the Wake of Cylinders and Spheres Using a Hot Wire Probe," Tech. Rept. WT-21, Brown Univ., 1957.

9. Roshko, A., "On the Development of Turbulent Wakes from Vortex Streets," NACA TN 2913, 1953.

10. Chuan, R.L., and Magnus, R.J., "Study of Vortex Shedding as Related to Self-Excited Torsional Oscillations of an Aerofoil," NACA TN 2429, 1951.

11. McGregor, D.M., "An Experimental Investigation of the Oscillating Pressures on a Circular Cylinder in a Fluid Stream," UTIA TN 14, 1957.

12. Prendergast, V., "Measurement of Two-Point Correlations of the Surface Pressure on a Circular Cylinder," UTIA TN 23, 1958.

13. Molyneux, W.G., "Measurement of the Aerodynamic Forces on Oscillating Airfoils," AGARD Rept. 35, 1956.

14. Molyneux, W.G., and Ruddleston, F., "A Technique for the Measurement of Pressure Distribution on Oscillating Aerofoils, with Results for a Rectangular Wing of Aspect Ratio 3.3," Br. ARC TR 18,018, 1956.

15. Smith, J.D., "An Experimental Study of the Aeroelastic Instability of Rectangular Cylinders," M.A.Sc. Thesis, Univ. Brit. Col., 1962.

16. Laub, J.H., "Externally Pressurized Journal Gas Bearings," Presented at the ASIE/ASME Lubrication Conference, Boston, Preprint 601C-15, 1960.

17. Perry, C.C., Lissner, H.R., "A Strain Gage Primer," McGraw-Hill Book Co., Inc., New York, 1962.

18. Heuter, T.F., "Sonics," John Wiley & Sons Inc., New York, 1955.

19. Fung, Y.C., "The Theory of Aeroelasticity," John Wiley & Sons, Inc., New York, 1955.

20. Brooks, N.P.H., "Experimental Investigation of the Aeroelastic Instability of Bluff Two-Dimensional Cylinders," M.A.Sc. Thesis, Univ. of Brit. Col., 1960.

21. Relf, E.F., Simmons, L.R.G., "The Frequency of Eddies Generated by the Motion of Circular Cylinders through a Fluid," Br. ARC, R&M 917, 1924.